Investigation on Effect of Vibrational Distribution and Reduction Analysis on Mercedes Benz City Bus

Submitted by

Temeru Bere

MSc Thesis Submitted to the department of Mechanical Engineering

College of Mechanical, Chemical and Materials Engineering

Office of Graduate Studies

Adama Science and Technology University

May, /2024

Adama, Ethiopia

Investigation on Effect of Vibrational Distribution and Reduction Analysis on Mercedice Benz City Bus

Submitted by

Temeru Bere

Advisor: Dr. Geleta Fikadu (Asst. Professor).

MSc Thesis Proposal Submitted to the department of Mechanical Engineering

College of Mechanical, Chemical and Materials Engineering

Office of Graduate Studies

Adama Science and Technology University

May, /2024

Adama, Ethiopia

DECLARATION

I declare that this thesis entitled "Investigation on Effect of Vibrational Distribution and Reduction Analysis on Mercedice Benz City Bus" is my own work and has not been submitted to any university for similar purpose. The references used in this proposal are duly recognized by proper citations.

Name of student	Signature	Date

RECOMMENDATION

I, the advisor/supervisor of this research thesis, hereby certify that I have closely advised/supervised the student while developing this thesis and read the draft thesis proposal entitled "Investigation on Effect of Vibrational Distribution and Reduction Analysis on Mercedice Benz City Bus" prepared under my guidance by Temeru Bere Therefore, I recommend the submission of the proposal to the department for further review and evaluation.

Major Advisor/Supervisor	Signature	Date
Co- Advisor/Co-Supervisor	Signature	Date

APPROVAL

I/we hereby certify that the recommendation and suggestion given by the thesis review committee are appropriately incorporated into the final thesis entitled "Investigation on Effect of Vibrational Distribution and Reduction Analysis on Mercedice Benz City Bus" by Temeru Bere.

____________________	____________________	________________
Major Advisor/Supervisor	Signature	Date
____________________	____________________	________________
Co- Advisor/Co-Supervisor	Signature	Date

APPROVAL OF BOARD OF REVIEWERS

We, the undersigned, members of the Board of Reviewers of the thesis open defence by Temeru Bere have read and evaluated the thesis proposal entitled "Investigation on Effect of Vibrational Distribution and Reduction Analysis on Mercedice Benz City Bus" and assessed the understanding of the candidate about the proposed research. This is, therefore, to certify that the thesis is accepted and we recommend the implementation of the thesis. ---

Chair Person	Signature	Date
Reviewer 1	Signature	Date
Reviewer 2	Signature	Date

Final approval and acceptance of the thesis is contingent upon submission of its final copy to the Office of Postgraduate Studies (OPGS) through the Department Graduate Council (DGC) and School Graduate Committee (SGC).

Department Head	Signature	Date
School Dean	Signature	Date
Office of post-graduate Studies, Dean	Signature	Date

ACKNOWLEDGEMENT

First and foremost, I would like to extend my heartfelt thanks to almighty God for providing me with the opportunities of joining this program and for enabling me to conduct this study. I would like to express my deepest gratitude and appreciation to my advisor Dr .Gelata Fikadu (PhD.) for his suggestion, guidance, encouragement, and giving constructive comment and continuous follow up toward my Work.

Finally, I would like to thank Mr. Garbe Chukulu (Phd Candidate) for technically supported me on Ansys Transient Multi body dynamics simulator.

Table of Contents

Content **pages**

ACRONYMY AND ABBREVIATION

FEA	Finite element analysis
ANSYS	Analysis Systems
CATIA	Computer Aided Three-Dimensional interactive application
ANSYS	Analysis system
RMS	Root mean square
DOF	Degree of freedom
BRC	Body Rubber Mounted to Chassis
ERC	Engine Rubber Mounted to Chassis
SRF	Seat Rubber Mounted to Chassis
BERC	Body and Engine Rubber Mounted to Chassis
BESRC	Body, Engine and Seat Rubber Mounted to Chassis

NOMENCLATURE

Symbol	Name	Units
M	*Sprung Vehicle Mass*	*kg*
m_{fl} , m_{fr}	*Mass supported by front left and right suspension*	*kg*
m_{rl} , m_{rr}	*Mass supported by rear left and right suspension*	*kg*
m_{wfl} , m_{wfr}	*Front left and right Unsprang Mass*	*kg*
m_{wrl} , m_{wrr}	*Rear left and right Unsprang Mass*	*kg*
k_{fl} ,k_{fr}	*Front left and right Suspension Stiffness*	*N/m*
k_{rl} ,k_{r}	*Rear left and right Suspension Stiffness*	*N/m*
c_{fl} ,c_{fr}	*Front left and right Suspension Damping*	*Ns/m*
c_{rl} ,c_{rr}	*Rear Suspension Damping*	*Ns/m*
k_{tfl}, k_{tfr}	*Front left and right Tire Stiffness*	*N/m*
k_{trl}, k_{trr}	*Rear left and right Tire Stiffness*	*N/m*
c_{trl}, c_{trr}	*Front left and right Tire Damping*	*Ns/m*
c_{trl},c_{tfr}	*Rear left and right Tire Damping*	*Ns/m*
I_x	*Mass moment of inertia of roll*	kgm^2
I_z	*Mass moment of inertia of pitch*	kgm^2
L	*Vehicle Wheelbase*	*m*
B	*Vehicle Wheel width*	*m*
a_1	*Length to Front Suspension from Centre of Mass*	*m*
a_2	*Length to Rear Suspension from Centre of Mass*	*m*
TR	*Transmissibility Ratio*	*N/N*
ST	*Suspension Travel*	*m/m*
RH	*Road Holding*	*N*
a_w	*Weighted root mean acceleration*	*m/s2*
CF	*Comfort Factor*	-

LIST OF TABLES

LIST OF FIGURES

ABSTRACT

The research examines the impact of vibrations on passenger comfort in Mercedes Benz city buses, which use passive suspension systems. It highlights the importance of vibration control for enhancing passenger satisfaction and overall bus performance, particularly in improving health and comfort. The study employs Ansys Transient Multi-Body Dynamics and MATLAB Simulink to analyze the vibrational dynamics of the bus, comparing existing models with modifications to rubber sealing positions between the engine and chassis, the bus body and chassis, and passenger seats. The results indicate that the full-sealed model (BESRC) offers superior vibrational performance, achieving a passenger comfort factor of 8.35, significantly higher than the existing model (WR) at 3.07. The general bus comfort (GBC) also showed improvements across different models, with BESRC achieving a score of 7.84 compared to WR's 6.75. MATLAB simulations confirmed these findings, with a GBC quality factor of 7.3, deviating by 8% from the transient analysis results. The study concludes that the BESRC model represents a high-quality passive suspension system that effectively enhances both bus body stability and passenger comfort during operation.

Key word; *Bus vibration, MATLAB, Mercedes-Benz, Suspension system, Vibration analysis, Vibration reduction*

CHAPTER ONE
INTRODUCTION

1.1 Background of the Thesis

Any motion that recurs after a certain amount of time is called vibration; alternatively, vibration is the oscillating motion of an item around an equilibrium point. In solids, liquids, and gasses, this motion can happen. Numerous things, including mechanical forces, electromagnetic forces, and acoustic waves, can create vibration. Potential energy is converted to kinetic energy and vice versa in this process. It's studied extensively in fields like mechanical engineering, civil engineering, and aerospace engineering, where understanding and controlling vibration is crucial for designing structures and machinery that operate efficiently and safely (Rifaie et al., 2022).

There for, Vibration is a crucial factor in the design, operation, and maintenance of vehicles in the field of automotive engineering. It describes how parts of the vehicle oscillate, or how the vehicle oscillates as a whole. Numerous components, including the engine, drivetrain, suspension system, wheels, and interactions with the road surface, can cause vibration in an automobile. Engine vibration is a result of the reciprocating pistons, spinning crankshafts, and other moving components of internal combustion engines. The purpose of engine mounts and balancing shafts is to reduce vibrations and guarantee smooth operation. Among other drivetrain parts, vibrations in the transmission, driveshaft, and differential can result in drivetrain vibration. Vibrations may be noticeable during acceleration or deceleration, in particular because of imbalances, misalignments, or wear in certain components(Desai & Guha, 2021).

One of the most crucial parts joining the vehicle's body to its wheels is the suspension system. This system's vibration has an adverse effect on not just the car's comfort during the trip, but also the safety of other drivers and the condition of the road. Concerning isolations, The designers of vibration and noise isolation systems focus significantly on vehicle transmission, engine, and gears (Chukulu Jarso et al., 2024). Therefore, matching specifications and optimizing the suspension system are crucial steps in enhancing the comfort of riding in a car. The optimal parameters of the passive suspension system are found to improve ride comfort and rollover resistance, including safety of the vehicle design. Previous researchers proposed the vibration optimization analysis based on parameters, used to improve the ride comfort, road holding, workspace, and preventing rollover. Researchers also presented a method for the optimized design of the vehicle suspension system, considering a full vehicle model with 11-DOF based on the vertical acceleration values of seats according to (Long et al., 2018).

The processes for measuring, assessing, and evaluating vibration as outlined in the two standards differ in a few ways. Among these, measuring vibration on a seat is advised by British standards BS 6841. Vibration measurement in several axes is covered in ISO 2631. In other circumstances Comfort while driving an automobile is a topic of great interest and the focus of research on vibration value reduction. Parts of the human body receive vibrations from the seat, engine, steering, wheels, and pedals. These vibration levels have decreased, primarily in the frequency range of 20 to 100 Hz. Reducing vibration communicated to the human body is a significant issue from the perspective of ride comfort and manoeuvrability. Car vibrations are directly related to the nature of the vehicle and the road surface, which affect drivers and passengers. Road conditions and tire force from the rough surface of the road are the origins of vibration. Reducing vibration also involves improving car suspension systems and road surface quality. Certain cars vibrate with greater intensity in the front or rear. Through the base and back of the seat, these vibrations are transferred along the vertebral axis to the occupants' backsides and backs. Drivers' entire body is exposed to vibration, which is caused by seating dynamics. Certain chairs can either minimize or increase vibration. The driver's hands and feet are also subjected to extra vibrations from the steering wheel and pedals. Both drivers and passengers experience tiredness, cramps, instability, shock, and some physical discomfort during lengthy trips. The posture of an individual in an automobile affects the amount of vibration that is communicated to the driver or passenger (Uzun, 2010).

Some transportation systems do not provide passengers with vibration control, even though these vibrations might be detrimental to health. Among these, the Mercedes-Benz city bus is one that makes use of passive and active suspension technologies. Mercedes-Benz city buses are widely used in Ethiopian urban transportation, making them ideal candidates for studying and enhancing passenger comfort through improved vibrational control strategies. Thus, the purpose of this study is to investigate how Mercedes Benz buses with passive suspension system are affected by vibrational distribution and how successful anti-vibration devices are used. These findings are assessed using Ansys Transient Multi-Body Dynamics and confirmed using a full bus model of the vibrational dynamics equation that is simulated using Matlab-Simulink. The figure 1.1 (a and b) shows the Mercedes Benz bus model and its suspension system.

Figure 1-1Mercedes Benz bus active and passive suspension picture taken from local ara.

1.2 Motivation

The performance of automobiles in terms of noise, vibration, and harshness is greatly impacted by the suspension system. Engineers can optimize suspension parts (like springs, dampers, and bushings) to improve ride comfort and stability by analyzing vibrations. Vibration analysis aids in maximizing the effectiveness of designs for practical use and passenger comfort. Durability and smooth operation are ensured by an understanding of the oscillatory motions of engines, transmissions, and suspension systems.There are several engineering productions that use vibration analysis during car manufacturing. Unwanted vibrations and structural faults could severely lower the product's quality when it is in use. The engineer can adjust the construction of the structure to avoid potential failure, malfunction, or undesirable vibrations by using vibration analysis to identify critical circumstances. Vibration analysis is also utilized to give a way of health monitoring while a structure or vehicles is in use.The aim of this research is to examine the effects of vibrational dispersion on the Mercedes-Benz buses and examine the efficacy of anti-vibration measures. Examining the impacts of vibrational distribution on Mercedes-Benz buses with passive suspension and the effectiveness of anti-vibration solutions are the goals of this research.

1.3 Statement of Problem

Vibration is one of the main concerning topic on vehicle suspension problem. One of the problem is from the viewpoint of ride comfort and manoeuvrability to reduce vibrations transmitted to the human body. The source of this vibration occurs in two ways: structural vibrations and engine vibrations in cars. Vibration influence is a considerable effective factor in car driving as it is a concern related to ride comfort (Uzun, 2010; Barone et al., 2016). Automotive industries are developing constantly and one of the important problems in this field is suspension and related vibration issues. which not only affects the vehicle ride comfort, but also has the negative effects on the road surface as well as safe driving (Long et al., 2018).

For some transit systems, passengers are not given the option to control vibrations, even though they may be harmful to their health. One of these that uses passive suspension technology is the

Mercedes-Benz city bus. The Mercedes-Benz city buses currently exhibit higher-than-acceptable vibration levels, especially during urban operations on uneven roads. This issue affects both passenger comfort and vehicle durability, highlighting the need for effective vibration reduction strategies. Existing literature and driver feedback indicate that Mercedes-Benz city buses often experience increased vibrational discomfort, particularly on uneven road surfaces. This study aims to quantify these vibrations and propose effective reduction strategies. While no direct measurements were taken on the specific bus model, previous studies have shown similar issues in buses with comparable suspension systems, warranting a detailed analysis.

Therefore, the goal of this study is to ascertain how vibrational dispersion affects Mercedes Benz buses and the effectiveness of anti-vibration measures. Ansys Transient Multi-Body Dynamics is used to evaluate these results, and Matlab Simulink is used to simulate a full bus model of the vibrational dynamics equation.

1.4 Objective of the study

1.4.1 General objective

The objective of this research is to investigate the distribution of vibrations in Mercedes-Benz city buses and develop effective strategies for vibration reduction to enhance passenger comfort and vehicle longevity.

1.4.2 Specific objectives

The specific objectives of the research is described as the following.

- To evaluate the baseline vibration characteristics of the Mercedes-Benz city bus under typical operational conditions.
- To develop a full-body simulation model using Ansys and MATLAB for analyzing vibrational responses.
- To implement and test anti-vibration solutions such as rubber mountings in different configurations.
- To validate simulation results against real-world data and recommend optimal vibration reduction strategies.

1.5 Scope of the research

The scope of the current issue is outlined in the following points: The impact of vibrational distribution on Mercedes-Benz City Bus's when driving cyclically in low-frequency vibration. The vehicle's dynamic response can be positively impacted by both an optimal energy distribution and effective vehicle damping, according to the findings.Basically the study comprises;

- 3d Modelling of Vehicle and its vibrational analysis by Ansys transient multibody dynamics and evaluation of its suspension performance and.
- Mat lab-Simulink Computer simulation is performed to validate the numerical transient multibody dynamic simulation results.

Generally, the study focuses on analysing the vibration distribution in the Mercedes-Benz city bus using a full-body simulation model. It examines the effects of various anti-vibration materials and configurations, specifically rubber mountings, on suspension performance and ride comfort. The study is limited to analysing vibrations within the 0-1000 Hz frequency range, commonly encountered in urban bus operations.

1.6 Significances of the research

The significance of the research is discussed as follows

- The vibration suppression can help to increase vehicle life span and passenger's comforts. And due to this maintenance cost or repairing parts can be minimized or increased maintenance intervals.
- On other hand the vibration analysis with numerical technique in this thesis can help to open the way for other researchers to do many work on vibration numerically within a component, machine, or structure to detect unusual vibration events and assess the overall condition of the test object.

1.7 Limitation of the research

The result from the simulation tool, which is called Ansys transient multi body dynamics, needs huge computing time, which can only be obtained by a high-processing unit computer to run simulation on a long-distance highway road surface, which may require a long journey to perceive the comfort quality of passengers and drivers. For this reason, the simulation time for a moving vehicle is limited to 3.1 seconds and a sinusoidal road with an amplitude of 0.1m and a longitudinal distance of 26.15m.

1.8 Organization of the research

This thesis is structured into five chapters: **Chapter 1** introduces the research background, objectives, and scope; **Chapter 2** reviews relevant literature on vibration analysis and reduction strategies; **Chapter 3** outlines the research methodology, including the materials and methods used; **Chapter 4** presents and discusses the research findings; and **Chapter 5** concludes the study with recommendations for further research.

CHAPTER TWO
REVIEW OF LITERATURE

2.1 Introduction

The synthesis of the body of knowledge about a study topic available is called a literature search. In order to explain the general understanding of the subject, this synthesis synthesizes findings from a wide range of sources, providing the groundwork for future research topics and primary investigations. Literature reviews are more than just annotated references; they should acknowledge sources and address the validity of the materials they include. It is important to examine all relevant sources of information, even if they are not included in this study project on vibration analysis of vehicles.

Vibration in Automotive Engineering

The oscillatory motions caused by internal and external forces in different components of a vehicle are referred to as vibration. Aerodynamic influences, road conditions, engine operations, and interactions between vehicle components can all produce these forces. Because vibration affects component longevity, passenger comfort, and vehicle performance, it is an important topic of research in automotive engineering. Vibration is a fundamental aspect of automotive engineering, affecting vehicle performance, safety, comfort, and durability. This literature review provides an overview of the significance of vibration in automotive applications, examining its sources, effects, and the methodologies employed to analyze and mitigate it. Understanding and managing these vibrations is essential for optimizing vehicle design and ensuring a satisfactory user experience. This paper investigates the many causes, consequences, and methods of vibration mitigation for automobiles.

Engine and Powertrain Dynamics: The engine is a primary source of vibrations due to the reciprocating motion of pistons and rotational forces from the crankshaft. Combustion, mechanical imbalances, and gear movements can cause vibrations. Various studies, such as those by Wu et al. (2018), highlight the need for advanced engine mounts and isolation systems to mitigate these vibrations. The integration of active vibration control systems has shown promise in enhancing comfort and reducing noise.

Structural Vibrations: The vehicle's structural components, including the chassis and body, can resonate under dynamic loading conditions. Studies by Zhang and Li (2019) explored finite element analysis (FEA) to predict and mitigate structural vibrations, demonstrating the importance of material selection and design optimization.

Road-induced vibrations: Vehicle interactions with road surfaces can induce significant vibrations. Potholes, uneven surfaces, and road texture contribute to vibrations transmitted through tires and suspension. Research by Karam et al. (2020) emphasizes the impact of road roughness and tire characteristics on vehicle vibration response. Understanding these interactions is crucial for developing suspension systems that can absorb shocks and improve ride quality.

Sources of Vibration:

Numerous factors, such as motor operations, uneven roads, aerodynamic forces, and imbalances in rotatin g parts, have been linked to vehicle vibration in studies.

Research by Ghosh and Chatterjee (2023) emphasize how crucial it is to locate these sources in order to c ontrol vibrations in electric cars.

Aerodynamics: Wind forces acting on the vehicle body can induce oscillations.

Components: Imbalances in rotating parts like wheels and drive shafts also contribute.

2.1.1 Basic vibration elements on car suspension system

The three essential components that present in any machine components are, Mass, spring and Damper. As a result, any machine part, like the one in the following diagram, can be modeled as a spring-mass-damper system.

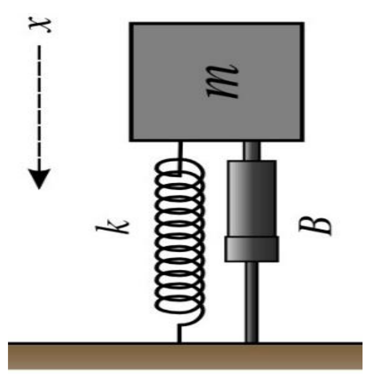

Figure 2-1 spring-mass-damper system

1. Mass

Any machinery component must, of course, have a particular mass that allows it to withstand external loads of any size with a magnitude of F = Ma (mass times acceleration).

2. Stiffness

Depending on the kind and direction of the applied load, a component will bend, deflect, or twist when it is subjected to it. The component will also resist the load in terms of stiffness, with a magnitude of F = Kx (i.e., stiffness times the displacement of the mass). The stiffness of a component is shown by the spring in Figure 2.7.

3. Damper

Damping decreases a component's velocity by gradually dissipating vibration energy in the solid medium, which resists the system's motion to the extent that F = Cv (i.e., the damping coefficient times the velocity) In Figure 2.7, the damping is represented by the piston and oil assembly. Generally speaking, the engineering parts that go into making machinery have an under damped condition, or a damping ratio of less than 1. The damping ratios of a few common engineering materials are shown in the following table.

Table 2-1 damping ratios of a few common engineering materials

Material	Damping Ratio
Steel Spring	0.005
Neoprene	0.05
Natural Rubber	0.05
Pre stressed Concrete	0.02 to 0.05

Vibration isolation is traditionally achieved by use of a passive system consisting of dampers and springs. Because it applies an opposing force proportionate to its displacement, the spring prevents the vibration from moving. The damper is made up of a conductor traveling in a magnetic field or a piston moving through a viscous fluid. It releases kinetic energy as heat. But, the spring has a natural resonance frequency that is determined by its force constant, k. When the vibration frequency gets close to this natural frequency, the spring turns into an amplifier. Vibrations lower than roughly 10Hz are too weak for this basic system to handle.

2.1.2 Harmonically excited vibrating systems

Systems that are one-DOF harmonically excited fall into four categories. (1) Base excitation: this is the most realistic model for vehicle vertical vibration; (2) Eccentric excitation: this model covers all rotary motor suspension types, including engines mounted on engine mounts. (3) Eccentric base excitation: this is a vibration model for any equipment installed on a motor vehicle or engine. (4) Forced excitation: this is the most basic forced vibration model, useful for teaching purposes, but it has very little real-world application. The harmonically excited vibrating systems are depicted in Figure 2.8.

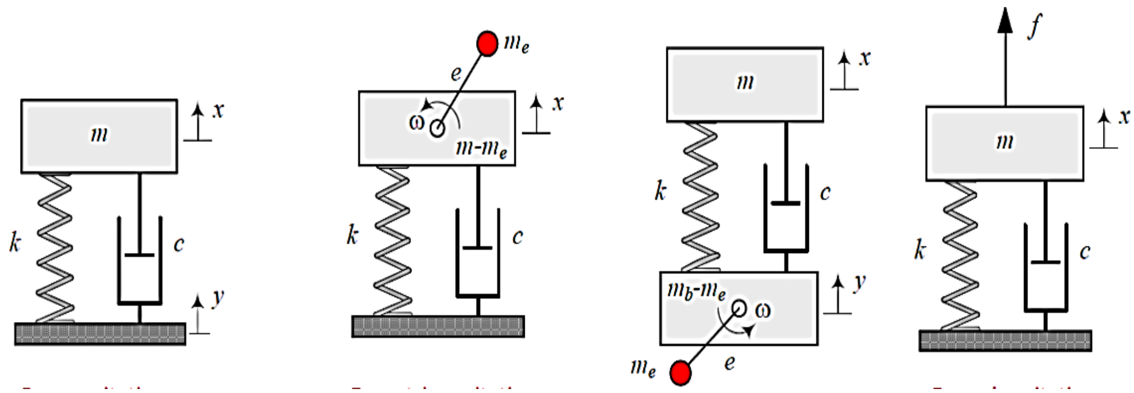

Base Excitation	Eccentric excitation	Eccentric base excitation	(4) Forced excitation

Figure 2-2harmonically excited vibrating systems

2.2 Basic of suspension system in car vibration

The suspension system of city buses is critical in determining ride comfort, stability, and overall vehicle performance. Various suspension types; passive, active, and semi-active, have been developed, each offering unique advantages and mechanisms for vibration control.

With increasing urbanization and the demand for efficient public transportation, understanding the various types of suspension systems is essential for optimizing bus design and functionality. This review examines the predominant suspension systems used in city buses, discussing their characteristics, advantages, and limitations based on existing literature

2.2.1 Passive Suspension System

Passive suspension systems consist of conventional components such as springs and shock absorbers that do not actively adjust to changing road conditions.

1. Leaf Spring Suspension

Leaf spring suspension is one of the oldest and most widely used systems in heavy vehicles, including city buses. According to Zhang and Li (2020), leaf springs provide a robust and cost-effective solution for supporting heavy loads, making them suitable for public transport applications. This system’s primary advantage is its durability and simplicity, which contributes to lower maintenance costs. However, a study by Almeida et al. (2021) points out that while leaf spring systems are effective for heavy loads, they often lead to a harsher ride quality, especially on uneven urban roads.

2. Air Suspension

Air suspension systems are becoming increasingly popular in city buses for their ability to provide superior ride comfort and adaptability to varying load conditions. Air suspension systems use inflatable air bags, which can be adjusted to optimize ride height and damping characteristics. This adaptability enhances passenger comfort and reduces vibrations transmitted to the vehicle structure. However, Smith et al. (2022) note that the complexity and higher initial costs of air suspension systems can present challenges, leading to increased maintenance and repair needs.

3. Independent Suspension

Independent suspension systems, where each wheel operates independently, offer enhanced handling and ride quality. Independent suspension improves tire contact with the road surface, enhancing stability and cornering performance. This is particularly advantageous in urban environments where road conditions can vary widely. Nonetheless, Johnson et al. (2023) point out that independent systems are generally more complex and costly to manufacture and maintain compared to traditional leaf spring systems.

4. Hydraulic Suspension

Hydraulic suspension systems utilize fluid-filled dampers to provide a smooth ride and dynamically adapt to changing load conditions. Research by Kim and Lee (2023) indicates that hydraulic systems can effectively reduce body roll and enhance passenger comfort, making them suitable for city buses that often navigate sharp turns and uneven surfaces. However, as Thompson et al. (2020) notes, the complexity and higher maintenance requirements of hydraulic systems can limit their widespread adoption in public transportation.

5. Torsion Bar Suspension

Zhang and Li (2020) highlight that torsion bar suspension systems, while compact and capable of good load-carrying capacity, may fall short in ride comfort compared to air or hydraulic systems, particularly on rough urban roads. Jiregna and Sirata (2020) explain that passive suspension systems manage pitch, roll, and vertical motion dynamics by using damping components, such as hydraulic shock absorbers, to maintain ride comfort and ensure proper tire-road contact. Martinez et al. (2022) emphasize that torsion bar suspension systems are valued for their compact design and weight savings but acknowledge limitations in comfort performance. Bianchi (2022) elaborates that the design of dampers, whether soft or stiff, aims to optimize the trade-off between ride comfort and handling, with soft absorbers enhancing comfort but reducing handling performance and stiffer absorbers improving handling while increasing body acceleration.

The choice of suspension systems for city buses significantly impacts ride quality, stability, and operational costs. Leaf spring systems remain a reliable and economical option, while air suspension systems are increasingly popular for their superior comfort and adaptability. Independent and hydraulic suspensions offer better handling and performance but at higher costs and greater complexity. Torsion bar systems provide a balance of compactness and load capacity but may not deliver the same level of comfort. As urban transportation demands evolve, ongoing research and technological advancements in suspension systems will be essential to improve the efficiency and effectiveness of city buses.

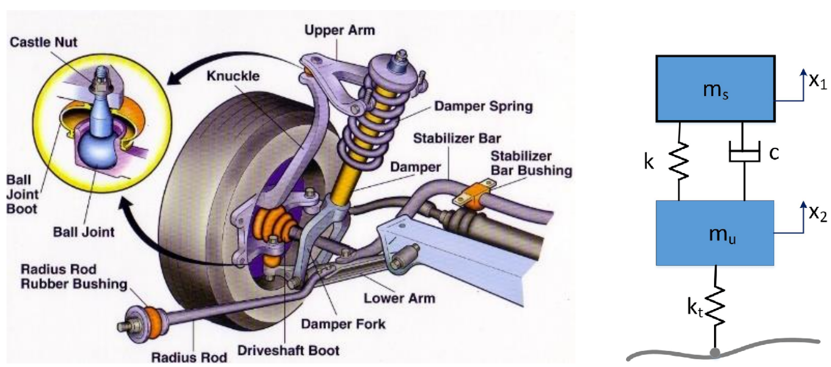

Figure 2-3 Passive Suspension System

2.2.2 Advantages of a passive suspension system

Passive suspension systems are commonly used in vehicles, including automobiles and buses, due to their simplicity, reliability, and cost-effectiveness. These systems primarily rely on mechanical components such as springs and dampers to absorb road shocks and provide ride comfort. The passive car suspension system has some advantages despite being an older model. First off, since cars have been using this suspension system since the 1920s, it is by far the most popular. Due to its extensive availability, almost all cars now on the market have it as the standard suspension. Compared to its rivals, cars using passive suspension systems are more accessible and less expensive.

The following review explores the advantages of passive suspension systems, drawing on existing literature.

1. **Cost-Effectiveness**

One of the primary advantages of passive suspension systems is their cost-effectiveness. According to Liu et al. (2018), passive systems require fewer components and less complex engineering compared to active or semi-active systems. This simplicity translates to lower manufacturing and maintenance costs, making passive suspensions an attractive option for budget-conscious vehicle manufacturers and operators.

3. **Simplicity of Design and Installation**

The simplicity of passive suspension systems facilitates easier design and installation. Research by Zhao et al. (2019) highlights that passive systems can be integrated into a vehicle's structure with minimal alterations. This ease of installation is particularly beneficial for manufacturers looking to streamline production processes or retrofit existing vehicles.

2. **Reliability and durability**

Passive suspension systems are known for their reliability and durability. As noted by Smith and Johnson (2020), the lack of electronic components or fluid dynamics in passive systems reduces the potential for failure. Their straightforward mechanical design means fewer parts are susceptible to wear and tear, resulting in longer lifespans and lower maintenance requirements. This reliability is crucial for public transportation systems where downtime can significantly impact service.

6. **Maintenance and Serviceability**

Maintenance of passive suspension systems is generally straightforward. As highlighted by Thompson et al. (2020), routine inspections and occasional replacement of springs and dampers can typically be performed with standard tools, reducing the need for specialized equipment or training. This ease of maintenance contributes to lower overall operational costs for fleet operators. So, passive suspension systems offer several advantages, including cost-effectiveness, reliability, simplicity, and good ride quality. Their durability and ease of maintenance make them a popular choice in various applications, particularly in public transportation. While they may not provide the advanced performance characteristics of active systems, the benefits they offer make them a viable option for many vehicles, particularly in urban settings where practicality and cost considerations are paramount.

Passive suspensions are known for their cost-effectiveness and reliability. Smith and Johnson (2020) note that their straightforward design leads to lower maintenance needs, making them suitable for budget-constrained transit operators. Research indicates that passive systems effectively mitigate vibrations under normal operating conditions through mechanical damping. These systems primarily rely on the inherent characteristics of springs and dampers to absorb shocks from road irregularities. However, while passive systems provide satisfactory comfort for moderate conditions, their performance can be limited during extreme events, such as potholes or abrupt stops (Zhang & Li, 2020).

5. **Performance under Varying Loads**

Passive suspension systems can handle varying loads effectively. According to research by Wang et al. (2022), the linear characteristics of springs and dampers allow passive systems to manage changes in load conditions without significant adjustments. This capability is particularly important for city buses and trucks that frequently experience fluctuations in passenger numbers and cargo weight.

4. **Good Ride Quality**

While passive suspension systems may not offer the same level of ride comfort as advanced active systems, they can still provide adequate ride quality under various conditions. A study by Kumar and Gupta (2021) emphasizes that well-designed passive systems can effectively dampen vibrations and shocks, offering a comfortable ride for passengers. The use of high-quality dampers and springs can enhance the performance of passive systems, especially in urban environments with frequent stops and uneven road surfaces.

2.2.3 Disadvantages of a passive suspension system

The main source of the passive suspension system's drawbacks is the advancement of technology. The passive suspension system is currently only adequate since the active suspension uses more advanced technology to achieve the same objectives more successfully. Naturally, this does not imply that passive suspensions are in any way undesirable. They are simply no longer at the top of the game.

The primary drawback is their inability to adapt dynamically to varying road conditions, which can lead to inadequate vibration control in certain scenarios (Kumar & Gupta, 2021).

2.3 Active suspension system

Active suspension systems use sensors and actuators to continuously monitor and adjust the suspension settings in real-time. These systems can change the damping characteristics based on road conditions and vehicle dynamics. Ultimate Suspension is another name for active suspensions. The vehicle body's vertical and horizontal movement in relation to the wheel and chassis is managed by an on-board system. Depending on the state of the road, active suspension raises or lowers each wheel's frame using pneumatic or hydraulic actuators. Actuator operations serve as the foundation for fully active suspension systems. The skyhook theory serves as the foundation for active suspension. According to the skyhook theory, a perfect suspension system would allow a car to maintain a stable posture independent of the state of the road, much like an imaginary hook in the sky. Although it is not feasible in practice, the suspension system can be designed using the skyhook theory (Kunanoppadol & Pathom, 2015; Seifi et al., 2016).

Studies, such as those by Wu et al. (2019), demonstrate that active systems significantly enhance vibration control by responding immediately to changes in road surface and vehicle behavior. This responsiveness allows for optimal load distribution and improved handling, effectively minimizing vibrations transmitted to passengers.

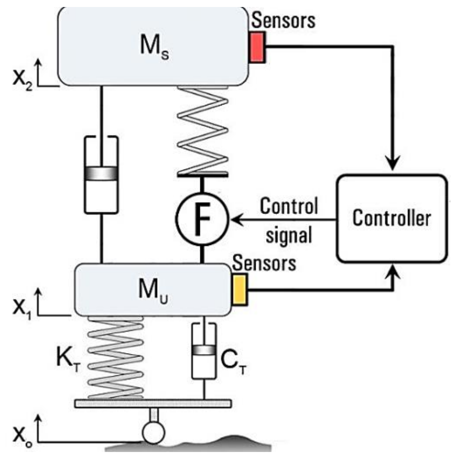

Figure 2-4 Active Suspension System (dos Santos Accioly Lins et al., 2021)

2.3.1 Disadvantages of an active suspension system

The cost is by far the biggest drawback of an active suspension system. When compared to their passive equivalents, active suspension systems are more expensive. Really, they just started with more expensive luxury cars due to the expense. The complexity of active suspension is another drawback, which is a problem if something goes wrong. In comparison to passive suspension repair, active suspension repair is more expensive.

However, active systems are generally more complex and expensive to implement and maintain, as noted by Thompson et al. (2020). Their reliance on electronic components may lead to higher service costs.

2.3.2 Advantages of an active suspension system

For contemporary cars, active suspension offers many advantages. Compared to passive suspensions, they yield superior results overall because of their high level of technological advancement. The car's passengers will have a smoother ride and the driver will have improved handling thanks to an active suspension.

Active suspensions provide superior ride quality, reducing body roll and maintaining consistent tire contact with the road, which is crucial for urban buses navigating uneven surfaces (Karam et al., 2021). Their advanced control strategies also enhance safety by improving vehicle stability.

2.4 Semi-active suspension system

One kind of automotive suspension system called semi-active suspension regulates the shock absorber's damping force in response to input from the continuously changing road surfaces. Its goal is to roughly carry out the active suspension. Numerous control strategies can be used to implement semi-active suspension. Skyhook control is a well-known example of typical technology.

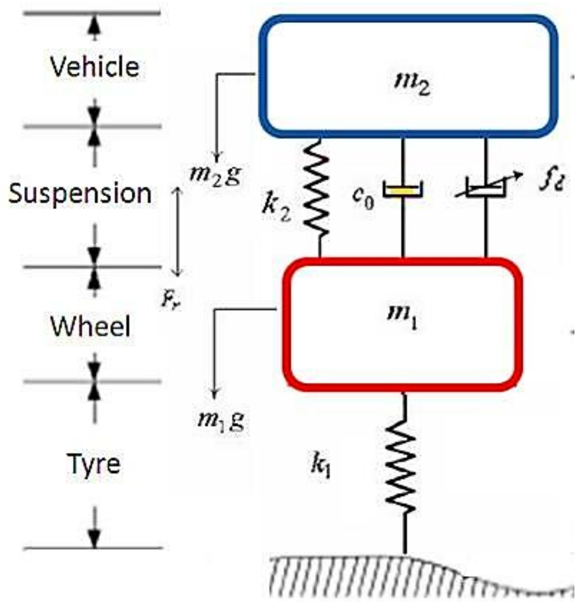

Figure 2-5 Semi-Active Suspension System

(Zhao et al. (2019), (Jiregna & Sirata, 2020) caution that, while semi-active systems are beneficial, they may not achieve the same level of vibration control as fully active systems under extreme conditions. Almeida et al. (2021) note that semi-active systems are a more cost-effective option than fully active systems, providing better performance than passive systems and enhancing passenger comfort with their adaptability to varying conditions, all without excessive complexity. Research by Wang et al. (2022) further supports the effectiveness of semi-active suspensions, highlighting their ability to improve stability and comfort across different loads and road conditions. Kim and Lee (2023) emphasize that semi-active systems strike a balance between ride comfort and handling by adjusting damping levels without complex actuators, reducing vibrations and avoiding the limitations associated with fully passive systems. The choice of suspension system—whether passive, semi-active, or active—significantly affects vibration control, ride quality, and operational efficiency. Passive systems are valued for their reliability and low cost, though they may lack adaptability to severe road conditions, while active systems offer superior control but involve higher costs and complexity. Semi-active systems serve as a middle ground, enhancing performance while maintaining simpler designs. Understanding these options is crucial for optimizing bus design and improving urban transportation services.

2.4.1 Quarter model car suspension

Within lumped-mass vehicle models, the quarter car model is the most basic representation of a vehicle. Analyses of vehicles and suspension, especially those pertaining to ride dynamics, employ it. The model is made up of two mass bodies a quarter vehicle and a wheel as well as lumped parameters for damping and stiffness in the suspension and tires (Desai et al., 2021).

One of a car's most important components is the suspension system. A properly designed suspension system ought to safeguard the car's occupants from harm and shield it from the effects of uneven roads. Fatigue damage is known to be significantly influenced by dynamic loads in vehicles as a result of irregularities in the road. Furthermore, vibrations from the ground may lessen the driver's ability to control the car and make them uncomfortable. In order to increase reliability and ride comfort at the same time, a vehicle's suspension system must reduce vertical vibrations (Desai et al., 2021). The integrated vehicle seat and suspension model with the driver's body is thus depicted in the next figure.

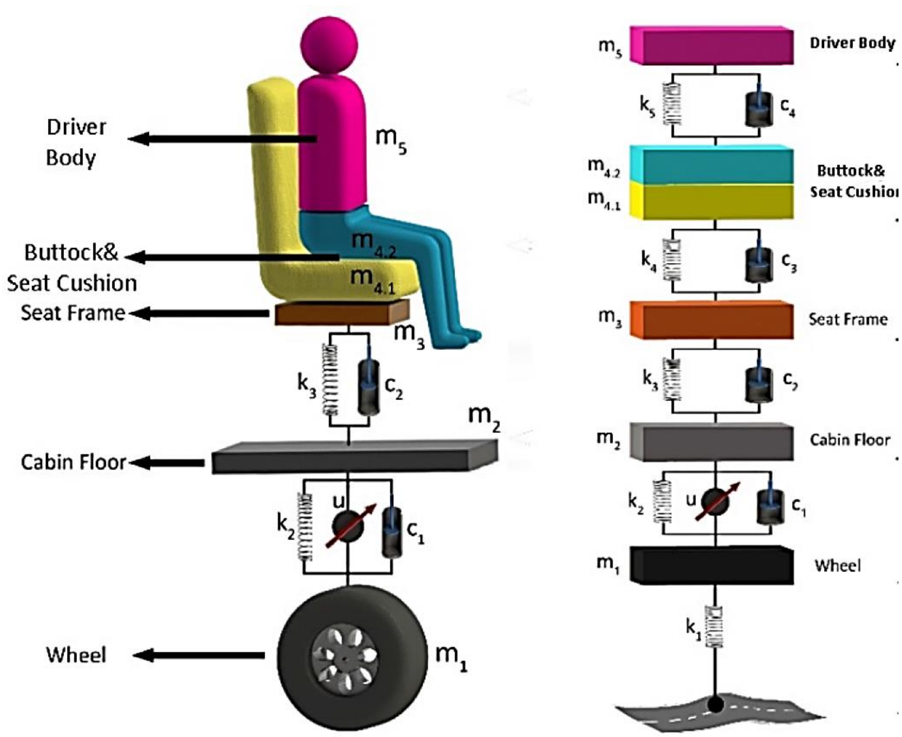

Figure 2-6 Integrated vehicle seat and suspension model with driver body (Yazici, 2016)Half model car suspension

2.4.2 Half model car suspension

Half of the car is taken into account in a half-car suspension model. Generally speaking, a "half-car model" refers to the left and right halves of the car and their pitch and bounce dynamics, though occasionally it takes into account the front or rear of the car (and their related roll dynamics). It should be noted that we also make the assumption that the suspension stays vertical, independent of the chassis pitch angle; this is related to the small angle approximation. These assumptions are reasonable approximations for small angular displacements (Desai et al., 2021).

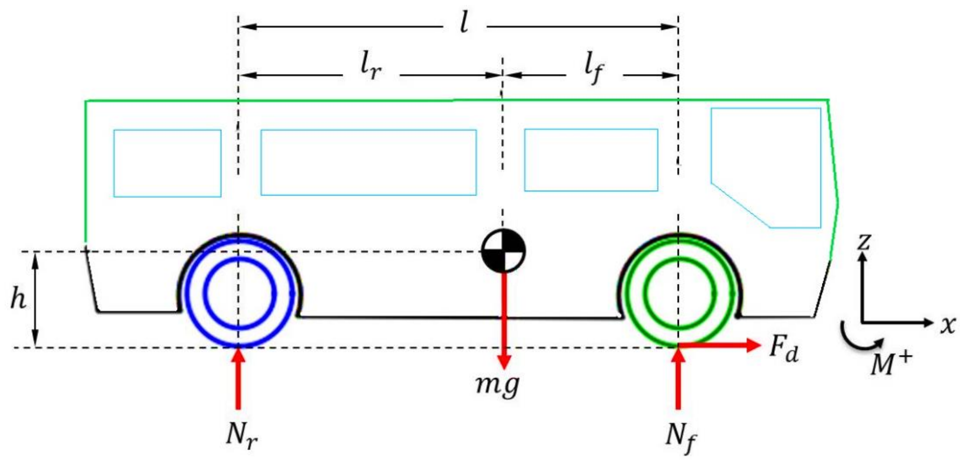

Figure 2-7 Free body diagram of half model of car

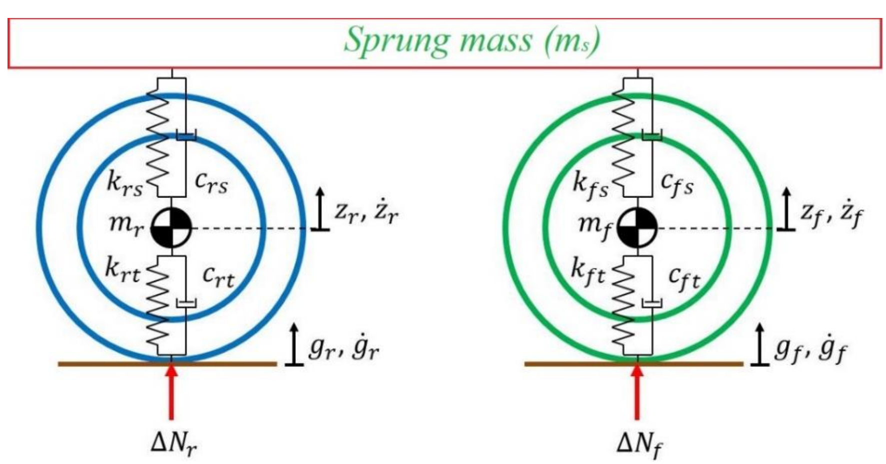

Figure 2-8 Free body diagram of half model of car with vibration elements

2.4.3 Half car VibrationMathematical model

$$\ddot{q} = [K]q + [C]\dot{q} + [K_g]g + [C_g]\dot{g} + n \quad (1)$$

$$[K]q = \begin{bmatrix} \frac{(K_{fs}+K_{rs})}{m_c} & \frac{l_r l_{rs} - l_f l_{fs}}{m_c} & \frac{k_{fs}}{m_c} & \frac{k_r}{m_c} \\ \frac{l_r k_{rs} - l_f k_{fs}}{I_{yy}} & \frac{-(l_f^2 k_{fs} + l_r^2 k_{rs})}{I_{yy}} & \frac{-l_f k_{fs}}{I_{yy}} & \frac{-l_r k_{rs}}{I_{yy}} \\ \frac{k_{fs}}{m_f} & \frac{l_f k_{fs}}{m_f} & \frac{-(k_{fs}+k_{ft})}{m_f} & 0 \\ \frac{k_{rS}}{m_r} & \frac{-l_r k_{rs}}{m_r} & 0 & \frac{-(k_{rs}+k_{rt})}{m_r} \end{bmatrix} \begin{Bmatrix} Z_c \\ \phi \\ Z_f \\ Z_r \end{Bmatrix} \quad (2)$$

$$[C]\dot{q} = \begin{bmatrix} \frac{-(C_{fs}+C_{rs})}{m_c} & \frac{l_r C_{rs} - l_f C_{fs}}{m_C} & \frac{C_{fs}}{m_C} & \frac{C_r}{m_C} \\ \frac{l_r C_{rs} - l_f C_{fs}}{I_{yy}} & \frac{-(l_f^2 C_{fs} + l_r^2 C_{rs})}{I_{yy}} & \frac{-l_f C_{fs}}{I_{yy}} & \frac{-l_r C_{rs}}{I_{yy}} \\ \frac{C_{fs}}{m_f} & \frac{l_f C_{fs}}{m_f} & \frac{-(C_{fs}+C_{ft})}{m_f} & 0 \\ \frac{C_{rS}}{m_r} & \frac{-l_r C_{rs}}{m_r} & 0 & \frac{-(C_{rs}+C_{rt})}{m_r} \end{bmatrix} \begin{Bmatrix} \dot{Z}_C \\ \dot{\phi} \\ \dot{Z}_f \\ \dot{Z}_r \end{Bmatrix} \quad (3)$$

$$[K_g]g + [C_g]\dot{g} + n = \begin{bmatrix} 0 & 0 \\ 0 & 0 \\ \frac{k_{ft}}{m_f} & 0 \\ 0 & \frac{k_{rt}}{m_r} \end{bmatrix} \begin{Bmatrix} g_f \\ g_r \end{Bmatrix} + \begin{bmatrix} 0 & 0 \\ 0 & 0 \\ \frac{C_{ft}}{m_f} & 0 \\ 0 & \frac{C_{rt}}{m_r} \end{bmatrix} \begin{Bmatrix} \dot{g}_f \\ \dot{g}_r \end{Bmatrix} + \begin{Bmatrix} 0 \\ 0 \\ \frac{\Delta N_f}{m_f} \\ \frac{\Delta N_r}{m_r} \end{Bmatrix} \quad (4)$$

2.5 Full model car suspension

Heave (vertical displacement), pitch, and roll are among the most complicated motions that are taken into consideration by the full-car model. It has seven degrees of freedom (DOF): pitch, roll, vertical motions of the four unsprang masses (wheels), and vertical motion of the sprung mass. Studying ride comfort, handling, and stability requires the full-car model. Real-world automobiles behave more like this model.

I. Sprung mass vertical acceleration

$$\ddot{x} = \left(\frac{c_f}{m}\right)\left(-(\dot{x}-x_1+b_1\dot{\emptyset}-a_1\dot{\theta})-(\dot{x}-\dot{x_2}-b_2\dot{\emptyset}-a_1\dot{\theta})\right)+\left(\frac{c_r}{m}\right)\left(-(\dot{x}-\dot{x_3}-b_1\dot{\emptyset}-a_2\dot{\theta})-(\dot{x}-\dot{x_4}+b_2\dot{\emptyset}+a_2\dot{\theta})\right)+\left(\frac{k_f}{m}\right)\left(-(x-x_1+b_1\emptyset-a_1\theta)-(x-x_2-b_2\emptyset-a_1\theta)\right)+\left(\frac{k_r}{m}\right)\left(-(x-x_3-b_1\emptyset+a_2\theta)-(x-x_4+b_2\emptyset+a_2\theta)\right) \quad (5)$$

where, cf,cr front and rear dumping constant respectively

k_f,kr front and rear spring stiffness constant respectively

a_1,a_2, distance from centre of gravity to front axle and rear axle respectively

b_1,b_2 distanse from center of gravity to right hand side and left hand side of base length respectively

II. Roll angular acceleration

$$\ddot{\emptyset}=\left(\frac{c_f}{I_x}\right)\left(-b_1\left(\dot{x}-\dot{x_1}+b_1\dot{\emptyset}-a_1\dot{\theta}\right)+b_2\left(\dot{x}-\dot{x_2}-b_2\dot{\emptyset}-a_1\dot{\theta}\right)\right)+\left(\frac{c_r}{I_x}\right)\left(b_1\left(\dot{x}-\dot{x_3}-b_1\dot{\emptyset}-a_2\dot{\theta}\right)-b_2\left(\dot{x}-\dot{x_4}+b_2\dot{\emptyset}+a_2*\dot{\theta}\right)\right)+\left(\frac{k_f}{I_x}\right)\left(-b_1(x-x_1+b_1\emptyset-a_1\theta)+b_2(x-x_2-b_2\emptyset-a_1\theta)\right)+\left(\frac{k_r}{I_x}\right)\left(b_1(x-x_3-b_1\emptyset+a_2\theta)-b_2(x-x_4+b_2\emptyset+a_2\theta)\right)-\left(\frac{k_R}{I_x}\right)\left(\emptyset-\frac{x_1-x_2}{w}\right) \quad (6)$$

where, Ix rolling moment inertia of sprung mass

k_R sway bar stiffness constant

w track length

III. Pitch angular acceleration

$$\ddot{\theta}=\left(\frac{c_f}{I_y}\right)\left(a_1\left(\dot{x}-\dot{x_1}+b_1\dot{\emptyset}+a_1\dot{\theta}\right)-a_1\left(\dot{x}-\dot{x_2}-b_2\dot{\emptyset}-a_1\dot{\theta}\right)\right)+\left(\frac{c_r}{I_y}\right)\left(-a_2\left(\dot{x}-\dot{x_3}-b_1\dot{\emptyset}-a_2\dot{\theta}\right)-a_2\left(\dot{x}-\dot{x_4}+b_2\dot{\emptyset}+a_2\dot{\theta}\right)\right)+\left(\frac{k_f}{I_y}\right)\left(a_1(x-x_1+b_1\emptyset-a_1\theta)+a_1(x-x_2-b_2\emptyset-a_1\theta)\right)+\left(\frac{k_r}{I_y}\right)\left(-a_2(x-x_3-b_1\emptyset+a_2\theta)-a_2(x-x_4+b_2\emptyset+a_2\theta)\right) \quad (7)$$

where, Iy pitching moment inertia of sprung mass

IV. Front Suspension right side unsprang mass vertical acceleration

$$\ddot{x_1}=\left(\frac{c_f}{m_f}\right)\left(\left(\dot{x}-\dot{x_1}+b_1\dot{\emptyset}-a_1\dot{\theta}\right)+\left(\frac{k_f}{m_f}\right)\left((x-x_1+b_1\emptyset-a_1\theta)\right)+\left(\frac{k_R}{m_f w}\right)\left(\emptyset-\frac{x_1-x_2}{w}\right)-k_{tf}(x_1-y_1)\right. \quad (8)$$

where, mf , ktf frontal suspension unsprang mass and front tire stiffness constant respectively

V. Front Suspension left side unsprang mass vertical acceleration

$$\ddot{x_2}=\left(\frac{c_f}{m_f}\right)\left(\left(\dot{x}-\dot{x_2}+b_2\dot{\emptyset}-a_1\dot{\theta}\right)+\left(\frac{k_f}{m_f}\right)\left((x-x_2+b_2\emptyset-a_1\theta)\right)+\left(\frac{k_R}{m_f w}\right)\left(\emptyset-\frac{x_1-x_2}{w}\right)-k_{tf}(x_2-y_2)\right. \quad (9)$$

Rear Suspension right side unsprang mass vertical acceleration

$$\ddot{x}_3=\left(\frac{c_r}{m_r}\right)((\dot{x}-\dot{x}_3+b_1\dot{\emptyset}+a_2\dot{\theta})+\left(\frac{k_r}{m_r}\right)((x-x_3+b_1\emptyset+a_2\theta)-k_{tr}(x_3-y_3) \quad (10)$$

where, mr ktr rear suspension unsprang mass and rear tire stiffness constant respectively

Rear Suspension left side unsprang mass vertical acceleration

$$\ddot{x}_4=\left(\frac{c_r}{m_r}\right)((\dot{x}-\dot{x}_4+b_2\dot{\emptyset}+a_2\dot{\theta})+\left(\frac{k_r}{m_r}\right)((x-x_4+b_2\emptyset+a_2\theta)-k_{tr}(x_4-y_4) \quad (11$$

(Campbell, 2009) Using accelerometer data, he examined vibration measurements on heavy-duty diesel cars traveling on the US-27 and I-75. Similar vibrations were observed on both roads, although there were notable variations between the manufacturers. Using the data gathered, two basic models were created; the accuracy of the models was increased by applying transducers to the body of interest. Nevertheless, because the tested trucks lacked mechanical characteristics, the model could not be confirmed.

(Uzun, 2010) studied the analysis of vibration effect in cars and driving quality. On-going studies are focusing on the quantification and identification of vibration sources. Vibration influence is a considerable effective factor in almost all industrial fields as well as in car driving as it is a concern related to ride comfort. Automotive industries are developing constantly and one of the important problems in this field is suspension and related vibration issues. Drivers and passengers in vehicles are directly affected by vibrations. In regard to this problem, vibration control is improving continuously in the automotive industry worldwide, including Turkey. Vibration occurs in two ways: structural vibrations and engine vibrations in cars. Vibration levels of a passenger car have been measured and simulated in his study by means of experimental method and developed program respectively.

(Senthil Kumar et al., 2013) Vibration Analysis and Improvement of a Vehicle Chassis Structure. The study is focused on analysing the existing chassis design and the noise, vibration, and harshness (NVH) characteristics. Modelling of chassis structure is carried out using 3D modelling package CATIA V5 and finite element model is created by meshing using Hyper mesh software. The main objective is to find the natural frequency and analyse the mode shape of the automotive chassis structure. Results of the analysis help to study the dynamic behaviour of the chassis structure with load application/real road condition and to improvise the car chassis structure assembly.

(Agostinacchio et al., 2014) The purpose of the study is to evaluate the dynamic load increases that the vehicle transfers to the road pavement, due to the generation of vibration produced by surface irregularities. The method used starts from the generation, according to the ISO 8608 Standard, of different road roughness profiles characterized by different damage levels. In particular, the first four classes provided by ISO 8608 were considered. Subsequently, the force exchanged between the pavement and three typologies of vehicles (car, bus, and truck) has been assessed by implementing, in Matlab, the QCM (Quarter Car Model) characterized by a quarter vehicle mass and variable speed from 20 to 100 km/h. The analysis allows determining the amount of dynamic overload that causes the vibrational stress. Results/Conclusions the paper shows how this dynamic overload may be predetermined as a function of the pavements surface degradation. This is a useful reference for the purposes of designing and maintaining road pavements.

(Kousikan & Sundaraj, 2014) Field measurements and a random vibration model were used to simulate the bus model. Acceleration PSD and frequency-weighted root mean square acceleration were used to validate the model. When the simulation results were utilized to assess how passengers felt about the journey, it became clear that both drivers and passengers would greatly benefit from the suggested new leaf spring design.

(Zhao et al., 2016) proposed the Boa web server, which displays the vibration comfort on the LCD installed in the bus and may switch on a warning bulb when the vibration reaches a certain threshold. The server estimated the vibration comfort degree of the bus using the vibration signals that passengers' smartphones captured and transmitted over WiFi. A practical running environment was used to evaluate the suggested model, and offline data was gathered and analysed during the entire voyage. As demonstrated by the result, such modes have been shown to be effective and the comfort level of vibration acquired from the testing system matched reality.

(Jugulkar et al., 2016) Simulink has been used to evaluate the prototype of a variable stiffness shock absorber that includes a variable fluid damper and two helical springs. When the prototype's performance was compared to the traditional passive approach, it showed a 15% increase in peak acceleration without noticeably degrading road-holding abilities. Further discussion was held regarding the system's design, which included sensors and actuators and showed how changeable stiffness may enhance the performance of a vehicle's suspension.

(Z. Liu et al., 2017) conducted the research on Full Vehicle Vibration and Noise Analysis Based on Substructure Power Flow. Based on a simple vehicle model, characteristics of vibration, noise, and power flow are studied. The comparison with the result of conventional FEM (finite element method), the new method is confirmed to be feasible. When it comes to a vehicle with the problem of low-frequency noise, finite element models of substructures for vehicle body and chassis are established. The substructure power flow method is also employed to examine the transfer characteristics of multidimensional vibration energy for the whole vehicle system. By virtue of the adjustment stiffness of drive shaft support and bushes at rear suspension lower arm, the vehicle interior noise is decreased by about 3dB when the engine speed is near 1050 rpm and 1650 rpm in experiment. At the same time, this method can increase the computation efficiency by 78%, 38%, and 98% when it comes to the optimization of chassis structure, body structure, and vibration isolation components, respectively.

(Musbah, 2017) Based on ISO 2631 (1997), the performance assessment of a hybrid MR damper on a quarter bus semi-active seat suspension was carried out. To improve damping force and obtain fail-soft capability in the event of an electrical failure, the damper was designed. When the design was contrasted with traditional MR dampers, the driver seat comfort was enhanced with the skyhook controller. Based on the simulated findings, the hybrid MR damper reduced driver discomfort to a minimum.

(Y. Liu et al., 2018) One of the main reasons why GIS technology fails is mechanical vibration. This work uses a vibration acceleration sensor to construct a vibration signal detection device and explores the mechanics of vibration. The GIS shell is tested on a laboratory test platform to identify both loose and normal faults. Spectrum analysis and judgment basis are used to obtain the vibration signal properties. According to the findings, vibration signals with an amplitude that is nearly equal to 100 Hz can be found in the GIS shell close to the insulator. An excessive vibration signal amplitude in the connector suggests a loose contact.

(Mrad et al., 2018) developed a methodology for vibration analysis in vehicles, proposing new suspension system setups to enhance passenger comfort. The study analysed the impact of these modifications on vibration levels, emphasizing dynamic behaviour in vehicle design. The study tested various rubber mountings, springs, and shock absorbers, identifying the best combination.

(Long et al., 2018) proposed a three-dimensional vibration model of bus with 10 DOF (degree of freedom) based on Dragan Sekulić model to analyse the suspension parameters directly influencing ride comfort. The suspension parameters, which include the stiffness and damping parameters, are analysed based on the weighted R.M.S. (root-mean-square) acceleration responses of the space of a driver, passenger in the middle part of the bus, and passenger in the rear overhang according to ISO 2631-1:1997. The results show that both stiffness and damping parameters of vehicle suspension have important influences on ride comfort. Especially, the stiffness and damping values of vehicle suspension are within the value ranges (0.5ko ≤ k ≤ 0.75 ko) and (0.5co ≤ c ≤ 0.75co) to improve the ride comfort of driver and passengers.

(Roslan & Priyandoko, 2019) his purpose of the study is to examine vibration at a Proton Wira's seat under various loads, speeds, and road conditions. Using accelerometer sensors, vibration data from tar, yellow line, and dirt roads were gathered. There was more vibration on the uneven terrain, especially on the dirt road. According to transmissibility results, load three reached its maximum value of 1.54 at 80 km/h, whereas load two attained its lowest value of 1.06 at 30 km/h. All speed profiles had a pleasant index; however, the tar road and yellow line road profiles had a slightly uncomfortable index.

(Vosoughi et al., 2019) This study used ISO 2631-1 measures to examine the relationship between whole-body vibrations and musculoskeletal diseases in intercity minibus drivers. The models' respective accelerations were found to differ significantly, with the 2011 model exhibiting the lowest acceleration (0.88 m/s^2) and the 2009 model exhibiting the highest acceleration (0.96 m/s^2). Furthermore, a strong relationship was found between daily vibration exposure and pain in several body parts. One significant component that effectively transmits vibration to drivers of minibuses is the production lifespan of the vehicle.

(Acosta, 2019) studied vibratory analysis of a public bus and evaluation of health, comfort, and perception. Transportation systems are generally the most efficient way in which people can commute. Government agencies from different countries have contributed to its expansion for improving citizens' quality of life. However, during regular operation of these transport systems, vibrations caused by their normal operation are transmitted to passengers. These vibrations can have negative effects on health; notwithstanding, some transport systems do not have vibration control for passengers. This research project aims to analyse how those vibrations in a public bus are distributed, and what is the effect on human health in accordance with ISO 2631-1.

(Gowtham et al., 2020) Whole-body vibration is a common occurrence for professional drivers, especially bus drivers, and can cause medical issues, including lower back pain. According to Scopus databases, mechanical vibration is a common workplace exposure for bus drivers, which may exacerbate lumbar spine pain. According to this comprehensive review, prolonged vibration exposure may increase the likelihood of developing these problems.

(Ma et al., 2020) To investigate the mapping relationship between vibration characteristics and deterioration characteristics of tracked vehicle components, a vibration test system is designed. A logarithmic linear regression model is used to examine test points and determine the relationship between vibration levels and vehicle speed. This study contributes to the evaluation of vehicle health and failure alerts, as well as the improvement of test point configurations.

(Road et al., 2020) Bus vibrations are a serious problem, especially when the roads are uneven. These vibrations were simulated using a 13-degree-of-freedom model. According to the model, properly installed mass-spring-damper passive absorbers decreased the amplitudes of vertical displacements in frequency responses, especially in the vicinity of resonant frequencies. The detrimental effects of vibrations caused by uneven roads are successfully reduced by this creative remedy.

(Edition, n.d., 2020) This study uses cognitive tests to look at how whole body vibration (WBV) affects bus fare collectors. 24 volunteers used a vibrating platform that was vertically vibrated at frequencies of 5 Hz and 30 Hz as part of the study. The findings indicated that while the frequency of 30 Hz improved cognition with longer exposure times, the frequency of 5 Hz decreased performance. In comparison to male participants, female volunteers demonstrated superior performance, and for brief exposure intervals, the residual impact lasted for less than ten minutes. Muscle comfort and easier concentration were linked to the 30-Hz frequency.

(Cheng et al., 2021) aims to investigate the correlation of the soft road excitation of different long-wave surfaces with the vehicle vibration response. Vibration equation between the vehicle and soft road surface system is established to produce an effective roughness model of the field soft road surface. In order to simulate the vehicle vibration state under different long-wave road surfaces, the soil rectangular pits with 21 kinds of different spans and depths are applied to the road surfaces, and a tractor vibration test system built for vibration test. Frequency spectrum analysis performed for the vibration response and the roughness signals of the road surfaces. The results showed that Coefficient (R2) of frequency correlation between the roughness excitation and the original unevenness at the excitation point at the rear end of the rectangular soil pit fell within 0.9641∼0.9969. The main frequency band of the vibration response fell within 0∼3 Hz, and the phenomenon of quadruple frequency existed. The correlation of roughness excitation with quadruple frequency fell within 0.992165∼1. The primary excitation points located at the rear end of the rectangular soil pit. In addition, it also indicated that when the vehicle is driven without autonomous power, the vehicle vibration frequency mainly depended on the excitation frequency of the field road surface and the frequency at the maximum vehicle vibration intensity is 2 or 3 times of that at the maximum field soft road excitation. These findings may provide a reference for optimal design of vibration reduction and control for agricultural vehicles.

(Lopes et al., 2021) examined the dynamic behaviour of a multi-body passenger bus articulated by a damping joint when it is in or out of operation. In addition to assessing any harm to the bus structure and passenger safety, the dynamic behaviour of the chassis under load was also assessed. The Finite Element Method (FEM) was used in the numerical analysis to simulate a single-joint articulated urban bus model. Therefore, several computational analyses were performed in order to assess the influence of external loads on the natural frequencies of the structure.

(Festa et al., 2021) studied human response to vehicle vibrations and acoustics during transient road excitations. Driving over rising and falling edges on roads and pavements, rails, manhole covers, or transverse joints can influence the driving impression regarding the driver’s perception of vibrations and acoustics. To be able to describe this, objective parameters are used to make the subjective ride comfort measurable and scalable. Previous studies have already contributed to the investigation of the subjective perception regarding the interaction of vibrations and acoustics. However, the results were individual. Aimed at improving the quality of objective analysis methods, driving manoeuvres were performed in a real vehicle to investigate the interaction of vibrations and acoustics due to transient road excitations. For this purpose, a sound reproduction system was used, which could provide the acoustic environment for the driver to adapt to while driving. With this method, subjective ratings by varying vibrations and acoustics were collected and with reference to objective parameters statistically evaluated. The results showed that both tactile and audible vibrations under transient influences had no significant interactive effects on the driver’s perception.

2.6 Research Gap

Generally, from the literature review or related works, the gaps are drawn and explained as follow.

- The researchers studied only the effects of vibration and comfort factors under partial vehicle body. But they didn't studied about vibration isolation System and vibration distribution with full model of bus. And the modification of vibration reduction system for general passengers didn't considered on seat zone and body mounted with chassis. This show that still there is rigid connection between body and chassis.
- In this thesis, the analysis of vibration distribution on the model of vehicle for the Mercedes-Benz city bus and the vehicle's vibrations were analyzed in three dimensions, and the efficiency of the suspension system was evaluated using Ansys transient multibody dynamics. Computer simulation is performed using Simulink in Mat Lab to verify the numerical transient multibody dynamic results.
- Vibration Frequency Range**:** Limited understanding of how different vibration frequencies affect passenger comfort and health. Research could focus on identifying the most problematic frequencies in various road conditions.

Previous research has primarily focused on partial vehicle models or specific components like the suspension system, without considering a full-body vibration analysis for city buses. This study fills the gap by developing a comprehensive full-body model and evaluating the effectiveness of various anti-vibration configurations using advanced simulation tools.

CHAPTER THREE
MATERIALS AND METHODS

3.1 Introduction

This chapter contains a list of materials used in this study. Various steps of the methodology are also described in this chapter. For materials and methods, the most important heading is to assess the overall quality of study distribution products. It is intended to explain to the reader the procedures, approaches, designs and actions used in the study. Replicate research. A full literature review aided in the appropriate selection of working materials, research methods, and simulation software. In this study, the design was performed using an appropriate selection of working materials.

3.2 Materials

This section will help ensure the reliability of the study. In other words, the materials and methods selected must be appropriate and valid to answer the research question. It also ensures the reproducibility of the method so that other studies can replicate the study. And it guides readers on how research is conducted and organized, telling compelling research stories. Researchers wonder what leadership has to do with writing. You may think. The materials to be used on this research are simply the raw materials, tools. Basically, it is the important details of what in this research. The following table 3.1 is used to describe the materials needed for this type of research.

Table 3-1 : Materials to be used

Characteristics of material	**Materials Name**
Simulation Software Tool's	Ansys Transient multibody Dynamics
Computer	Minimum Processor Unit, 32 RAM

The materials used in this research include Ansys Transient Multi-Body Dynamics software for simulating vibration responses and MATLAB for system validation. Rubber mountings of various stiffness values were selected for the anti-vibration configurations.

3.3 Methodology

This section describes the methodology used to achieve the research objectives. This means that the section review the methods used in the theory or principles behind them to develop an approach that is consistent with our goals. Figure 3.1 below details the article workflow.

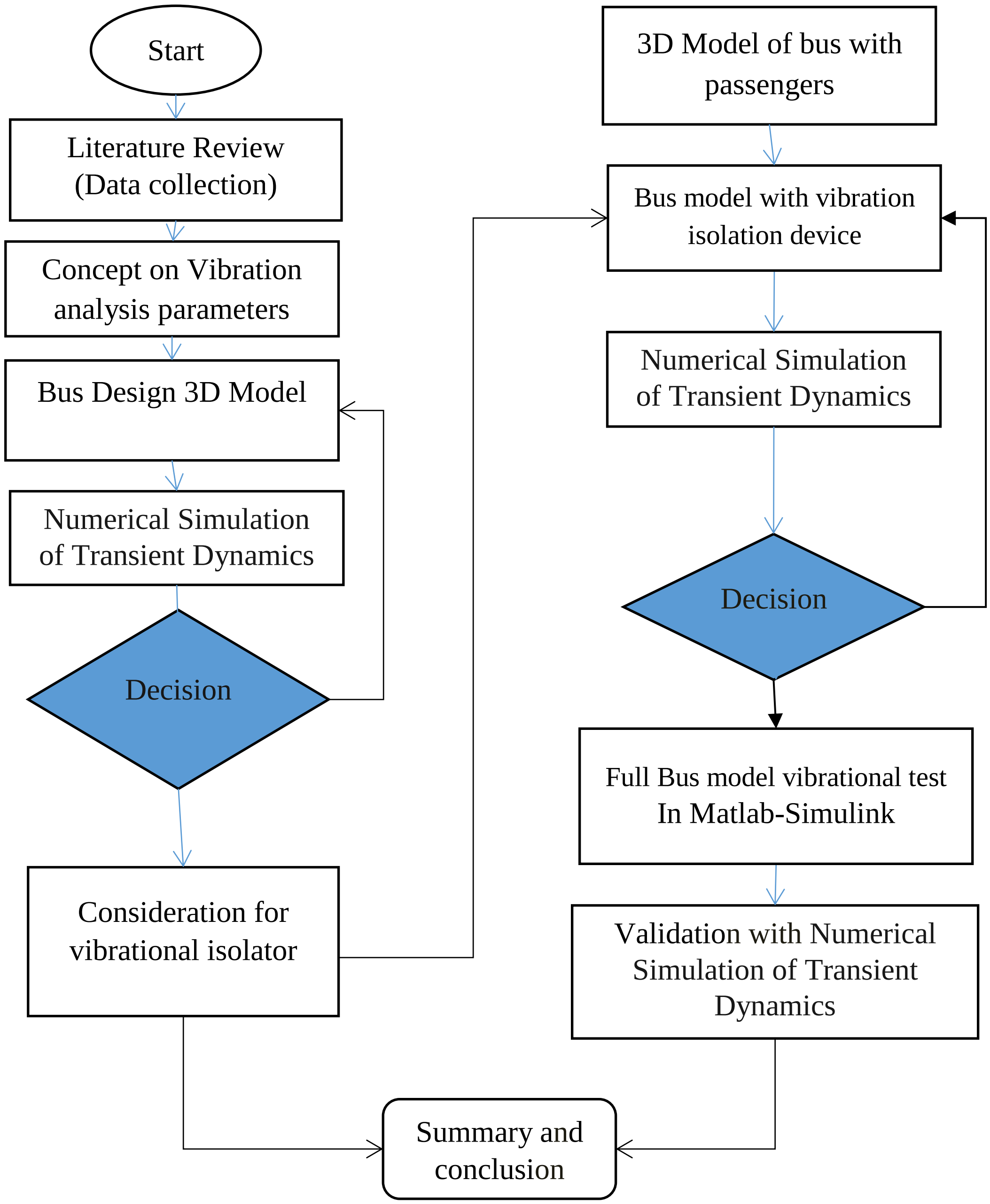

Figure 3-1 Methodology

3.2. Data collection Method

It is recognized that, data is the information collected by a reviewer to inform a literature review. As a result, the literature review process can be considered as a data collection tool that is, a method of gathering a body of material relevant to a certain topic of interest. Therefore, the collected data for the analysis of bus vibration analysis is based on primary and secondary type of data.

3.3.1 Primary Data

Collected primary data for this research work is based on questioning, observing from some target group of local area bus owners and drivers. The following points is the detail information asked as questionnaire on as bus vibration issue specified model Mercedes Benz city bus.

Figure 3-2 Mercedes Benz city bus picture captured at Addis A**b**a**b**a

Primary data collection was conducted to obtain first-hand information on the perceived vibration issues and their impact on passenger comfort. This data, combined with secondary sources, provides a comprehensive view of the problem.

3.3.1.1 Questionnaire

1. Are High vibration amplitudes (depending on road types)?
2. Is increase in travel time due to traffic congestion affects comfort?
3. How vibrations are created (generated) in a public bus?
4. What types of vibrations are transmitted to passengers through seats and floor?
5. What model of bus is this?
6. Do you have Bus technical specification and structure?
7. Year, weight, for how many time it work per day, types of passenger seats, how many nu mbers of seat it has?
8. Numbers of doors, has it vibration isolations, at where? And due to what high vibration is created in it?
9. Can you estimate the average mass of passengers in Ethiopia?
10. What is the total mass on your bus?

3.3.1.2 Response to Questionnaire

The type of road obviously has an impact on the bus's vibrational characteristics.It follows that la rge dynamic loads transmitted by high vibration amplitudes could damage the bus's structure as well as the people within.High vibration amplitudes, contingent on road kinds, are observed in nu merous cases of automobile vibration and comfort quality of bus vibration in the overall case stu dy.Though not traffic congestion, comfort can be impacted by persistently unpredictable amplitu de increases in journey time.There is a rise in contact energy when the road excitation meets the s peed of the automobile.This is the process by which a public bus generates vibrations.The bus bo dy and passenger compartment might absorb and dissipate this energy.According to the interviewer, the Mercedes-Benz City Bus has two doors. It also features vibration isolations at the corner edges, which reduce shock during the forced opening and closing of the door. On the other hand, these vibrations are frequently caused by road stimulation or dynamic operations. The bus has a total mass of about 8000 kg. Age, gender, and luggage are some of the variables that affect the average mass of travelers in Ethiopia. Nonetheless, a recent poll indicates that the average weight of all passengers is roughly 76.3 kg. The average passenger weight for people traveling with carry-on luggage is approximately 84.0 kg. On the other hand, these vibrations are frequently caused by road stimulation or dynamic operations. The bus has a total mass of about 16000 kg. Age, gender, and luggage are some of the variables that affect the average mass of travelers in Ethiopia. Nonetheless, a recent poll indicates that the average weight of all passengers is roughly 76.3 kg. The average passenger weight for people traveling with carry-on luggage is approximately 84.0 kg.

3.3.1.3 Technical specifications of the Mercedes-Benz O305Bus

The effect of the vibration on the human body may get worse depending on the frequency and the amount of time in which people have been exposed to the aforementioned vibrations (Conç et al., 2018).

Mercedes-Benz produced the O305, a single deck, at its Mannheim, West Germany, facility. It was constructed as a bus chassis or as an entire bus. The German VöV-Standard-Bus design, which was manufactured by multiple bus manufacturers, included the O305. The bus came in many versions and had an underfloor engine located in the back. The following are some important details of the double-decker O305. The following table shows the detail of data obtained from primary as well as secondary.

Table 3-2. Detail Technical specifications of the Mercedes-Benz O305 Bus.

Mechanical part	Description
Transmission	6-speed manual
Engine	2800 CC. inline-6 cylinder turbo-diesel
Suspension	Semi-elliptical Hotchkiss leaf
Number of wheels	6
Power	128 H.P. @ 2800 r.p.m.
Engine location	Longitudinal. Rear of the bus
Gross weight	12220kg + 45 Seating =16,000 kg
1st Axle Mass unladed	2950 kg
2nd Axle Mass unladed	5950 kg
1st Axle Mass laden	6000kg
2nd Axle: laden	10000kg
Length	10,750mm
Width	2,500 mm
Height:	4,478 mm (unladen)

3.3.2 Secondary Data

Secondary data was collected from academic journals, technical reports, and manufacturer documentation. These sources provided baseline information on the bus's suspension system and previous research on vibration reduction.

3.3.2.1 Theoretical Back Ground of Vibration

Spindling machinery and moving structures display the physical phenomenon known as vibration, regardless of their health. Vibration can be caused by a wide range of elements, including angular rotations, combustion events, rolling bearing components, rotating electric fields, rotating shafts, and meshing gear teeth. Because vibration is so widely used, it is very helpful in assessing the status and operating state of rotating machinery and structures. Vibrations can be explained in a number of ways, such as by acceleration, velocity, and displacement. While displacement and velocity describe how far the measuring point has travelled, respectively, acceleration is self-explanatory. While all three categories are often utilized, acceleration is the most widely used category for dynamic fault diagnostics because to its wider frequency range.

3.3.2.2 Modal Analysis

The mathematical models known as Finite Element Analysis (FEA) models may be used to forecast the mode shapes and natural frequencies of a structure, also known as the modal parameters. The application of boundary conditions establishes the loads exerted, as well as how the structure is supported or fastened to the ground. After the model has been established, the mode shapes and natural frequencies are estimated using a mathematical technique. Before a building is ever completed, this information aids the design of the structure and in understanding vibration characteristics. Between 2 and 2.5 Hz is the natural frequency in performance cars, where managing the vehicle comes above comfort during the journey (Sharma et al., 2020). The primary source of external stimulation for a bus operating on a roadway is uneven pavement. The highest frequency of road excitation, according to pertinent data, is between 2 and 5 Hz. Another significant external source of excitation is engine excitation. The engine typically runs at 600–800 r/min when it is idle, and the vibration frequency is typically 30–40 Hz.

3.3.2.3 Frequency Response of Vibrating Systems

The steady-state solution to the equations of motion when the system is excited harmonically is known as the frequency response. A steady-state response occurs when the starting conditions no longer have an influence and there is a constant amplitude oscillation. Any combination of sinusoidal functions applied to a vibrating system is called a harmonic excitation. A harmonic excitation produces a harmonic response with a frequency-dependent amplitude if the system is linear. The goal of frequency response analysis is to find the oscillation's steady-state amplitude as a function of the excitation frequency. The outcomes of this thesis are solved in the time domain and then transformed into the frequency domain.

3.3.2.4 Amplitude

A vibrating object moves to a certain maximum distance on either side of its stationary position. Amplitude is the distance from the stationary position to the extreme position on either side and is measured in meters (m). The intensity of vibration depends on amplitude. The standard road amplitude considered in this work is 0.1m. The following figure 3. 3 shows the half wave representation of sinusoidal road speed breaker used as signal input for both transient and mat lab simulation on this research.

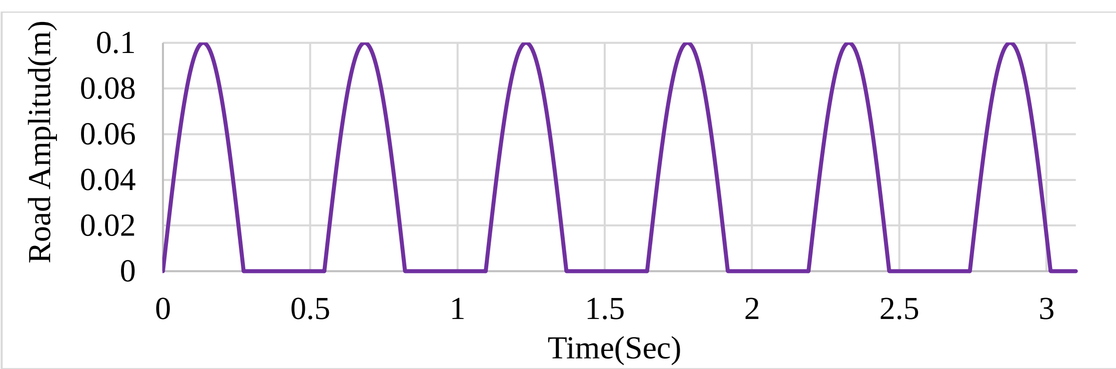

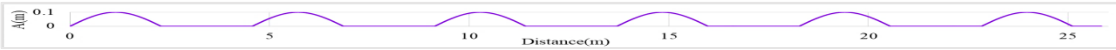

Figure 3-3 half wave representation of sinusoidal road speed breaker (Mohanty et al., 2021)

3.3.2.5 Acceleration (measure of vibration intensity)

Every vibration cycle causes an object to vibrate at a different speed—from zero to maximum. As it goes from its naturally motionless position to an extreme position, it moves at its fastest speed. As it gets closer to the extreme, the vibrating object slows down, stops, and then proceeds through the stationary position in the opposite way toward the other extreme. Meters per second (m/s) is the unit of measurement for vibration speed. The speed at which a change in speed occurs over time is called acceleration. Units of measurement for acceleration are meters per second (m/s^2) or meters per second squared (m/s^2).

3.3.2.6 Resonance

Everything has an inclination to vibrate at a certain frequency, which is called the natural frequency. The composition, size, structure, weight, and form of an object all affect its natural frequency. When a force vibrates at a frequency that matches the intrinsic frequency of an object, resonance happens. The most energy is transmitted to the target object by a vibrating machine when it vibrates at the resonance frequency of the object.

3.4 Concept of rubber based mounting system

3.4.1 Body rubber mounting with chassis (BRC)

Mercedes-Benz buses usually have a separate chassis from the body. Typically constructed of steel, the chassis and bus body are assembled separately. The bus body is then built by the body builder onto the chassis. Bus bodies are constructed using a variety of techniques. One notable method for creating bus bodies with a system of joints is the Co-Bolt aluminium extrusion technique (Nordin, 2018),(*HESS LOW ENTRY – REGIONAL PHENOMENAL MOBILITY FOR CITY*, n.d.). But there is drawback on bus body connection with chassis due it transfer dynamic load that can fracture the window glass as well as periodic damaging of whole body. In order to address these issues, it is advised according to this research to put rubber between the bus body and chassis. The problem's fixation depends on factors including energy dissipation and transmissibility load.

Figure 3-4 Co-Bolt and example of separated bus body from chassis

3.4.2 Seat rubber mounting with chassis (SRC)

The floor was simply in contact with the seat frame in the prior installation method for the passenger seat with the floor or chassis. Amplified load is made to the passenger sitting by this direct attaching technique. As a result, this research suggests using rubber between the seat frame bars that come into contact with the floor in order to address these problems. Factors such as quality acceleration, comfort factor, energy dissipation, and transmissibility load that could endanger passengers all play a role in how the problem is fixed.

Figure 3-5 Example of previous seat direct contact with floor face

3.4.3 Engine rubber mounting with chassis (ERC)

Engine mounts, sometimes referred to as motor mounts, are essential for maintaining engine stability and reducing vibrations. They absorb shocks, keep the engine in good alignment, and fasten it to the car's structure (Kamaruddin et al., 2019). Under the cover, there are typically four motor mounts. A few choices is looking for Mercedes-Benz motor mounts the image in figure are examples of theses. Depending on the precise material composition and production method, engine mounting rubbers might have different moduli of elasticity. Engine mount elastomeric materials typically have a modulus of elasticity between approximately 0.01 GPa and 0.1 GPa (10 MPa to 100 MPa) which is about 50Mpa (Diniță et al., 2023). However, the researcher thought about changing the type of engine mounting rubber because there is a better rubber with modulus material than traditional varieties.

(a) (b)

Figure 3-6 Example of previous *e*ngine rubber mount with floor

3.5 Evaluation of performance of a suspension system

When assessing vehicle vibrations, safety, occupant comfort, and suspension characteristics are all taken into account. Vibration affects are evaluated by scientific assessments, and techniques for optimization can improve performance as a whole.The following four aspects should be considered

3.5.1 Vibration Isolation (Transmissibility Ratio)

Evaluated by the response of the sprung mass (output) to the excitation from the ground (input). Usually, the transmissibility ratio (or transfer function) can be used as a basis for assessing the vibration isolation characteristics of a linear suspension system.

$$TR = \frac{F_T}{F_o} = \frac{\sqrt{1 + \left(2\xi \frac{\omega}{\omega_n}\right)^2}}{\sqrt{1 - \left(\frac{\omega}{\omega_n}\right)^2 + \left(2\xi \frac{\omega}{\omega_n}\right)^2}} \tag{12}$$

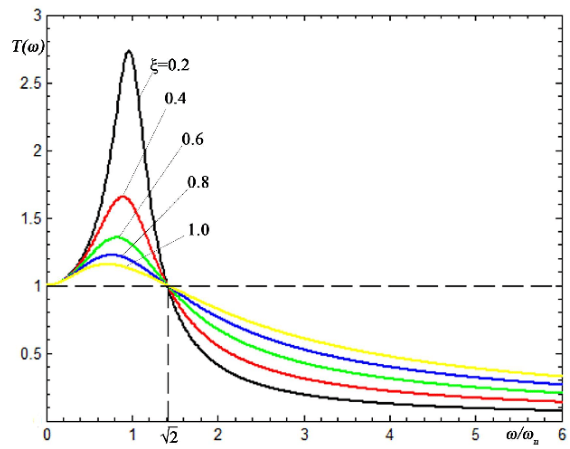

Figure 3-7 Transmissibility curve for different damping ratio(Introduction, 2011)(Zou et al., 2014)

3.5.2 Suspension Travel

Measured by the deflection of the suspension spring or by the relative displacement between the sprung and unsprang mass. It defines the space required to accommodate the suspension spring movement between bump and rebound stops, commonly known as the "rattle space. “

$$Suspension\ Travel = \frac{(X_s - X_u)}{Y} \tag{13}$$

Y is amplitude of sinusoidal road profile(Park et al., 2018)

3.5.3 Road Holding

The typical force acting between the tire and the road fluctuates when the vehicle system vibrates. The dynamic tire deflection or the displacement of the unsprang mass relative to the road surface can both be used to visualize the normal force acting between the tire and the road during vibration (Baronti et al., 2008). The vibration of the tire impacts the road holding ability and has an impact on the handling and performance of the vehicle since the cornering force, tractive effort, and braking effort created by the tire are connected to the normal load on the tire.

Table 3-3 Suspension Constant ad rubber

No.	Parameter Name	Values
1	Spring free length	294mm
2	Spring compressed length	228mm
3	Suspension dumping ratio (ξ)	0.35
4	Rubber damping ratio for chassis (ξ)	0.05
5	Rubber damping ratio for engine (ξ)	0.05

3.5.4 The Weighted RMS acceleration

The RMS value of a signal is its root-mean-square value. Possible to calculate the square root of a digitized signal by squaring each value, then taking the arithmetic mean of those squared values. It roughly corresponds to the average "power" of a signal. Is computed as;

$$a_w = \sqrt{\frac{(w_1^2 a_1^2 + w_2^2 a_2^2 + \cdots w_n^2 a_n^2}{w_1^2 + w_2^2 \ldots w_n^2})} \tag{14}$$

International criterion ISO 2631-1997 agrees that human physique has diverse sensitivity for not the same frequencies of vibration, consequently dissimilar frequencies of vibration ought to be weighted, separately.

Weight for vertical component,

$$w_y(f) = \begin{cases} 0.5, & 0.5 < f < 2 \\ \frac{f}{4}, & 2 < f < 4, \\ 1, & 4 < f < 12.5, \\ \frac{12.5}{f}, & 12.5 < f < 80, \end{cases} \tag{15}$$

Weight for horizontal and lateral component,

$$w_{xy}(f) = \begin{cases} 1, & 0.5 < f \leq 2 \\ \dfrac{1}{f}, & 2 < f \leq 80, \end{cases} \tag{16}$$

Vibration quality criteria

Vibration quality criteria are standards or guidelines that are used to quantify and evaluate the level of vibration in a system or piece of equipment. These guidelines help to ensure the longevity and proper operation of the machine by assisting in assessing whether the vibration levels are within permissible ranges. Although the specific standards may vary depending on the industry and application, they usually consider vibrational properties such as amplitude, frequency, and duration (Conç et al., 2018) ,(Barone et al., 2016).

Table 3-4 Comfort and discomfort passengers' reactions to vibration

a_v m/s^2	**Comfort reactions**
Less than 0,315	not uncomfortable
0,315 to 0,63	a little uncomfortable
0,5 to 1	fairly uncomfortable
0,8 to 1,6	uncomfortable
1,25 to 2.5	very uncomfortable
Greater than 2	extremely uncomfortable

Comfort factor

When designing bus structure that ensure human comfort, the comfort factor in vibration is a crucial parameter to take into account. The factor is represented by the (15).

$$P = 0.74a_w^2 - 6.426a_w + 10.592 \tag{17}$$

3.5.5 Equation of parameters estimation

The act of separating a vibration-producing object, such as a piece of equipment, from its source is known as vibration isolation. Methods have been developed to stop vibration from reaching designed systems and inhabited areas, two domains where vibration is most undesired. Mechanical waves are used to transmit vibrations, and some mechanical links are better at conducting vibrations than others. Materials and mechanical linkages that absorb and dampen these mechanical waves are used in passive vibration isolation. Sensors and actuators that generate disruptive interference to cancel out incoming vibration are used in active vibration isolation. In contrast to "active vibration isolation" or "electronic force cancellation," which uses electric power, sensors, actuators, and control systems,

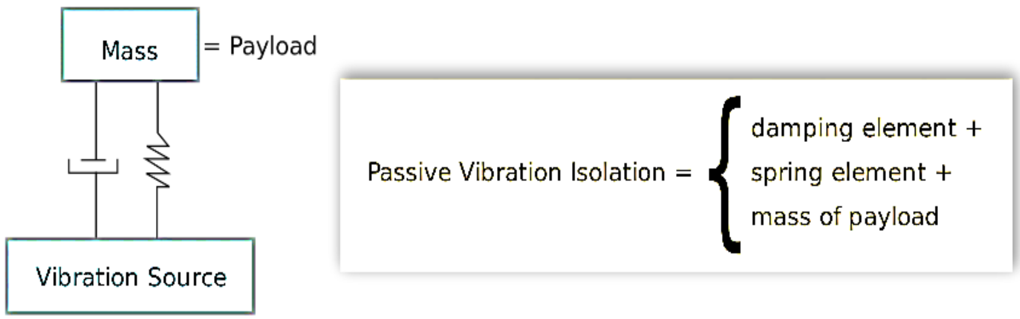

Figure 3-8 Vibration element model for parameters estimation

Equivalent Stiffness of Suspension spring

$$k_{eq} = k_{fr} + k_{fl} + k_{rr} + k_{rl} = 4k \quad (18$$

Equivalent damping coefficient of Suspension

$$C_{eq} = c_{fr} + c_{fl} + c_{rr} + c_{rl} = 4c \quad (19)$$

Equivalent rubber stiffness of body to chassis

$$k_{beq} = k_{bfr} + k_{bfl} + k_{brr} + k_{brl} = 4k_{BC} \quad (20)$$

Equivalent rubber damping of body to chassis

$$C_{beq} = c_{bfr} + c_{bfl} + c_{brr} + c_{brl} = 4c_{BC} \quad (21)$$

Equivalent rubber stiffness of engine to chassis

$$k_{eeq} = k_{efr} + k_{efl} + k_{err} + k_{erl} = 4k_{EC} \quad (22)$$

Equivalent rubber damping of engine to chassis

$$C_{eeq} = c_{efr} + c_{efl} + c_{err} + c_{erl} = 4c_{EC} \quad (23)$$

Equivalent rubber stiffness of seat to chassis

$$k_{seq} = k_{s1} + k_{s2} + k_{s3} \ldots\ldots k_{45} = 45k_{SC} \quad (24$$

Equivalent rubber damping of seat to chassis

$$C_{seq} = c_{s1} + c_{s2} + c_{s3} \ldots\ldots c_{45} = 45c_{SC} \quad (25)$$

Based on the automotive sealing rubber damping ratio 0.04 - 0.084 according to (Kattimani et al., 2017), the equivalent stiffness and damping constants are determined and labeled in the following table 3.6. Spring stiffness and dumping coefficient for suspension, engine rubbers and chassis rubbers can be calculated as follows

$$F = k_c x = mg \tag{26}$$

$$k = \frac{mg}{x} = \frac{EA}{t} \tag{27}$$

$$c = 2\xi\sqrt{mk} = 2\xi\sqrt{\frac{mEA}{t}} \tag{28}$$

Where, t is thickness of rubber, E is young's modulus of rubber

3.6 Bus 3d model

The process of creating three-dimensional models of a surface or object is known as 3D modelling. A mathematical coordinate-based depiction of an item in three dimensions is referred to in this setting as a 3D model. Using Ansys space claim in addition to CATIA V5, the following three-dimensional bus chassis, body, and tire are developed.

A. Real model of front and rear suspension leaf spring

   One kind of suspension system seen in both light and big commercial vehicles is the leaf spring. It gets its name from the way it resembles stacked leaves. These springs, which have been there for millennia, absorb bumps in the road to provide reasonably smooth transportation.

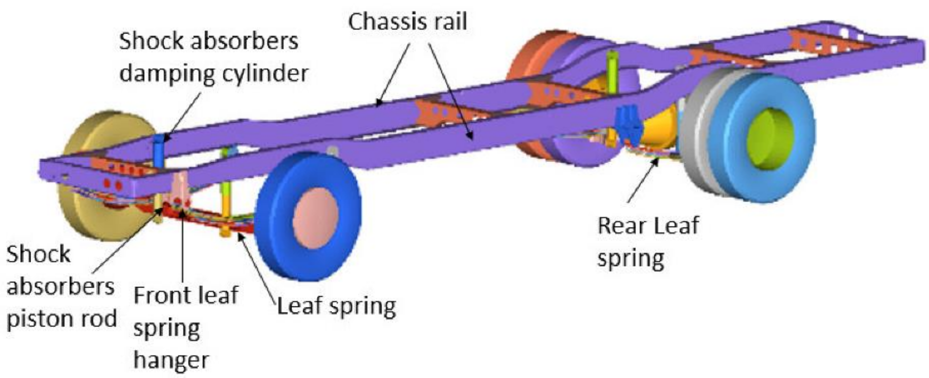

Figure 3-9 Simple bus chassis suspension system assembly

B. Representation of above chassis with assumed state of rigid slab.

The chassis portion is represented by a very basic rig slab model for depiction of the entire chassis, including axle, engine, and passenger seat weights, in order to simplify the complexity of the suspension system.

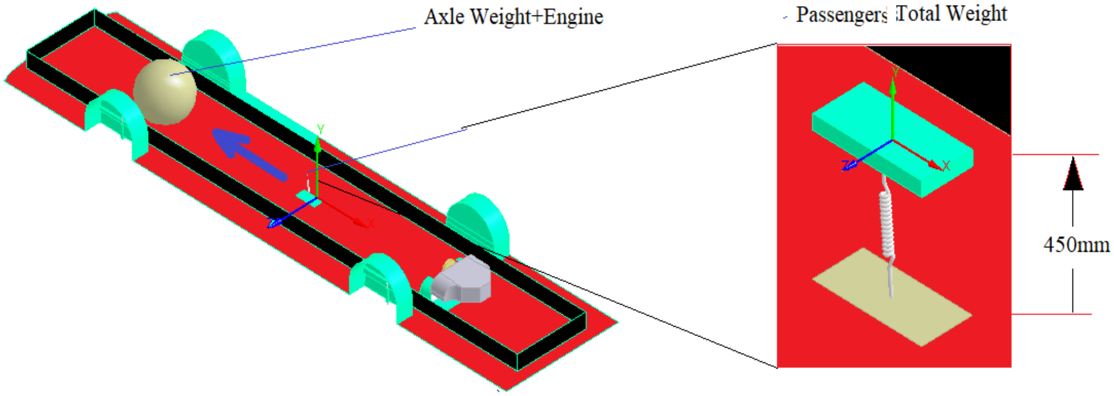

Figure 3-10 Basic rig slab model for depiction of the entire chassis

C. Representation of engine model

Because the engine is an oscillatory body caused by the flywheel's spinning, it operates under a h armonica excitation system in the vibrational analysis of the vehicle. As a result, the occupants an d other body parts of the car may experience vibration energy. The following figure shows the rep resentation detail of engine with oscillatory.

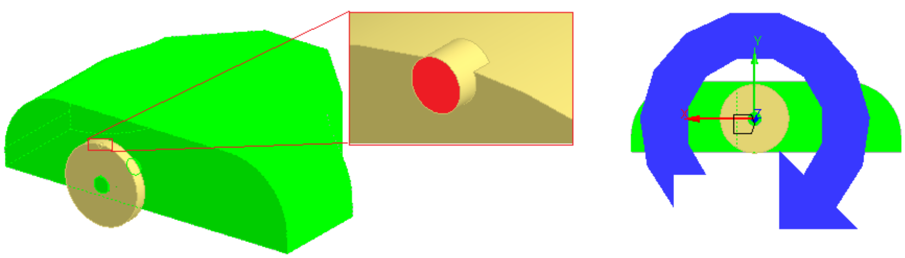

Figure 3-11 Representation of engine model

D. Representation of suspension spring and shock absorber

To resolve the leaf spring assembly with a shock absorber. The next ring, which rotates with the tire but translates with the spring and suspension damper, has been taken into consideration. The suspension model has rings built into each of its four corners.

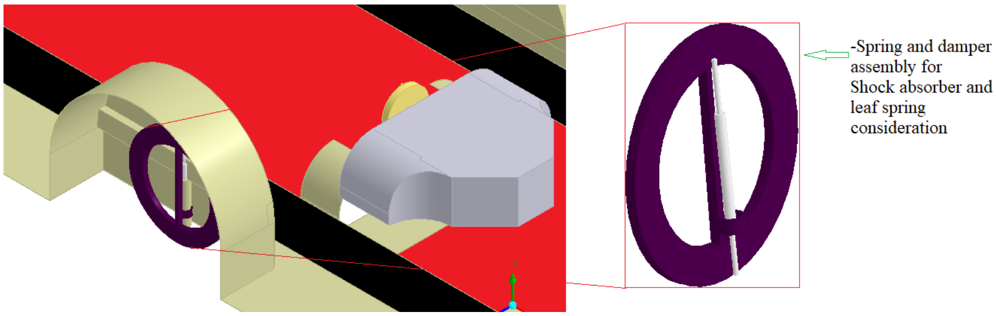

(a)

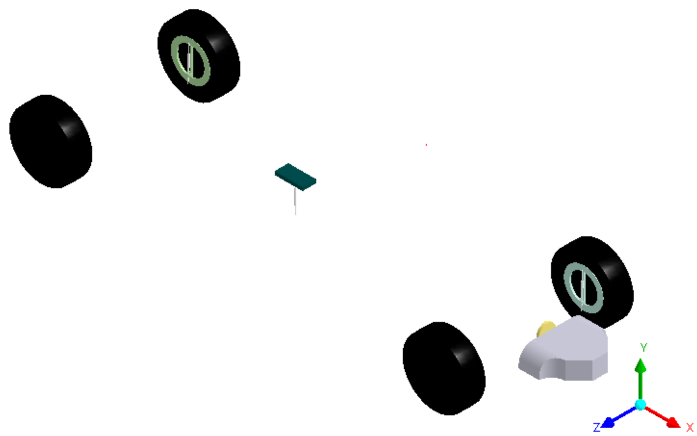

(b)

Figure 3-12 Representation of suspension spring and shock absorber

E. Bus body

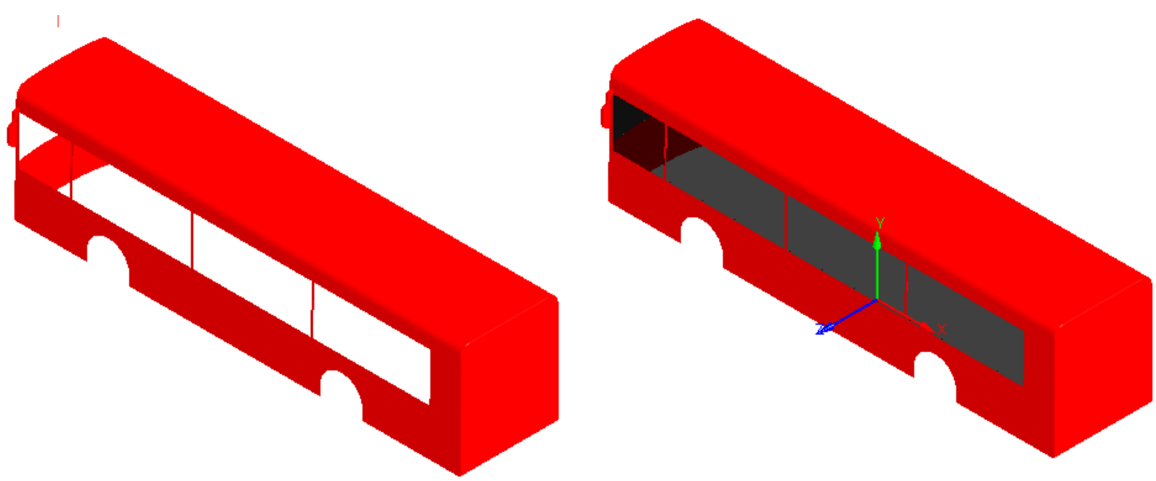

Figure 3-13 3d model of bus body depiction

F. 3D Mercedes model of suspensions assembly

The following figure represent the assembly system of bus 3d model with 100mm half wave road amplitude and 26m long road.

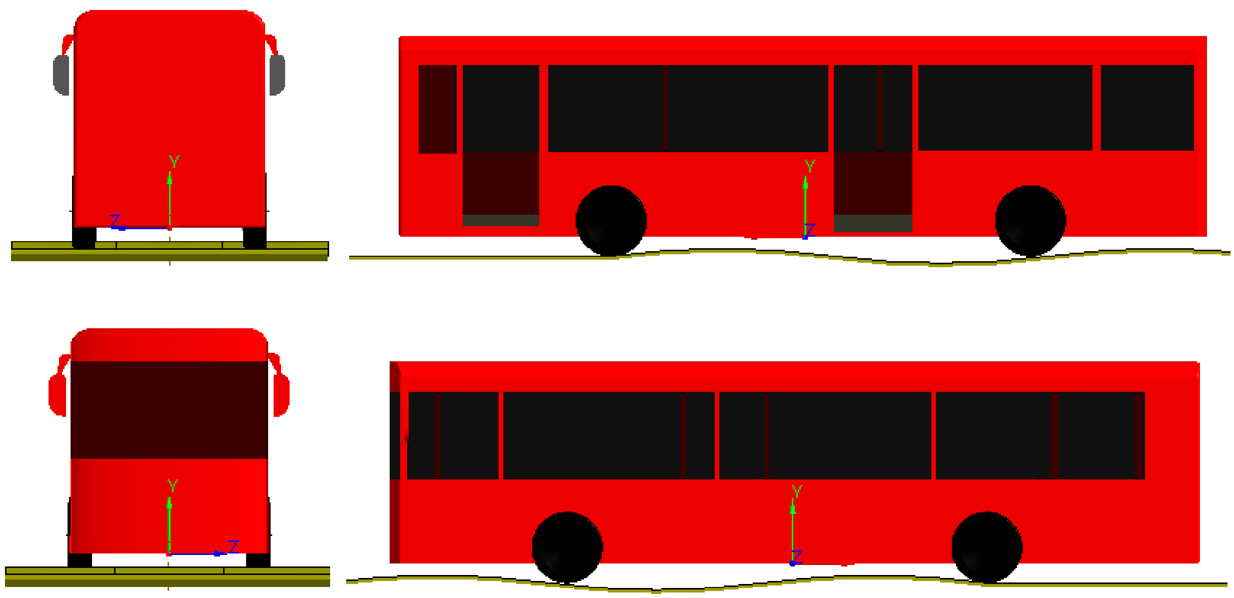

Figure 3-14 Mercedes bus modeled assemble

3.7 Numerical Simulation of Transient Dynamics

Simulations of transient dynamics examine how mechanical systems behave over time while accounting for inertial factors. Usually, when we examine the vibration of a stiff body, it concentrate on the motion caused by outside forces or starting conditions.

3.7.1 Boundary/initial Condition

A boundary condition explains how a function behaves at the edge (border) of its defined region. Similar to a boundary condition, but applied to the time-direction. Although some boundary conditions may not have solutions, physics often provides guidance.

The assumptions made on the vibrational analysis of bus are,

- Consideration of the bus without weighting and with weighting
- The dynamics axis of vibration is Y-axis which considered as vertical dynamics, because maximum acceleration values were found for this axis.
- For the rear part is critical parts of the vehicle when it is moving, receiving strong vibrations caused by road conditions. But in addition to this the front part also included, because for it contains most puller articulated buses, the engine is mounted under the floor between the rear and middle axles that can affect the vibrational behaviour of buses.
- The geometry of the speed breakers is based on IRC 99, which states that speed breakers should be 3.7 m wide and 0.1 m tall for urban roads. According to the codal requirements,

cars should be able to traverse the speed breaker at an advisory speed of 30 km/h. (Mohanty et al., 2021).

Table 3-5 Initial conditions on Shock and leaf sprig

Suspension input Parameters	**Constant Value**
Rear spring Stiffness (K_{rr})	758,000 (N/m)
Front spring Stiffness (K_{fr})	455,000 (N/m)
Rear spring Stiffness (K_{rl})	758,000 (N/m)
Front spring Stiffness (K_{fl})	455,000 (N/m)
Rear Damping Coefficient (C_{rr})	43000
Rear Damping Coefficient (C_{rl})	43000
Front Damping Coefficient (C_{fr})	26000
Front Damping Coefficient (C_{fl})	26000
Gross Weight of the Bus	16000kg

Table 3-6 Initial conditions on rubber sealing

Body to chassis four corner joint	Values
k_{bl}, k_{br}	1,1600N/mm
c_{bl}, c_{br}	8.2Ns/mm
Engine to chassis four corner joint	
k_e	1,1600N/mm
c_e	1.2Ns/mm,3.2 Ns/mm
Seat to chassis rubber single joint	
k_s	3800N/mm
c_s	38 Ns/mm
Rubber Diameter and thickness	Ø50mmx50mm

3.7.2 Transient Rigid dynamics analysis Settings

Transient multi-rigid body dynamics gives scientists and engineers important insights into the behavior of coupled bodies, enabling them to correctly simulate mechanical systems. Effective simulations and design optimization depend on an understanding of rigid body dynamics, which is necessary for assessing robotic motion, vehicle dynamics, and other complex systems. In Ansys the following setting has been carried out.

Table 3-7 Transient Rigid dynamics analysis Settings

1	Step Controls	
	Number Of Steps	1
	Current Step Number	1
	Step End Time	3.1s
	Auto Time Stepping	On
	Initial Time Step	1.e-002 s
	Minimum Time Step	1.e-005 s
	Maximum Time Step	1.e-002 s
2	Solver Controls	
	Time Integration Type	Program Controlled
	Correction Type	Program Controlled
	Assembly Type	Program Controlled
3	Nonlinear Controls	
	Energy Accuracy Tolerance	Program Controlled
4	Output Controls	
	Store Results At	All Time Points

Table 3-8 Boundary value settings

Object Name	*Standard Earth Gravity*
Definition	
Coordinate System	Global Coordinate System
X Component	0. mm/s²
Y Component	-9806.6 mm/s²
Z Component	0. mm/s²
Direction	-Y Direction

Object Name	*Joint - Velocity*	*Joint - Rotational Velocity*
State	Fully Defined	
Joint	Translational - floor To road	Revolute flywheel to engine
Definition		
DOF	X Displacement	Rotation Z
Type	Velocity	Rotational Velocity

Magnitude	-8300. mm/s (step applied)	62.832 rad/s (step applied)

Table 3-9 Boundary output Parameter settings

Name	y	v_x	v_y	v_z	a_x	a_y	a_z
Type	Directional Deformation	Directional Velocity			Directional Acceleration		
Orientation	Y Axis	X Axis	Y Axis	Z Axis	X Axis	Y Axis	Z Axis
By	Time						
Display Time	Last						
Coordinate System	Global Coordinate System						
Time History	Yes						

Name	F_1	F_2	F_3	F_4
Contact Region	Frictional Sliding - tire.1 To road	Frictional Sliding - tire.2 To road	Frictional Sliding - tire.3 To road	Frictional Sliding - tire.4 To road
Orientation	Global Coordinate System			
Contact Force	Y axis			

3.8 Vibrational analysis for Full Car Model in MATLAB / Simulink

Model for computer simulation in MATLAB/Simulink. The MATLAB/Simulink computer simulation models of the above-formulated passive suspension systems are used to validate and test mathematical formulations using transient finite element rigid body dynamics. The primary elements of the simulation models are chosen to include the input road profile, tire, suspension system, vehicle body, and four corners vertical motions (output parameters). The four cases of uneven road terrain that are considered are step (road bump), period (sinusoidal), impulse (road bump), and random (white noise) uneven road bumps. Road profile is chosen as the primary input for the simulation model. The body of the vehicle is assumed to be a rigid slab, this slab has a mass m, which is the total body mass, a longitudinal mass moment of inertia Ix, a lateral mass moment of inertia Iy, and The moments of inertia are only the body mass moments of inertia not the vehicle's mass moments of inertia. In that order, the masses of the wheels are m1, m2, m3, and m4. However, ktf and ktr, which stand for the front and rear tire stiffness, respectively, are typically represented by the equations $mf = m1 = m2 = mr = m3 = m4$. Tire damping can be ignored for computational simplicity because it is significantly less than shock absorber damping. Stiffness kf and damping cf up front and stiffness kr and dampening cr down back make up the car's suspension system. Typically, the left and right wheel suspensions are made. They therefore share the same rigidity and damping. Additionally, the vehicle may include antiroll bars with torsional stiffness values of k_{Rf} and k_{Rr} on the front and rear of the car. The torque M_R provided by the antiroll bar is proportional to the roll angle φ, as determined by a basic model. Most cars just have a front antiroll bar. For these vehicles, the antiroll bar's moment simplifies to

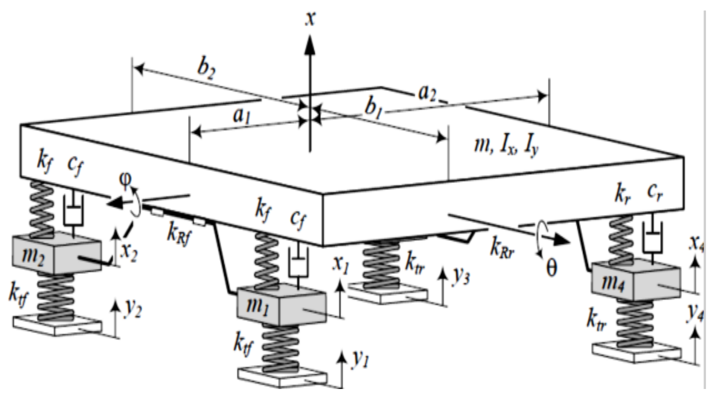

Figure 3-15 Full Car Model of vibrational rigid slab(Solhmirzaei et al., 2012)

If we use $w_f \equiv w = b_1 + b_2$ and $K_{Rf} = K_R$

3.8.1 Mat lab Input output function with

In the MATLAB script, the following variables are used:

- xdd: Second derivative of displacement (acceleration) in the x-direction.
- pidd: Proportional Integral Derivative controller output.
- thdd: Second derivative of angular displacement (angular acceleration). Each of these variables represents a component of the bus's vibrational response under different conditions.

i. Sprung mass acceleration

```
function xdd = fcn(a1,a2,b1,b2,m,kf,kr,cf,cr,x,xd,x1,x1d,x2,x2d,x3,x3d,x4,x4d,pi,pid,th,thd)
xdd=(cf/m)*(-(xd-x1d+b1*pid-a1*thd)-(xd-x2d-b2*pid-a1*thd))+(cr/m)*(-(xd-x3d-b1*pid-
a2*thd)-(xd-x4d+b2*pid+a2*thd))+(kf/m)*(-(x-x1+b1*pi-a1*th)-(x-x2-b2*pi-a1*th))+(kr/m)*(-
(x-x3-b1*pi+a2*th)-(x-x4+b2*pi+a2*th));
```

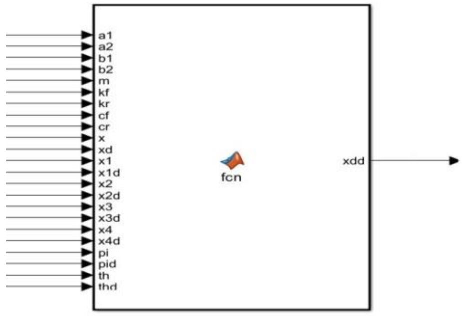

Figure 3-16 Simulink block of Unsprang acceleration of bus

ii. Rolling and pitching angular acceleration of bus

Function[pidd,thdd] =

fcn(a1,a2,b1,b2,w,Ix,Iy,kR,kf,kr,cf,cr,x,xd,x1,x1d,x2,x2d,x3,x3d,x4,x4d,pi,pid,th, thd)

pidd=(cf/Ix)*(-b1*(xd-x1d+b1*pid-a1*thd)+b2*(xd-x2d-b2*pid-a1*thd))+(cr/Ix)*(b1*(xd-x3d-b1*pid+a2*thd)-b2*(xd-x4d+b2*pid+a2*thd))+(kf/Ix)*(-b1*(x-x1+b1*pi-a1*th)+b2*(x-x2-b2*pi-a1*th))+(kr/Ix)*(b1*(x-x3-b1*pi+a2*th)-b2*(x-x4+b2*pi+a2*th))-(kR/Ix)*(pi-(x1-x2)/w);

thdd=(cf/Iy)*(a1*(xd-x1d+b1*pid-a1*thd)+a1*(xd-x2d-b2*pid-a1*thd))+(cr/Iy)*(-a2*(xd-x3d-b1*pid+a2*thd)-a2*(xd-x4d+b2*pid+a2*thd))+(kf/Iy)*(a1*(x-x1+b1*pi-a1*th)+a1*(x-x2-b2*pi-a1*th))+(kr/Iy)*(-a2*(x-x3-b1*pi+a2*th)-a2*(x-x4+b2*pi+a2*th));

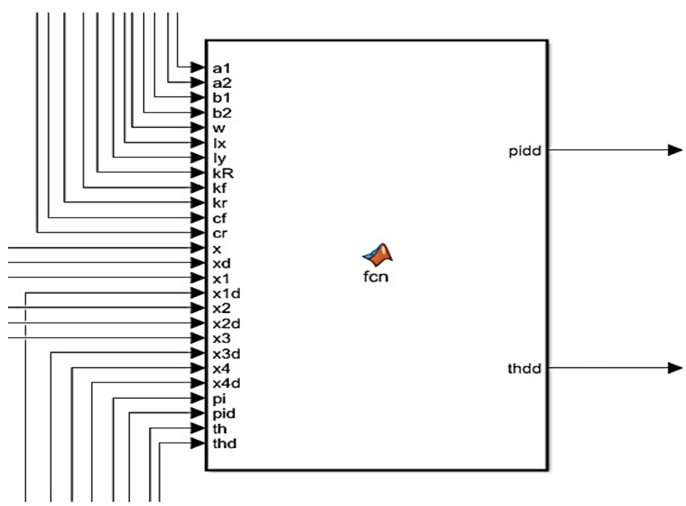

Figure 3-17 Simulink block of Rolling and pitching angular acceleration of bus

iii. All suspension of unsprang mass acceleration

function[x1dd,x2dd,x3dd,x4dd] =

fcn(a1,a2,b1,b2,w,mf,mr,kf,kr,ktf,ktr,cf,cr,kR,x,xd,x1,x1d,x2,x2d,x3,x3d,x4,x4d,y1,y2,y3,y4,pi,pid,th,thd) x1dd=(cf/mf)*((xd-x1d+b1*pid-a1*thd)+(kf/mf)*((x-x1+b1*pi-a1*th))+(kR/(mf*w))*(pi-(x1-x2)/w)-ktf*(x1-y1));

x2dd=(cf/mf)*((xd-x2d-b2*pid-a1*thd)+(kf/mf)*((x-x2-b2*pi-a1*th))-(kR/(mf*w))*(pi-(x1-x2)/w)-ktf*(x2-y2));

x3dd=(cr/mr)*(xd-x3d-b1*pid+a2*thd)+(kr/mr)*((x-x3-b1*pi+a2*th)-ktr*(x3-y3));

x4dd=(cr/mr)*(xd-x4d+b2*pid+a2*thd)+(kr/mr)*((x-x4+b2*pi+a2*th)-ktr*(x4-y4));

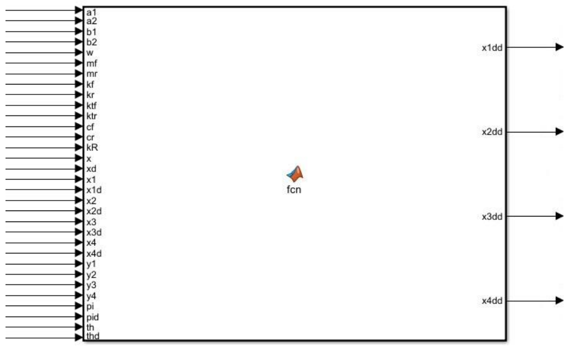

Figure 3-18 Simulink block of All suspension of unsprang mass acceleration

iv. Input Road condition

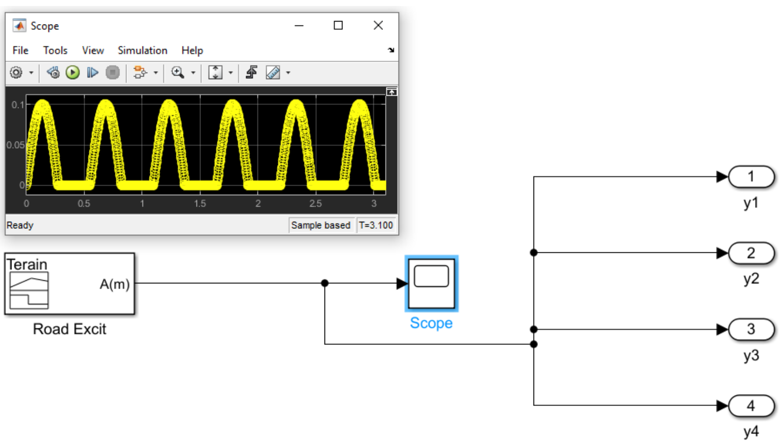

Figure 3-19Simulink block of Input Road condition

V. Complete Simulink Block Diagram for full car model vibrational analysis

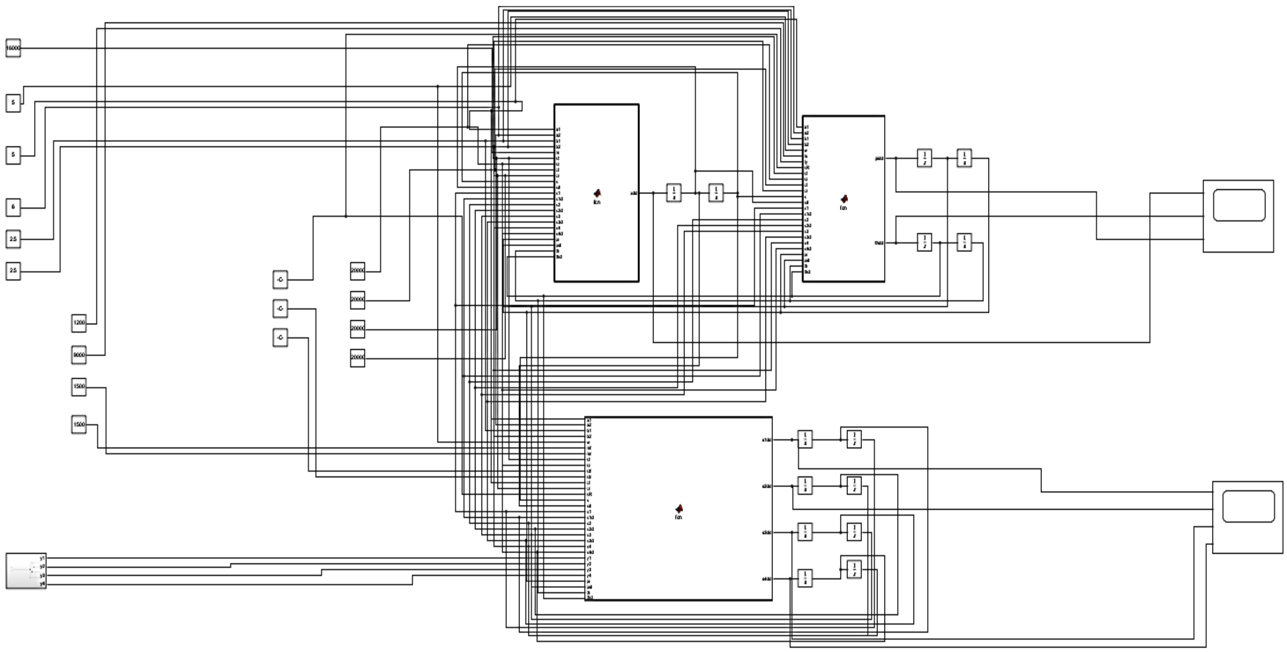

Table 3-10 Simulink data for simulation analyses

Parameters	Symbol	value	units
Sprung Vehicle Mass	M	16000	kg
Mass supported by front left and right suspension	m_{fl} , m_{fr}	1650	kg
Mass supported by rear left and right suspension	m_{rl} , m_{rr}	2350	kg
Front left and right Unsprang Mass	m_{wfl} , m_{wfr}	120	kg
Rear left and right Unsprang Mass	m_{wrl} , m_{wrr}	250	kg
Front left and right Suspension Stiffness	k_{fl} ,k_{fr}	455000	N/m
Rear left and right Suspension Stiffness	k_{rl} ,k_{r}	758000	N/m
Front left and right Suspension Damping	c_{fl} ,c_{fr}	26000	Ns/m
Rear Suspension Damping	c_{rl} ,c_{rr}	43000	Ns/m
Front left and right Tire Stiffness	k_{tfl}, k_{tfr}	400000	N/m
Rear left and right Tire Stiffness	k_{trl}, k_{trr}	500000	N/m
Front left and right Tire Damping	k_{trl}, k_{trr}	150	Ns/m
Rear left and right Tire Damping	c_{trl},c_{tfr}	200	Ns/m
Mass moment of inertia of roll	I_x	5000	kgm^2
Mass moment of inertia of pitch	I_z	42000	kgm^2
Vehicle Wheel span	w	2.936	m
Length to Front Suspension from Centre of Mass	a_1	6.3	m
Length to Rear Suspension from Centre of Mass	a_2	4.79	m

CHAPTER FOUR
RESULT AND DISCUSSION

4.1 Introduction

Without making assumptions about the causes of the outcomes, the results chapter or section simply and objectively summarizes what discovered. The discussion explains the significance of the findings, interprets their significance, and places them in their proper context. On the other hand, this results part is a section that describes the key findings of a study, whereas the discussion section analyses the findings for readers and explains their significance. The discussion and outcomes of vibration analysis with Modification and without Modification are described in further detail along with simulations and case studies of the outcomes of each of modified models. With simulations and case studies of each outcome, the result and discussion of vibration analysis are described in more depth. Here each analysed models have their own different case studies.

4.2 Vibrational Analysis on Mercedes Benz City Bus

Before the simulation of modified model of bus with vibration reduction device, the baseline model which didn't considered with devise or rubber sealing is analysed and next, the modified model with vibration reduction devise is examined with Ansys transient rigid dynamics. The results are described in the graphical form and summarized with tables which comprises the analysis of Suspension displacement, velocity, acceleration, reaction force from the ground and energy dissipations that used to evaluate the performance parameters, Transmissibility ratio (TR), Road Holding (RH), Suspension travel (ST) and Comfort factor (CF). These parameters are solved for Body rubber mounted to chassis (BRC), Engine rubber mounted to chassis (ERC), Seat rubber mounted to floor (SRF). The combined form showed as bus without rubber (WR), Body Rubber Mounted to Chassis (BRC), Body and Engine Rubber Mounted to Chassis (BERC), and Body, Engine and Seat Rubber Mounted to Chassis (BESRC)

Transmissibility Ratio (TR): The ratio of the amplitude of the output to the input in a vibrational system, indicating the efficiency of vibration transmission.

Suspension Travel (ST): The vertical displacement of the suspension system components relative to their static position, indicating the suspension's capacity to absorb vibrations.

4.2.1 Analysis of base line of Mercedes bus model (WR)

A. WR model suspension displacement (SD)

The suspension displacement (SD) and travel (ST) for base line or (WR) model Mercedes bus is graphical plotted in the following figure 4.1.

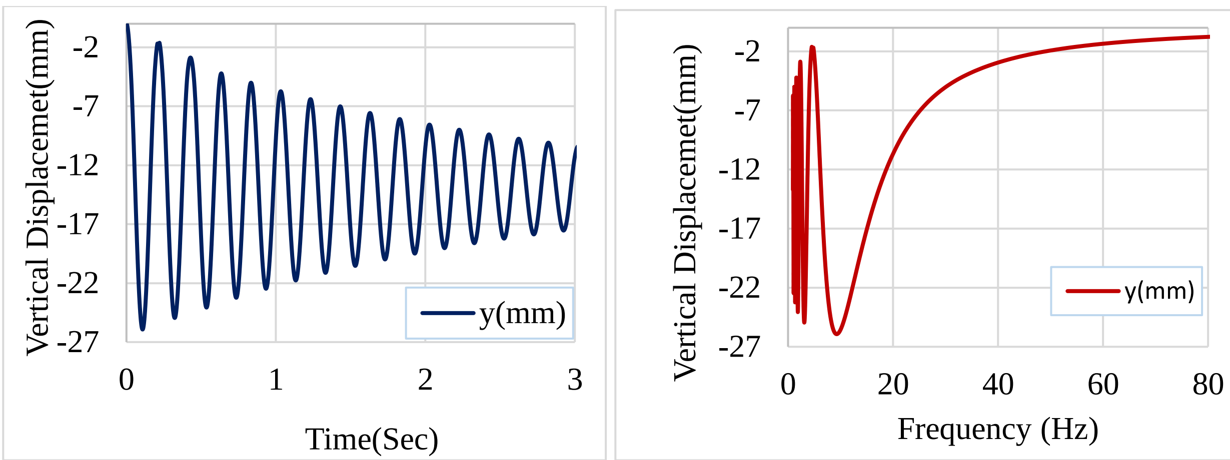

(a) (b)

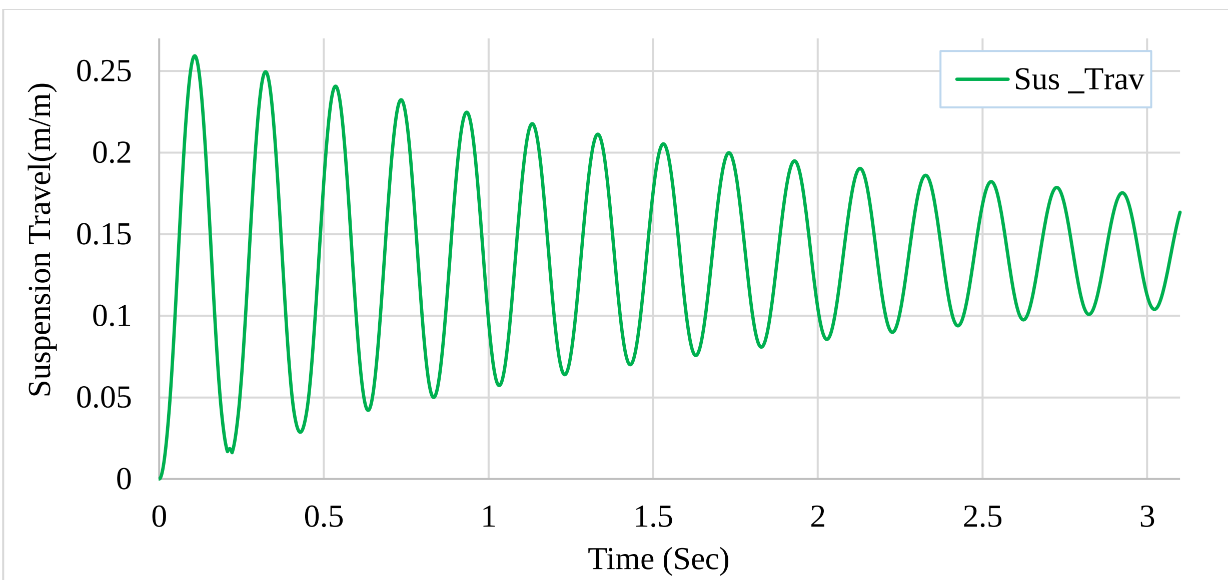

(c)

Figure 4-1 (a, b, c) Suspension displacement (SD) of WR model above unsprang mass vs Time(s) and Excitation frequency (Hz) and Suspension travel (ST)

The graphical plots of suspension dynamics from figure 4.1 for baseline model of bus shows that, the maximum SD of bus structure above the unsprang mass is 25.93mm which compared with road amplitude and gives ST maximum about 0.2593 m/m. And the graph plots of figure 4.1 (c) shows that this maximum suspension travel (ST) is obtained at the base excitation frequency of 9.242Hz.

B. WR model suspension velocity (SV)

The suspension velocity (SV) for base line or (WR) model Mercedes bus is graphical plotted in the following figure 4.2.

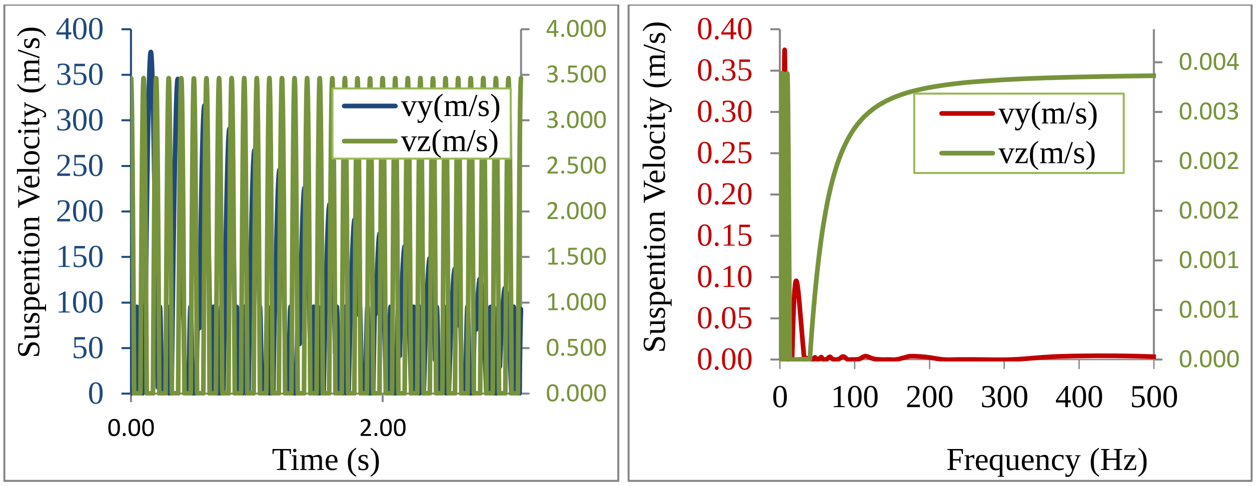

(a) (b)

Figure 4-2 (a, b) Suspension Velocity (SV) above unsprang mass vs Time(s) and Excitation frequency (Hz) of (WR) Model

According to the graphical displays of suspension dynamics from Figure 4.2 for the base line model of the bus (WR), the bus structure's maximum SV above the unsprang mass is 375.05 mm/s, whereas the maximum velocity after dumping is 92.629 mm/s. The maximum suspension velocity (SV) is reached at the base excitation frequency of 6.33 Hz, as indicated by the graph plots in figure 4.2 (b).

C. WR model suspension acceleration (SA)

The accompanying figure 4.3 is a graphical map of the suspension acceleration (SA) for the base line model (WR) designed to show each acceleration component.

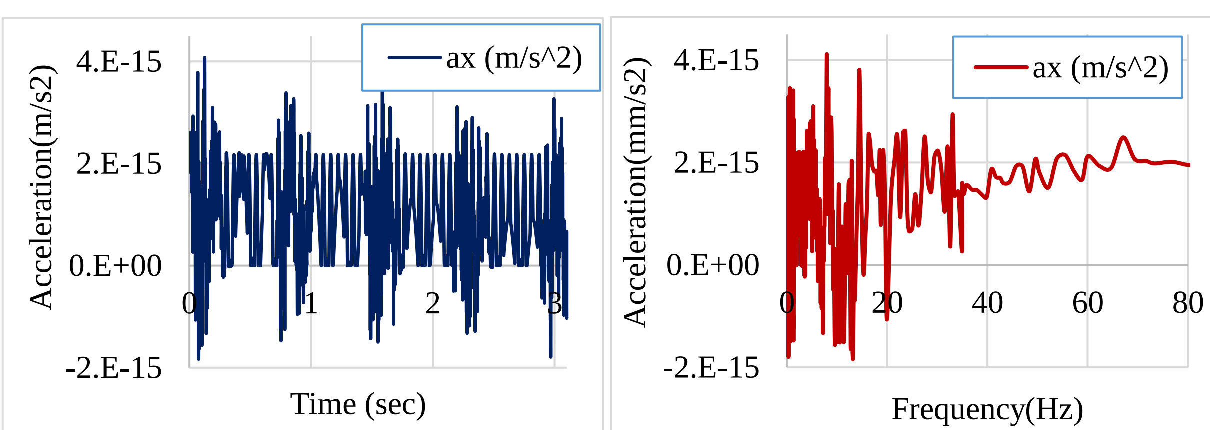

(a) (b)

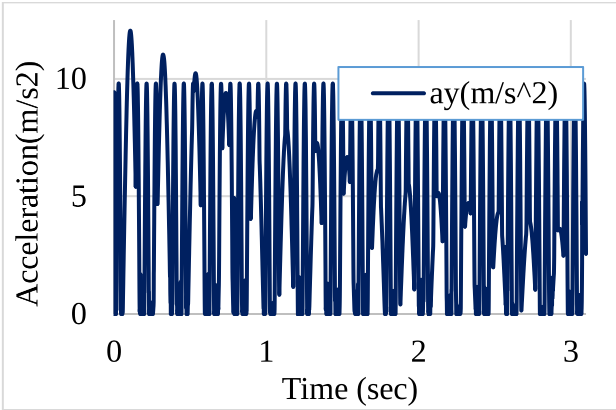

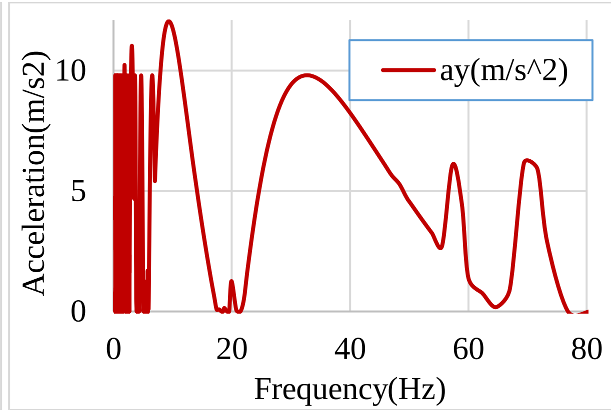

(c) (d)

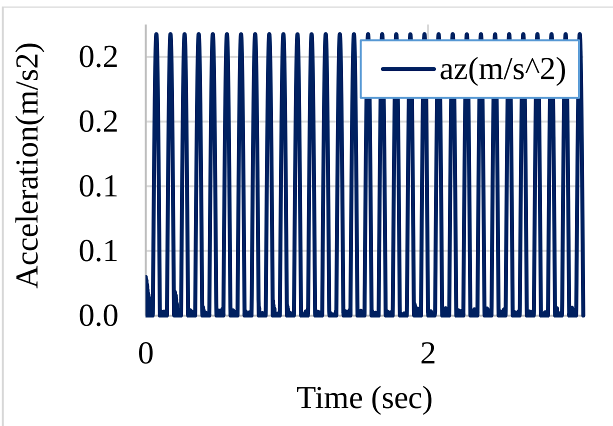

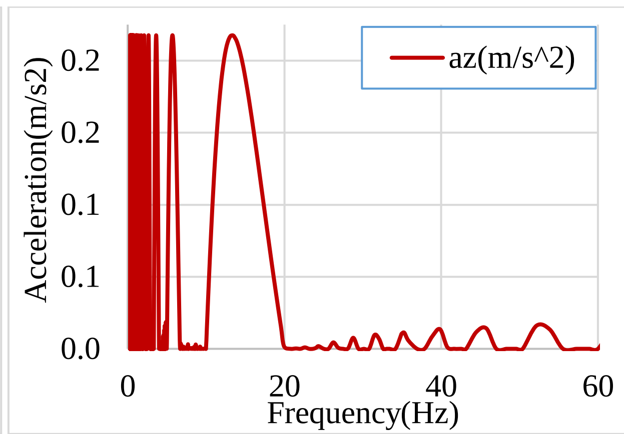

(e) (f)

Figure 4-3 (a, b, c, d, e, f) Suspension acceleration (SA) above unsprang mass vs time(s) and excitation frequency (Hz) for WR

The maximum SA of the bus structure above the unsprang mass for the WR model is 12049mm/s2, according to the suspension dynamics acceleration graphical charts in figure 4.3. The maximum suspension acceleration is governed by y axis acceleration (SA), which is reached at the base excitation frequency of 9.33 Hz, as shown by the plots in figure 4.3d. According to ISO 2631, the comfort factor is assessed as CF 6.75 and the quality factor of the weighted root mean acceleration is determined as 647mm/s2 based on the overall suspension system study. Depending on the usual quality factor criteria, this is fairly uncomfortable.

D. WR model Passengers' weight with seat acceleration (PSA)

The accompanying image 4.4 is meant to graphically plot the passengers' weight with seat acceleration (PSA) for the base line model, or WR, and shows each acceleration component.

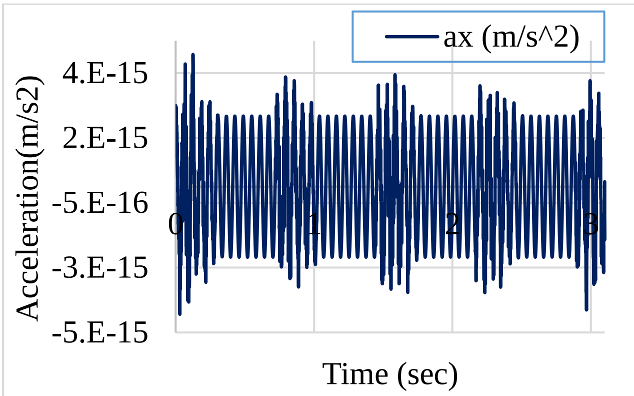

(a)

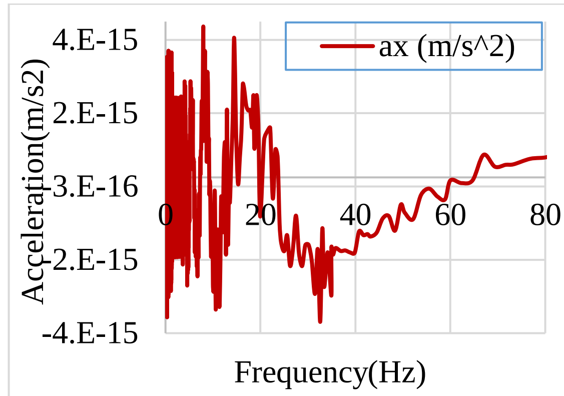

(b)

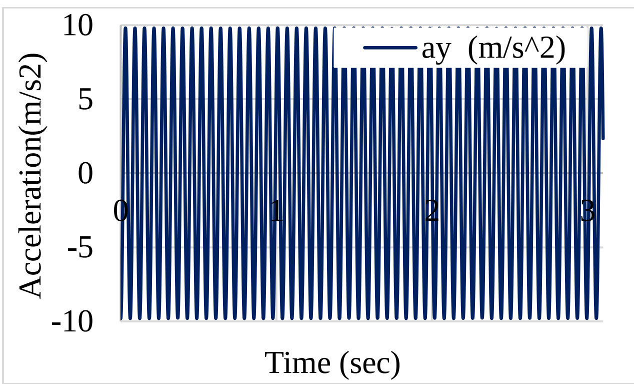

(c)

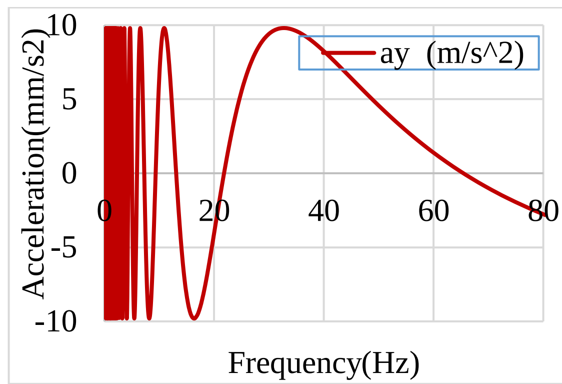

(d)

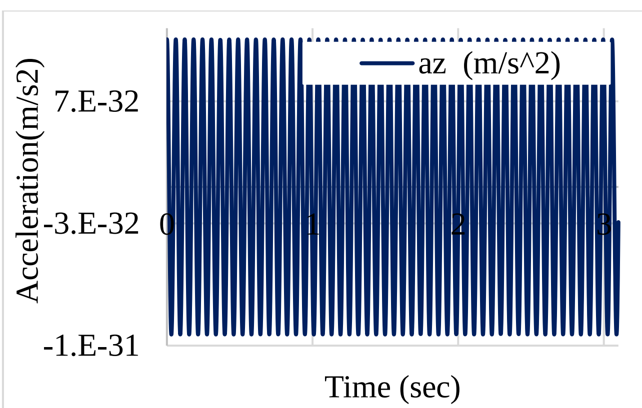

(e)

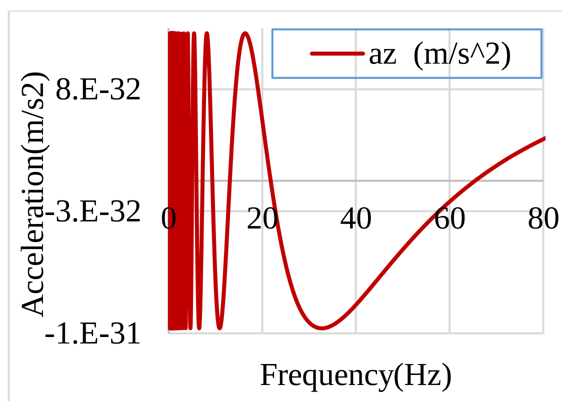

(f)

Figure 4-4 (a, b, c, d, e, f) Passengers weight with seat acceleration (PSA) vs time(s) and excitation frequency (Hz) for WR Model

According to figure 4.4 of WR, which shows graphical graphs of suspension dynamics for passenger weight with seat acceleration (PSA), the maximum PSA is 9806.4 mm/s2. Figure 4.4D graphs demonstrate that the y-axis acceleration (PSA) dominates the maximum acceleration, which is reached at 6.543 Hz base excitation frequency. The weighted root mean acceleration analysis quality factor, as calculated by the general overview of passenger weight with seat, is 1400 mm/s^2, and the comfort factor, as assessed by ISO 2631, is CF 3.07. The usual quality factor requirements state that this is uncomfortable.

E. WR model Transmitted Force (N)

The force Transmitted from base excitation of Model WR at successive time step and excitation frequency shown by figure 4.5.

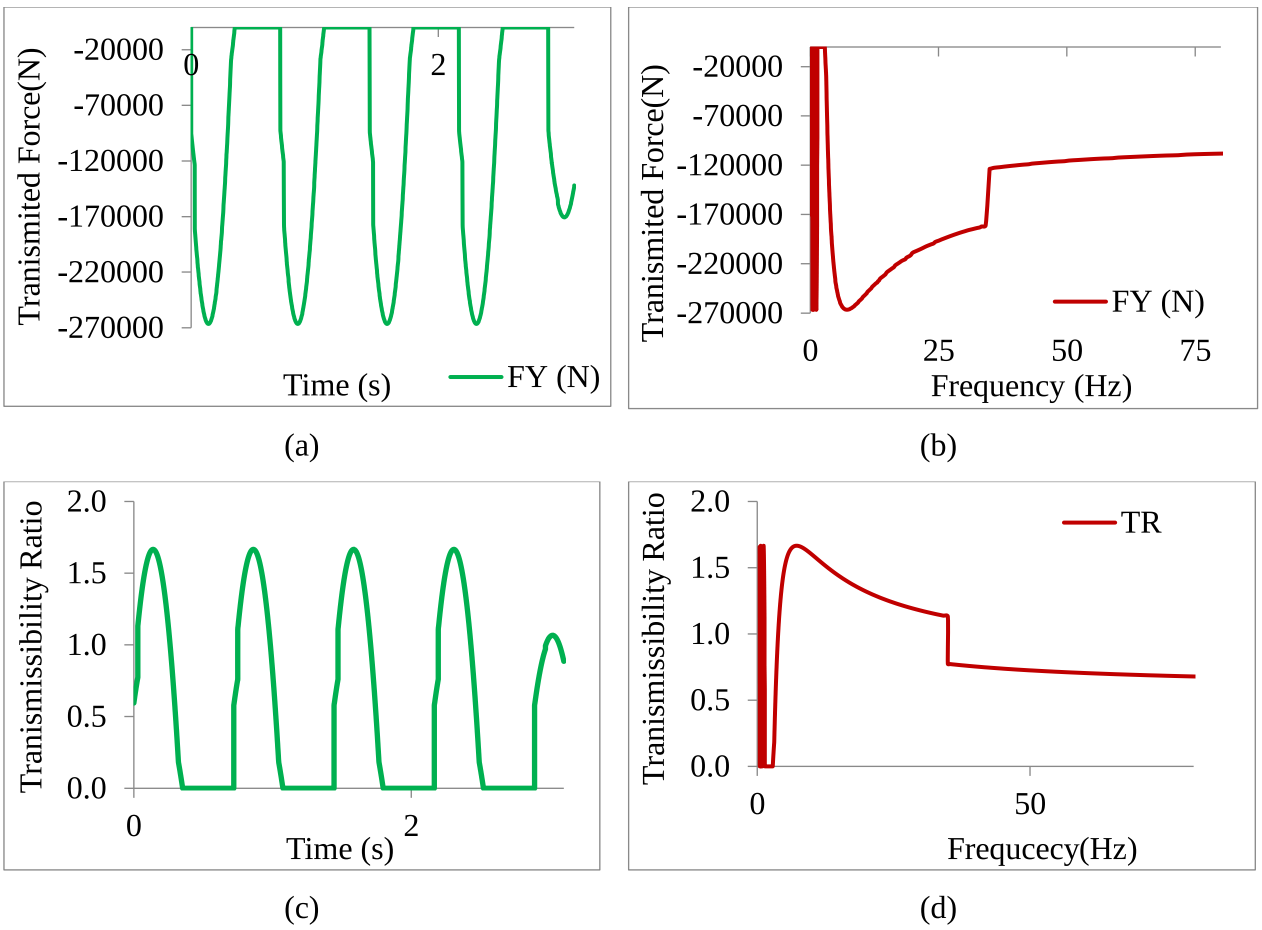

Figure 4-5 (a, b, c, d) Force Transmitted (FT) from base excitation and Transmissibility ratio (TR) vs time(s) and excitation frequency (Hz) for WR model

The force transmitted (FT) from base excitation and the transmissibility ratio of WR are plotted graphically in the suspension dynamics According to the model shown in Figure 4.5, the maximum FT is 266.53kN and the maximum TR is 1.658. The graphs in Figure 4.5d demonstrate that the base excitation frequency of 7.21 Hz, which is also common for TF, is where the highest TR is reached. This TR demonstrates why it is not advised for design quality, although it have average road holding capability (RH) 95693N.

F. WR model Vibrational Energy above unsprang mass

The baseline model WR's bus vibrational energy at each time step and excitation frequency above unsprang mass are displayed in figure 4.6.

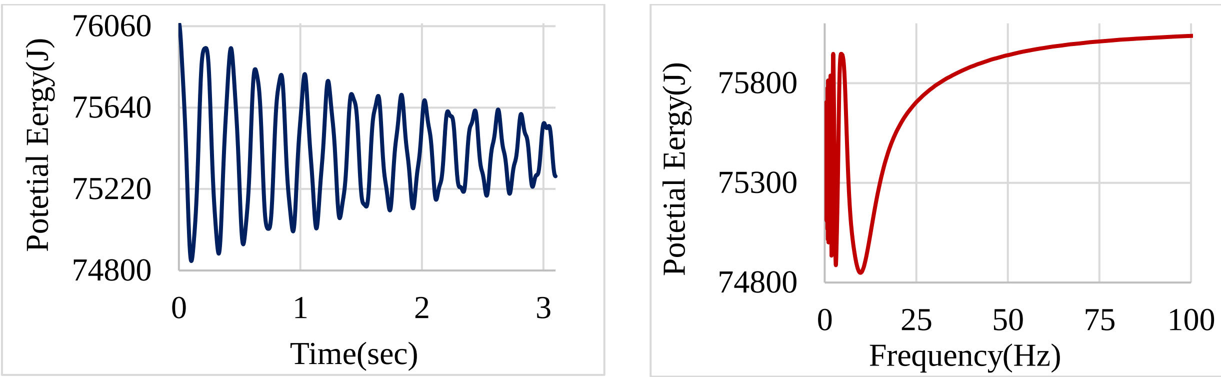

(a) (b)

Figure 4-6 (a, b) Vibrational energy at successive time step and excitation frequency of WR

According to figure 4.6's graphical plots of suspension dynamics for the vibrational energy of WR model at each time step and excitation frequency, the maximum energy is 76075 J, and the damped energy is 75545 J at 3.047. Figure 4.6b demonstrate that the maximum energy is reached at the standard base excitation frequency of 1000 Hz for common to TF. This indicates that suspension dampers are causing energy to be dispersed with amount 530J.

4.2.2 Analysis of Body Rubber mounted to Chassis (BRC)

A. BRC model suspension displacement above unsprang mass

The suspension displacement (SD) and travel (ST) for body rubber mounted to chassis of Mercedes bus is graphical plotted in the following figure 4.7.

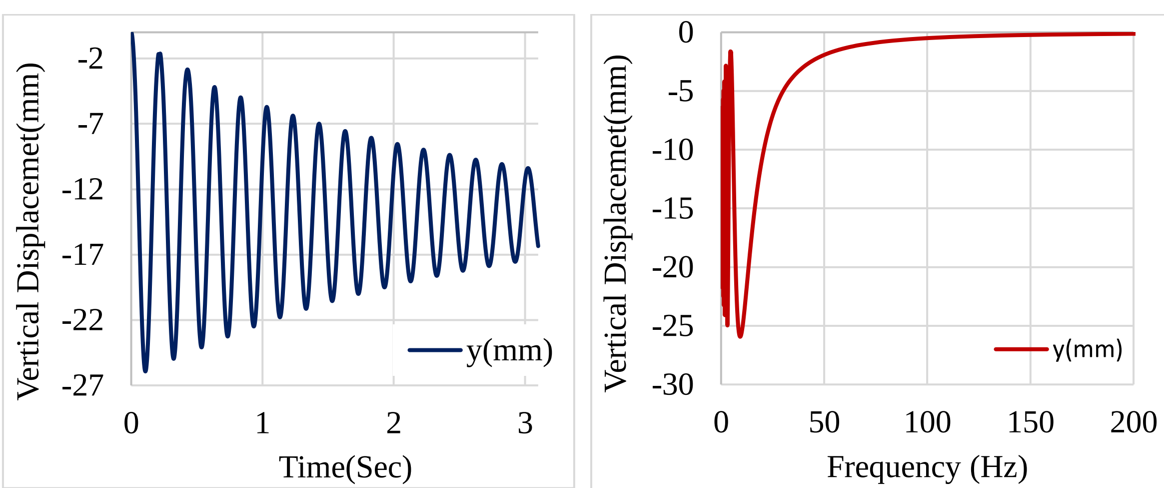

(a) (b)

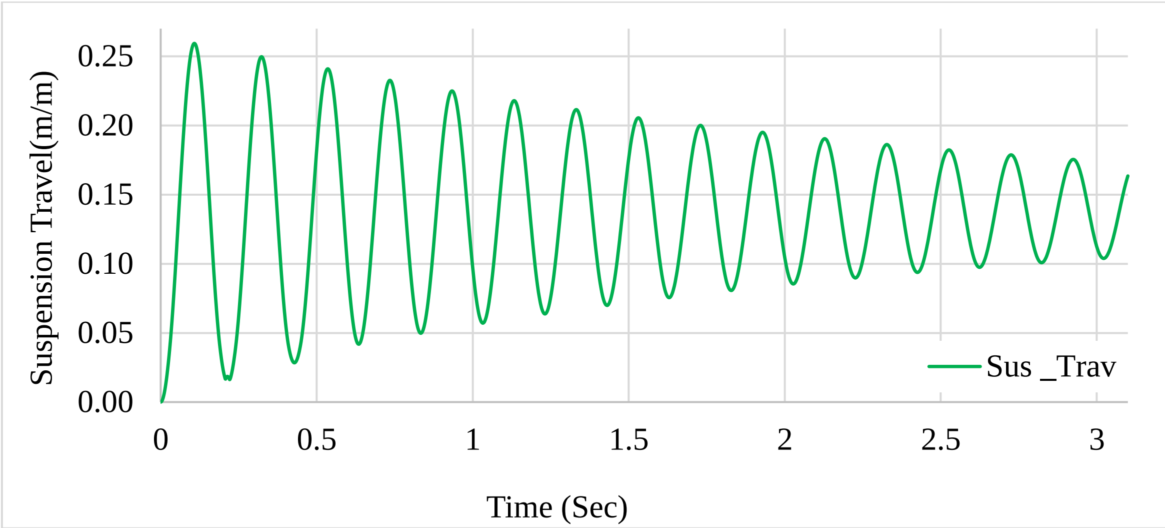

(c)

Figure 4-7 (a, b, c) Suspension displacement (SD) above unsprang mass vs Time(s) and Excitation frequency (Hz) and Suspension travel (ST) for BRC

The maximum SD of the bus structure above the unsprang mass is 25.93 mm, which, when compared to the road amplitude, yields a ST maximum of around 0.2593 m/m, according to the graphical plots of suspension dynamics in figure 4.7 of the BRC bus model. Furthermore, figure 4.7 (c)'s graph plots demonstrate that this maximum suspension travel (ST) is achieved at 9.32 Hz, which is the base excitation frequency.

A. BRC model suspension velocity above unsprang mass

The suspension velocity (SV) for BRC bus model is graphical plotted in the following figure 4.8.

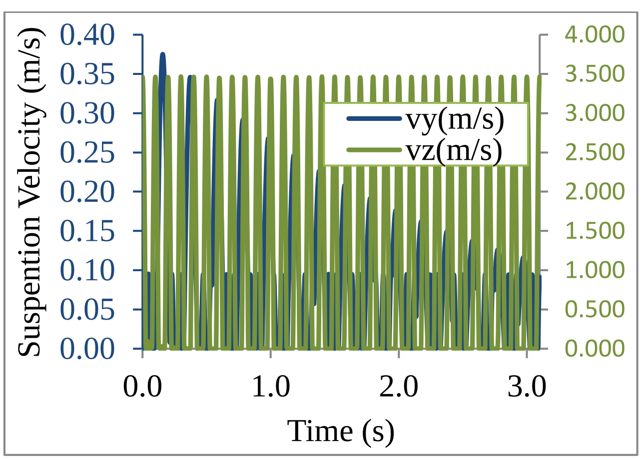

(a)

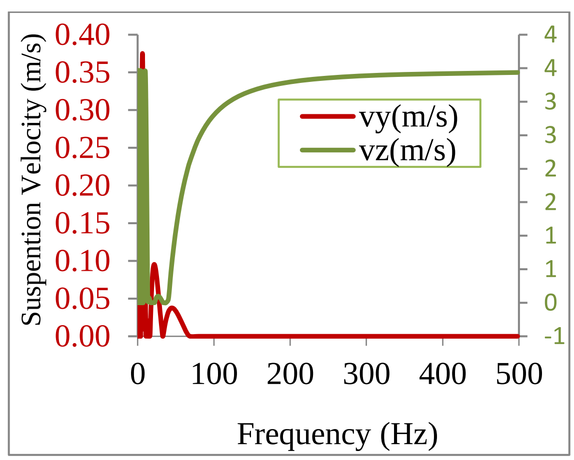

(b)

Figure 4-8 (a, b) Suspension Velocity (SV) above unsprang mass vs Time(s) and Excitation frequency (Hz) of BRC

The graphical plots of suspension dynamics on figure 4.8 for BRC model of bus displays that, the maximum SV of bus structure above the unsprang mass is 375mm/s which compared with after dumped maximum velocity 91mm/s. The graph subversions of figure 4.8 (b) shows that the maximum suspension Velocity (SV) is achieved at the base excitation frequency of 6.3 Hz.

B. BRC model suspension acceleration (SA) above unsprang mass

The suspension acceleration (SA) for BRC model is graphical plotted in the following figure 4.9 shows each accelerations components.

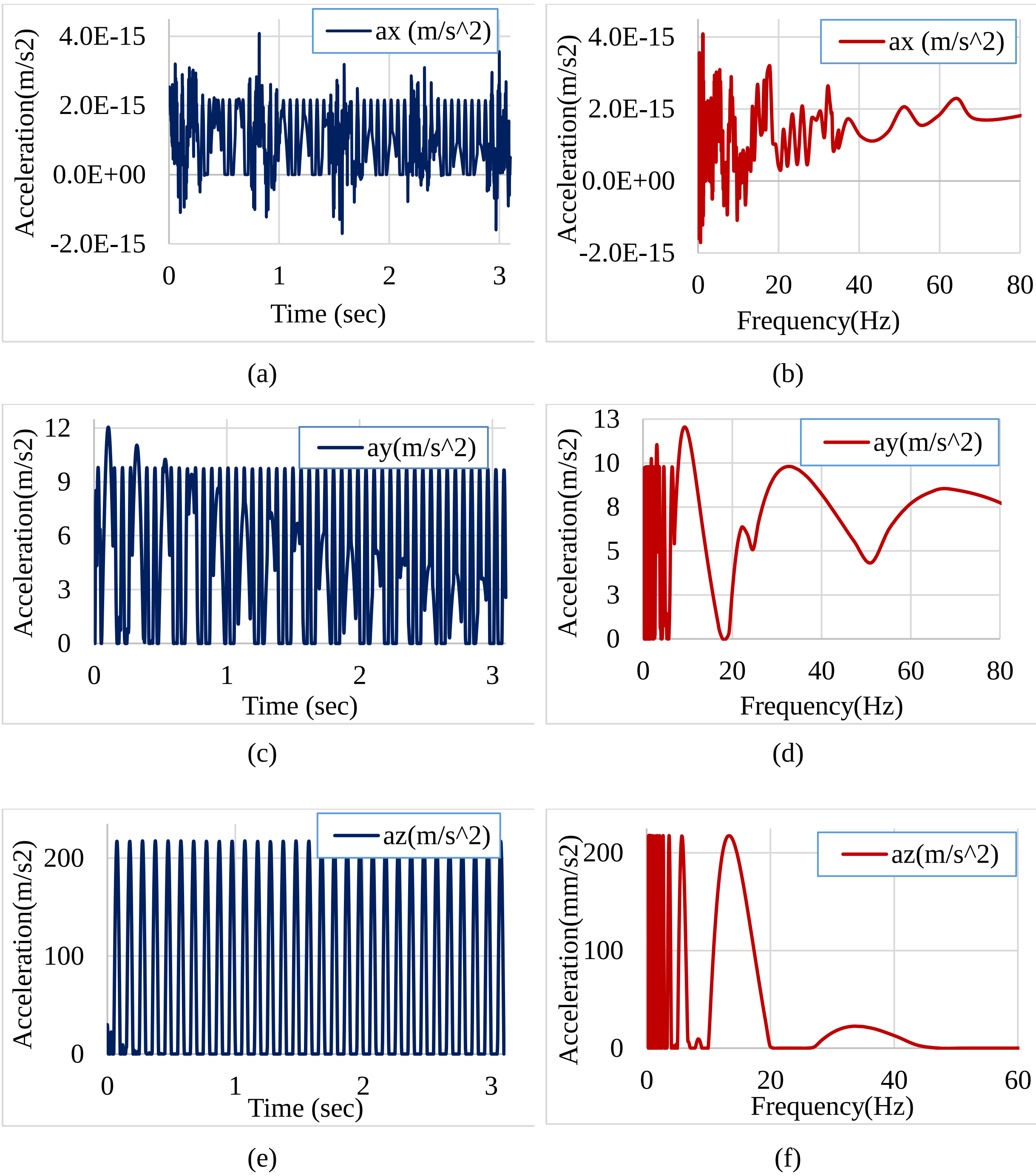

Figure 4-9 (a, b, c, d, e, f) Suspension acceleration (SA) above unsprang mass vs time(s) and excitation frequency (Hz) of BRC

The graphical plots of suspension dynamics acceleration from figure 4.9shows that, the maximum SA of BRC bus structure above the unsprang mass is 12052mm/s^2 subjugated by y axis. The plots of figure 4.9 d shows that the maximum suspension acceleration (SA) is attained at the base excitation frequency of 9.32 Hz. From the general over view of suspension system analysis the quality factor of weighted root mean acceleration is determined as 560mm/s^2 and the comfort factor is evaluated CF 7.23 according to the ISO 2631. This is a little uncomfortable according to the standard quality factor criteria.

C. BRC model Passenger's weight with seat suspension acceleration

The passenger's weight with seat acceleration (PSA) for BRC model is graphical plotted in the following figure 4.10 intended that displays each accelerations component.

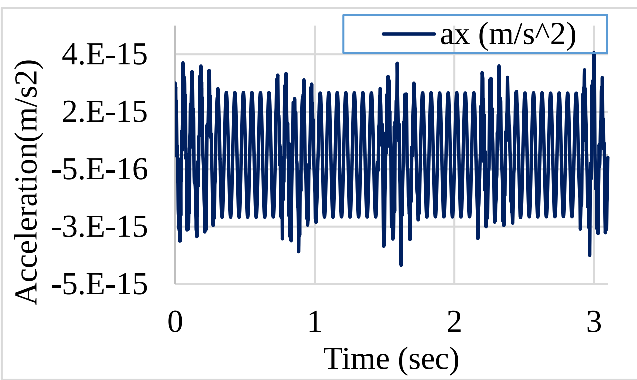

(a)

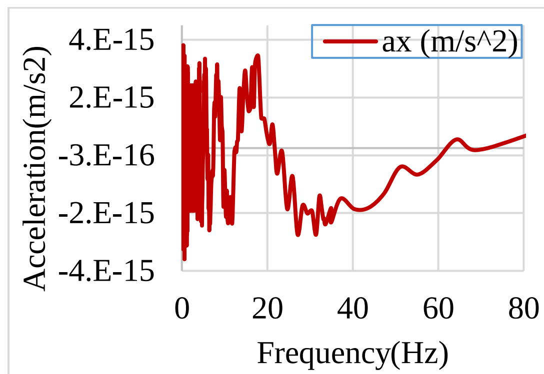

(b)

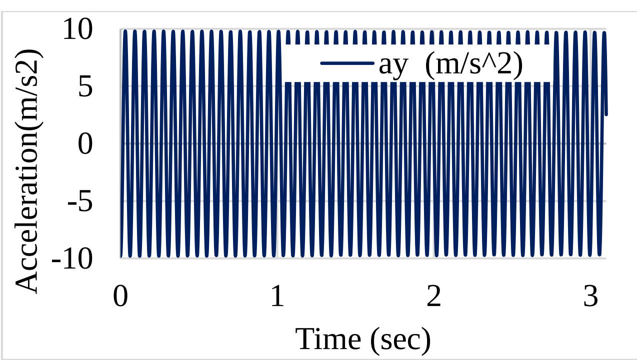

(c)

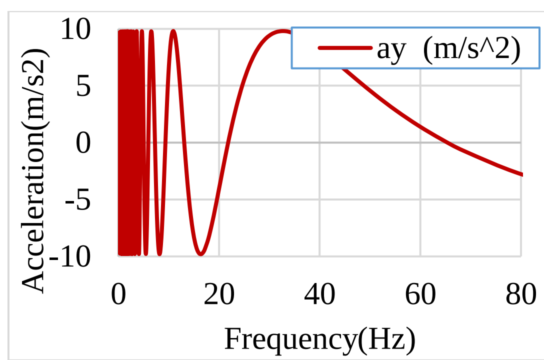

(d)

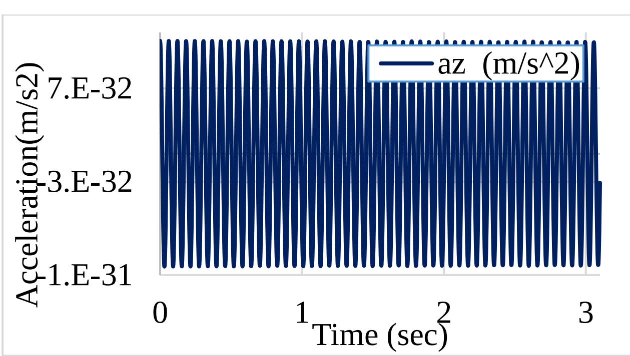

(e)

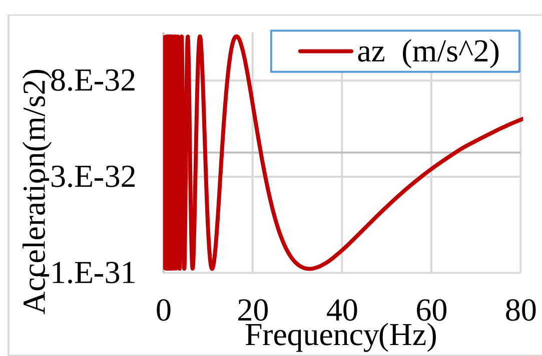

(f)

Figure 4-10 (a, b, c, d, e, f) BRC Passengers weight with seat acceleration (PSA) vs time(s) and excitation frequency (Hz)

The graphical plots of suspension dynamics for BRC passengers weight with seat acceleration (PSA) from figure 4.10 displays that, the maximum PSA is 9806 mm/s^2. The plots of figure 4.10 d shows that the maximum acceleration is controlled by y axis BRC acceleration (PSA) is attained at the base excitation frequency of 32.76Hz. From the general over view of passenger weight with seat for BRC, the analysis quality factor of weighted root mean acceleration is determined as 1191mm/s^2 and the comfort factor is evaluated CF 4 according to the ISO 2631. This is uncomfortable according to the standard quality factor criteria. But it is enhanced by 15% from base line model.

D. BRC model Transmitted Force (N)

The force Transmitted from base excitation at successive time step and excitation frequency show by figure 4.5 to the bus body.

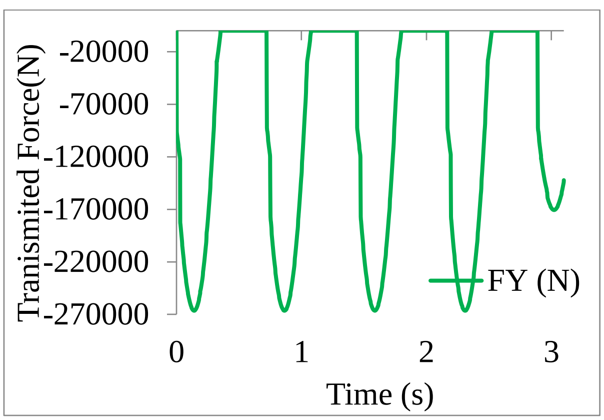

(a)

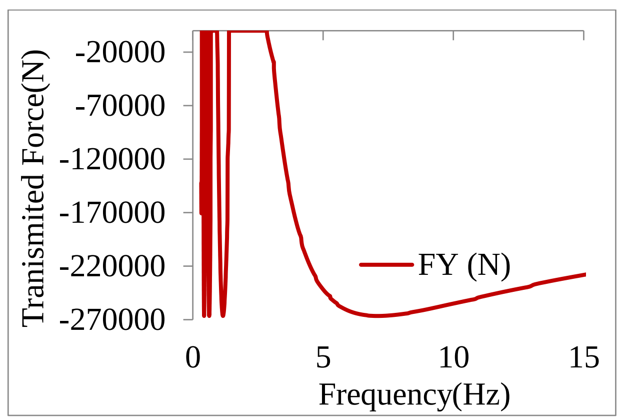

(b)

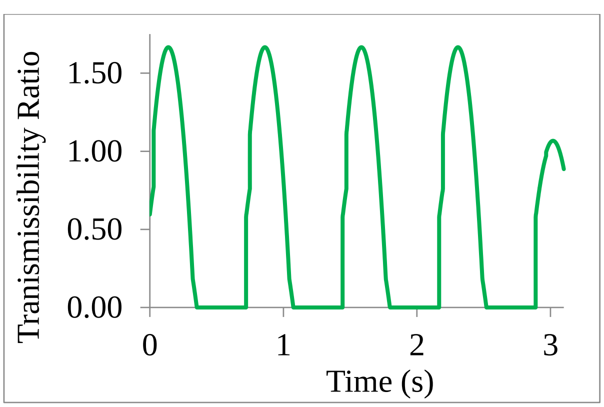

(c)

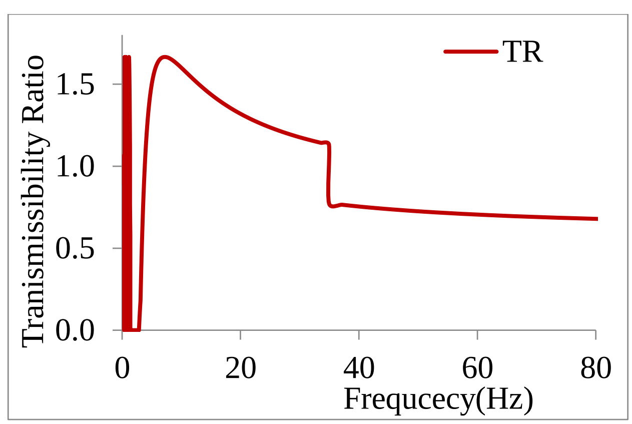

(d)

Figure 4-11 (a, b, c, d) Force Transmitted (FT) from base excitation and Transmissibility ratio (TR) vs time(s) and excitation frequency (Hz) for BRC

The graphical plots of suspension dynamics for Force Transmitted (FT) from base excitation and Transmissibility ratio from figure 4.5 displays that, the maximum FT is 266.52kN and TR is 1.6657. The plots of figure 4.11 d shows that the maximum TR is attained at the base excitation frequency of 7.26 Hz which is common for also TF. This TR shows that it is not recommended for quality of design but it is reduced by 10N from WR model and it have average road holding capability (RH) 95978N.

E. BRC model vibrational energy

The vibrational energy at successive time step and excitation frequency shown by figure 4.12.

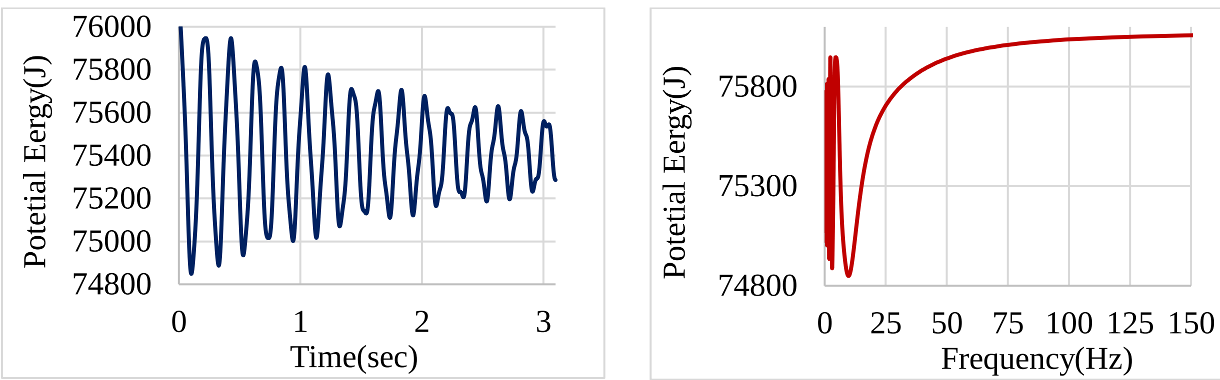

(a) (b)

Figure 4-12 (a, b) Vibrational energy of BRC above unsprang mass at successive time step and excitation frequency

The graphical plots of suspension dynamics for the vibrational energy of BRC at successive time step and excitation frequency from figure 4.12 displays that, the maximum energy vibrational energy is 76075 J and the damped energy is 75540J at 3.08 second. The plots of figure 4.12 b shows that the maximum energy is attained at the base excitation frequency of 500 Hz. This shows that there is 535J energy dissipated due to suspension dampers.

4.2.3 Analysis of Body, Engine Rubber Mounted to Chassis (BERC)

A. BERC Suspension displacement

The suspension displacement (SD) and travel (ST) for body, Engine rubber mounted to chassis of Mercedes bus is graphical plotted in the figure 4.13.

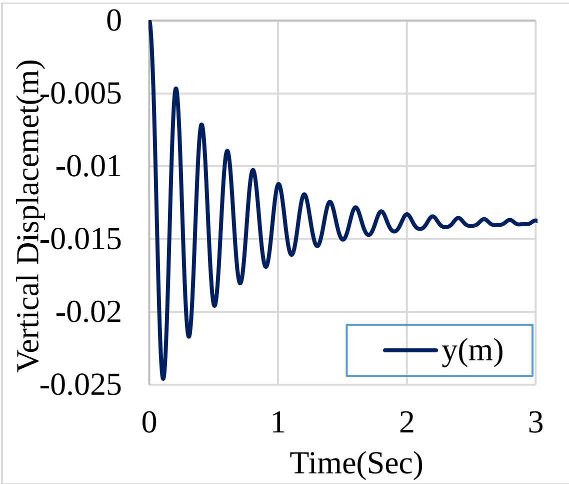

(a)

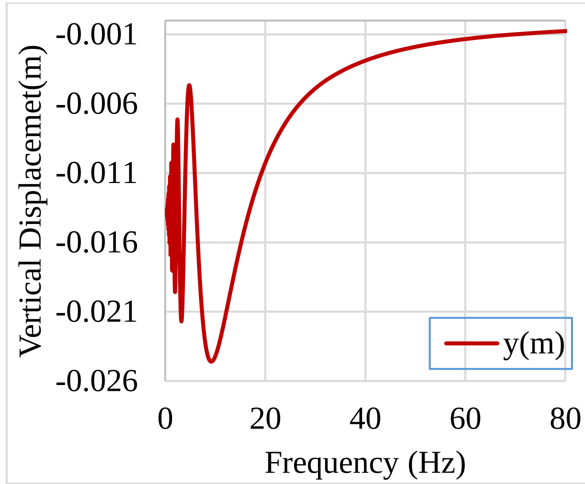

(b)

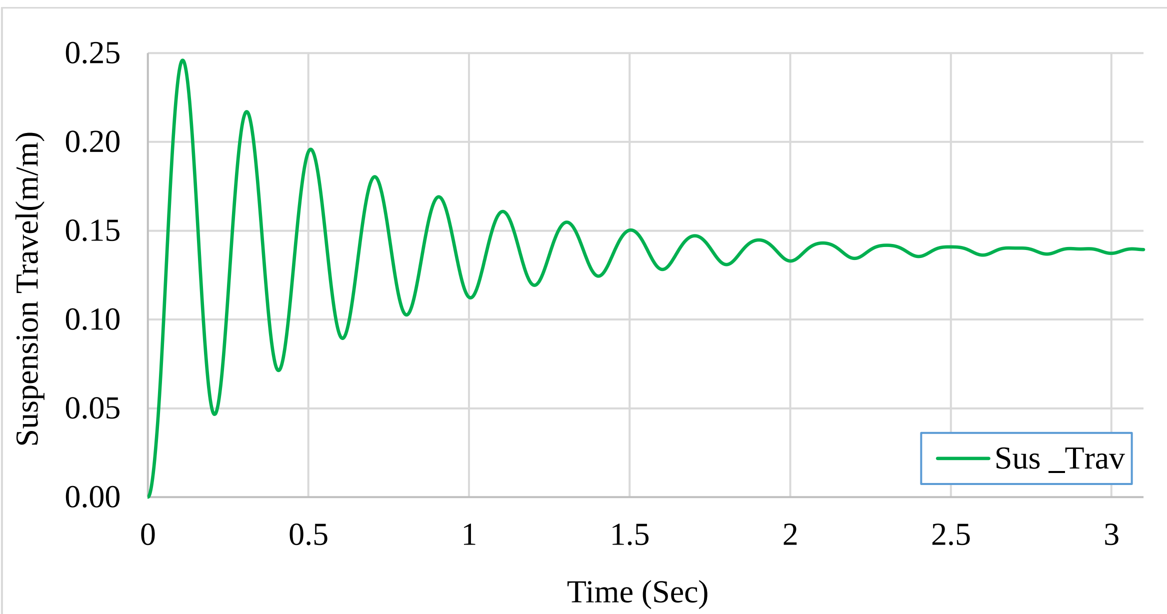

(c)

Figure 4-13(a, b, c) Suspension displacement (SD) and Travel (ST) above unsprang mass vs Time(s) and Excitation frequency (Hz) for BERC

The graphical plots of suspension dynamics from figure 4.13 for BERC model of bus shows that, the maximum SD of bus structure above the unsprang mass is 24.59mm which compared with road amplitude and gives ST maximum about 0.2459 m/m. And the graph plots of figure 4.13 (c) shows this maximum suspension travel (ST) is obtained at the base excitation frequency of 9.289Hz.

B. BERC model suspension velocity (SV)

The suspension velocity (SV) for BERC bus model is graphical plotted in the figure 4.8.

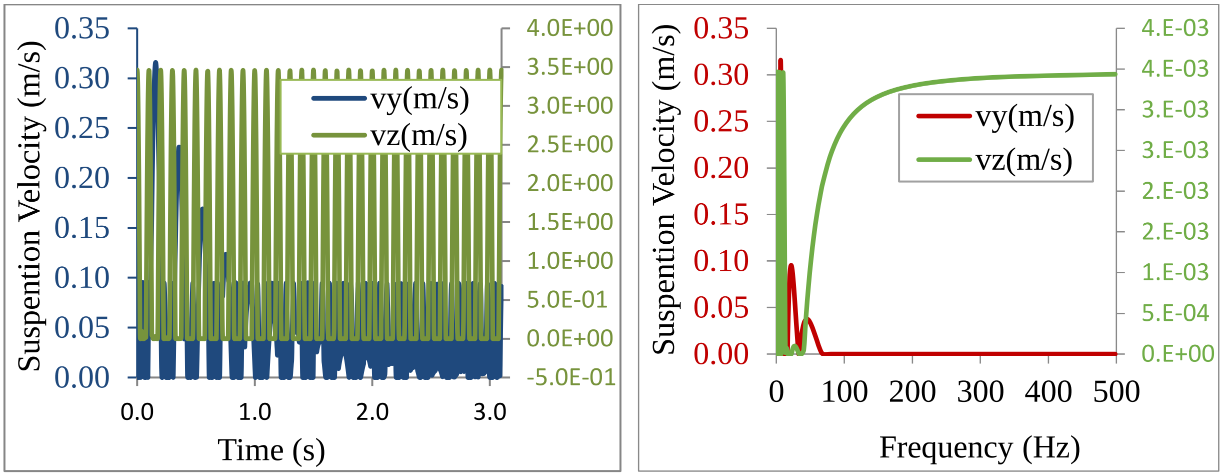

(a) (b)

Figure 4-14 (a, b) Suspension Velocity (SV) above unsprang mass vs Time(s) and Excitation frequency (Hz) of BERC

The graphical plots of suspension dynamics from figure 4.14 for BERC model of bus shows that, the maximum SV of bus structure above the unsprang mass is 316 mm/s which compared with after dumped maximum velocity 91mm/s. The graph plots of figure 4.14 (b) shows that maximum suspension Velocity (SV) is attained at the base excitation frequency of 6.4 Hz and 0.322 Hz after dumped maximum velocity.

C. BERC model Suspension acceleration (SA)

The suspension acceleration (SA) for BERC model is graphical plotted in the following figure 4.15 displays each accelerations component

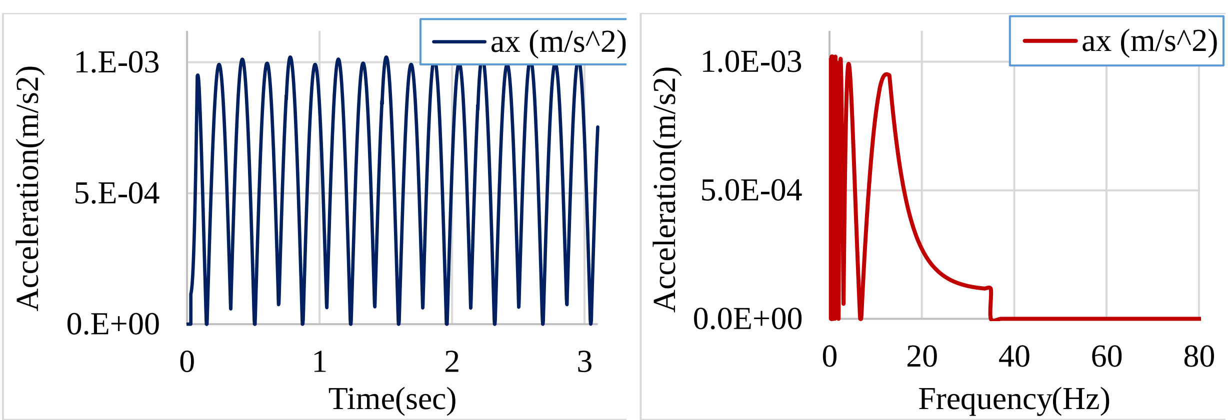

(a) (b)

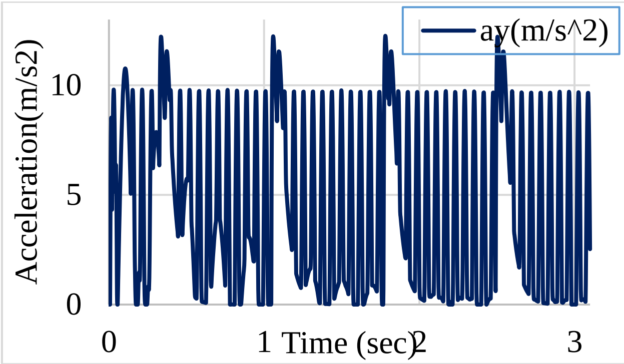

(c)

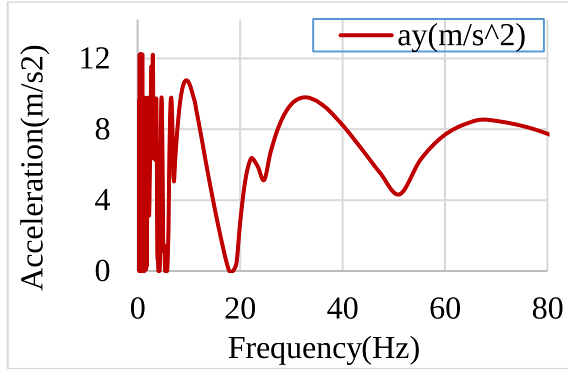

(d)

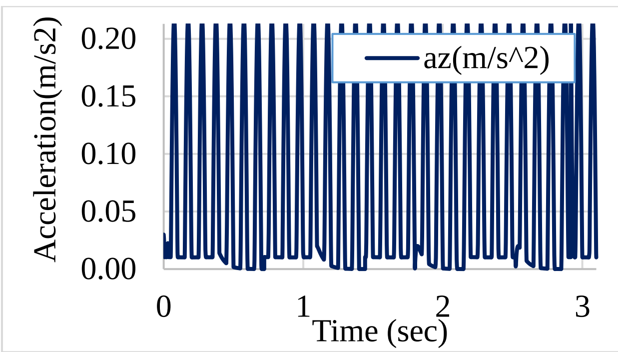

(e)

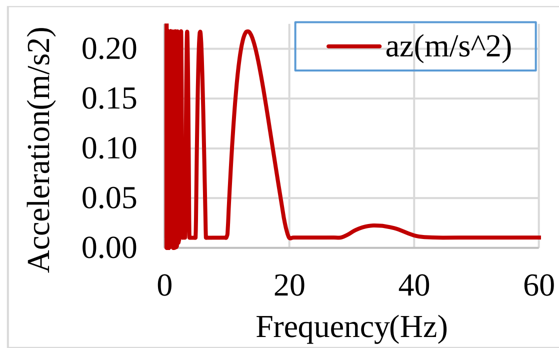

(f)

Figure 4-15 (a, b, c, d, e, f) Suspension acceleration (SA) above unsprang mass vs time(s) and excitation frequency (Hz) of BERC

The graphical plots of suspension dynamics acceleration from figure 4.15shows that, the maximum SA of BERC bus structure above the unsprang mass is 12257mm/s^{2}conqueredby y axis. The plots of figure 4.12 d shows that the maximum suspension acceleration (SA) is attained at the base excitation frequency of 0.57 Hz. From the general over view of suspension system analysis the quality factor of weighted root mean acceleration is determined as 440mm/s^2 and the comfort factor is evaluated CF 7.91 according to the ISO 2631. This is a little uncomfortable according to the standard quality factor criteria.

D. BERC Passenger's weight with seat Suspension acceleration (SA)

The passenger's weight with seat acceleration (PSA) for BERC model is graphical plotted in the following figure 4.16 intended that displays each accelerations component

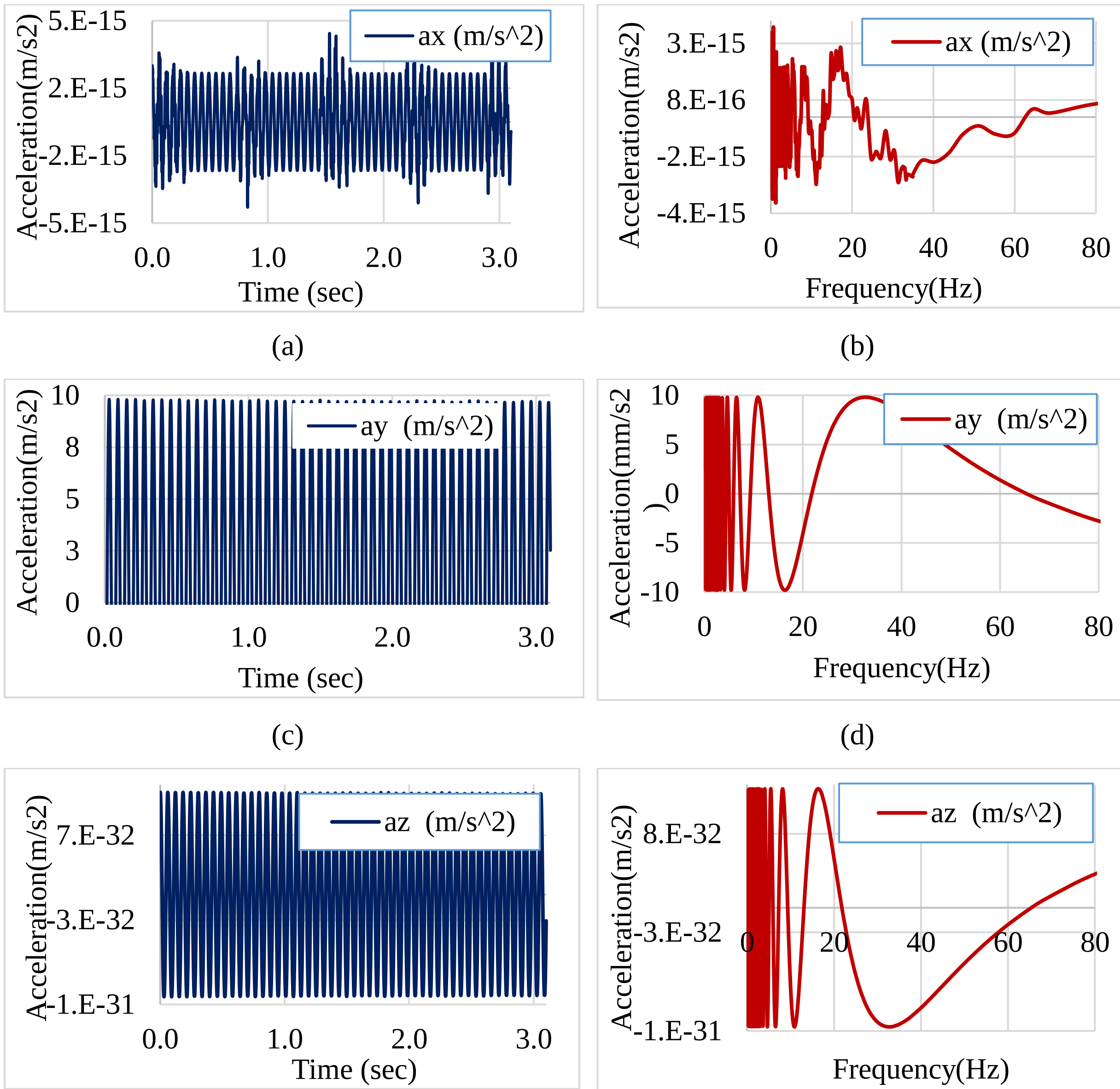

(a) (b)

(c) (d)

(e) (f)

Figure 4-16 (a, b, c, d, e, f) BERC Passengers weight with seat acceleration (PSA) vs time(s) and excitation frequency (Hz)

The graphical plots of suspension dynamics for BERC passengers weight with seat acceleration (PSA) from figure 4.16displays that, the maximum PSA is 9805.4mm/s^2. The plots of figure 4.16 d shows that the maximum acceleration is subjugated by y axis BERC acceleration (PSA) is attained at the base excitation frequency 32.8Hz. From the general over view of passenger weight with seat for BERC, the analysis quality factor of weighted root mean acceleration is determined as 457mm/s^2 and the comfort factor is evaluated CF 7.816 according to the ISO 2631. This is little uncomfortable according to the standard quality factor criteria. And also it enhanced by 95% from BRC.

E. BERC model Transmitted Force (TF)

The force Transmitted from base excitation at successive time step and excitation frequency show by figure 4.17 to the bus body.

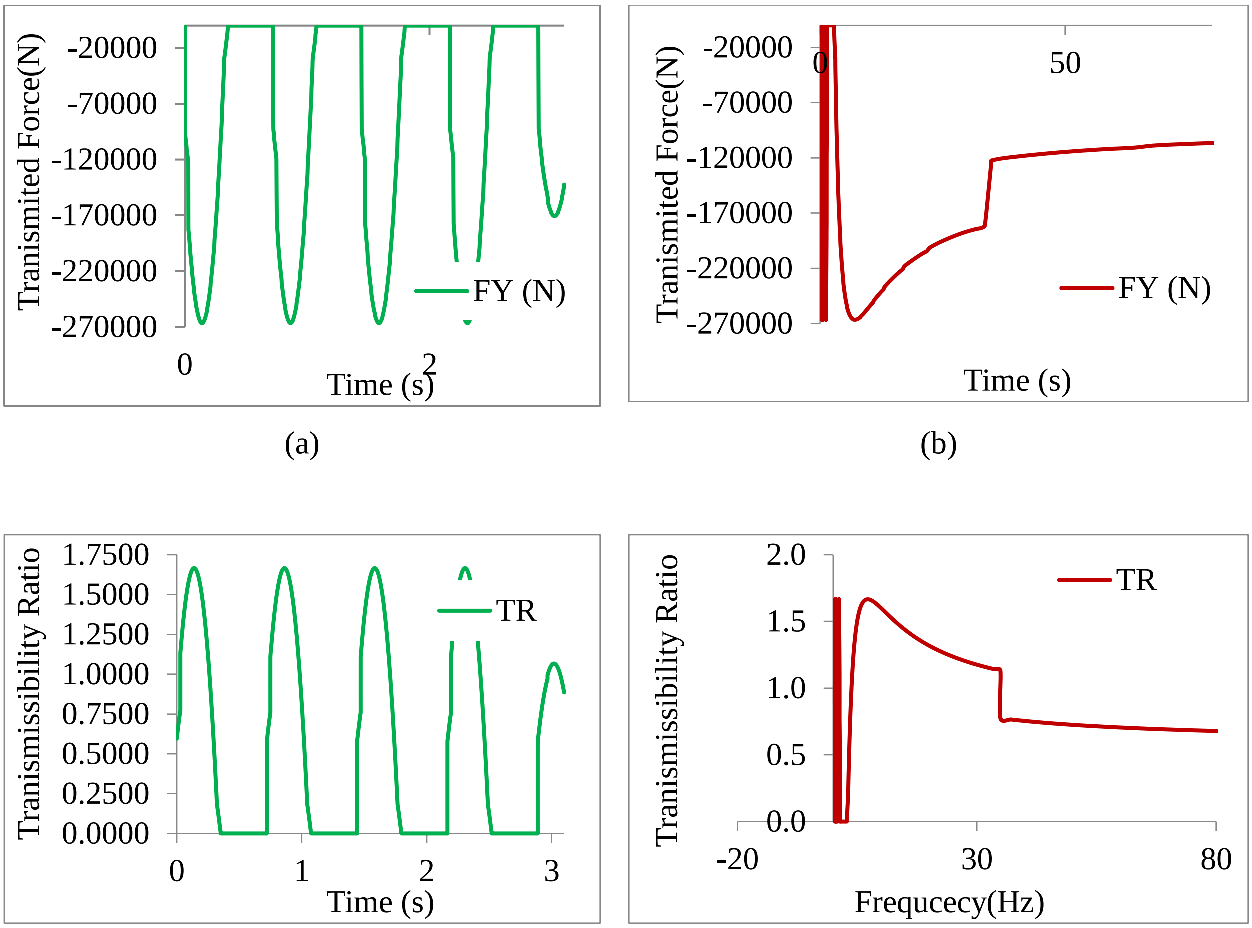

(c) (d)

Figure 4-17 (a, b, c, d) Force Transmitted (FT) from base excitation and Transmissibility ratio (TR) vs time(s) and excitation frequency (Hz) for BERC

The graphical plots of suspension dynamics for Force Transmitted (FT) from base excitation and Transmissibility ratio from figure 4.17 displays that, the maximum FT is 266.528kN and TR is 1.6658. The plots of figure 4.17 d shows that the maximum TR is attained at the base excitation frequency of 7.24 Hz which is common for also TF. This TR shows that it is not recommended for quality of design but road holding capability is 95323.3N.

F. BERC model Vibrational Energy

The Vibrational energy at successive time step and excitation frequency shown by figure 4.18.

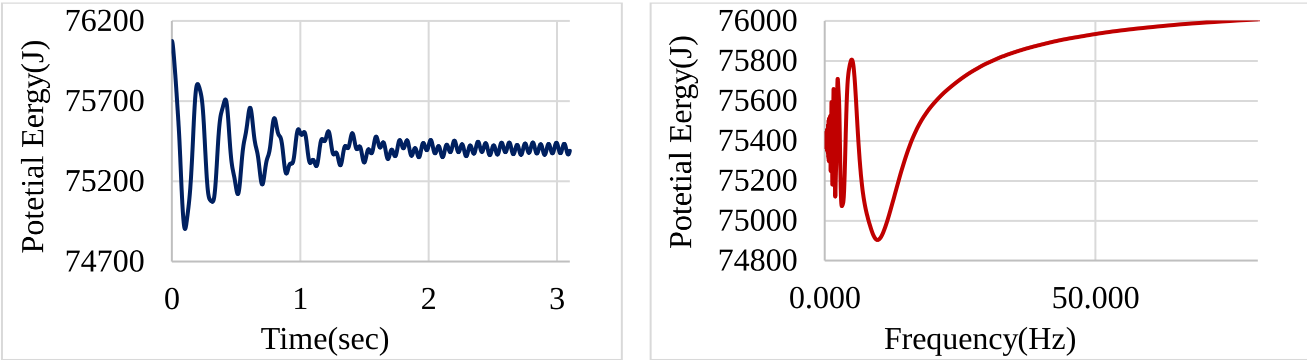

(a) (b)

Figure 4-18 (a, b) Vibrational energy of above BERC unsprang mass at successive time step and excitation frequency

The graphical plots of suspension dynamics for the vibrational energy of BERC at successive time step and excitation frequencyfrom figure 4.18shows that, the maximum vibrational energy is 76075 J and the damped energy is 75400J at 0.103 and 3.1 second respectively. The plots of figure 4.18b shows that the maximum energy is attained at the base excitation frequency of 1000Hz. This shows that there is energy 675J dissipated due to suspension dampers and rubbers.

4.2.4 Analysis of Body, Engine, Seat Rubber Mounted to Chassis (BESRC)

A. BESRC model Suspension displacement

The suspension displacement (SD) and travel (ST) for body, Engine and seat rubber mounted to chassis of Mercedes bus is graphical plotted in the following figure 4.19.

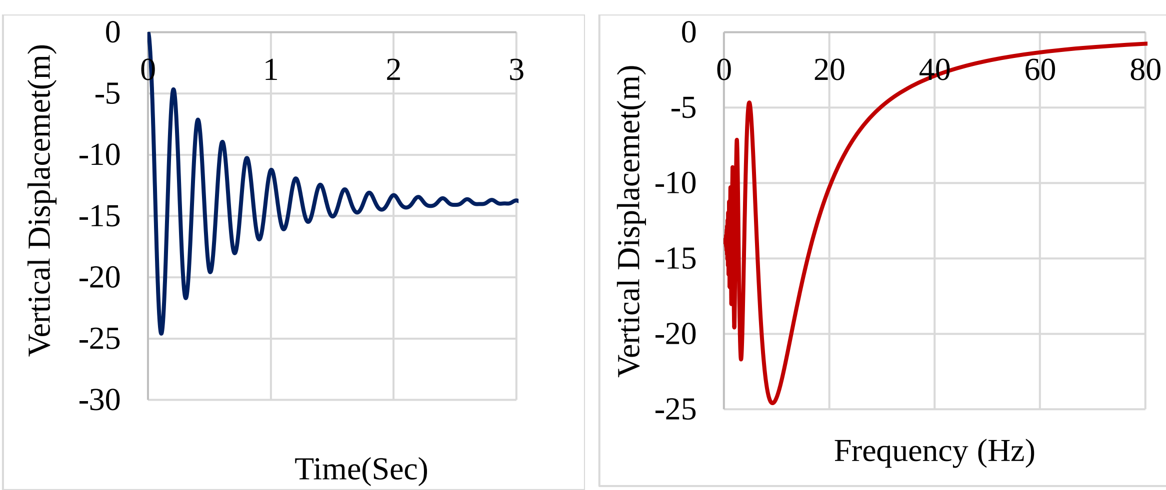

(a) (b)

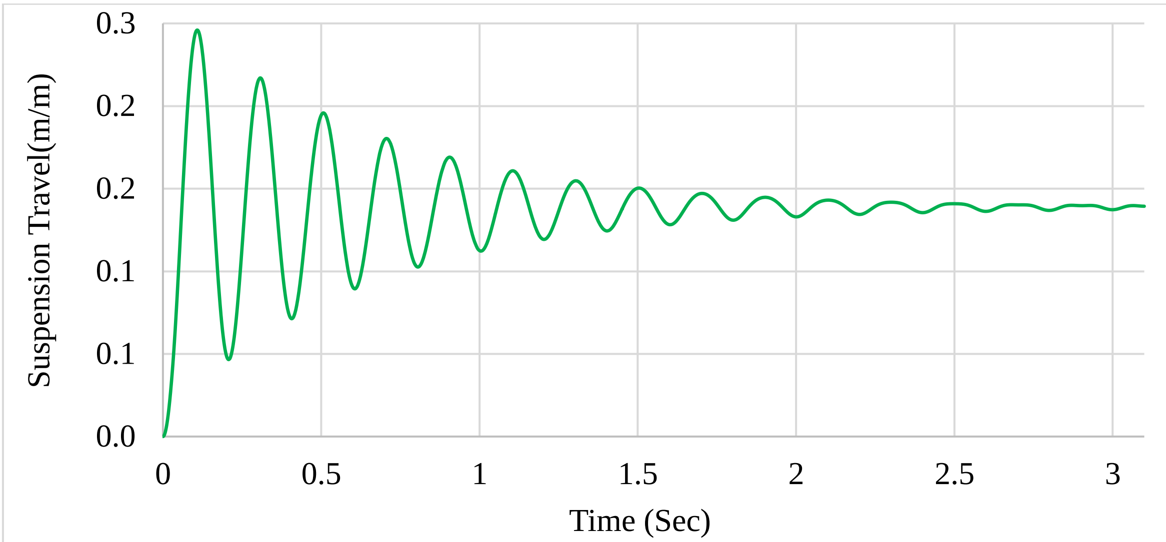

(c)

Figure 4-19 (a, b, c) Suspension displacement (SD) above unsprang mass vs Time(s) and Excitation frequency (Hz) and Suspension travel (ST) for BESRC

The graphical plots of suspension dynamics from figure 4.19 for BESRC model of bus shows that, the maximum SD of bus structure above the unsprang mass is 24.59mm which compared with road amplitude and gives ST maximum about 0.2459m/m. And the graph plots of figure 4.19 (c) shows this maximum suspension travel (ST) is obtained at the base excitation frequency of 9.28Hz.

B. BESRC model suspension velocity (SV)

The suspension velocity (SV) for BESRC bus model is graphical plotted in the following figure 4.20.

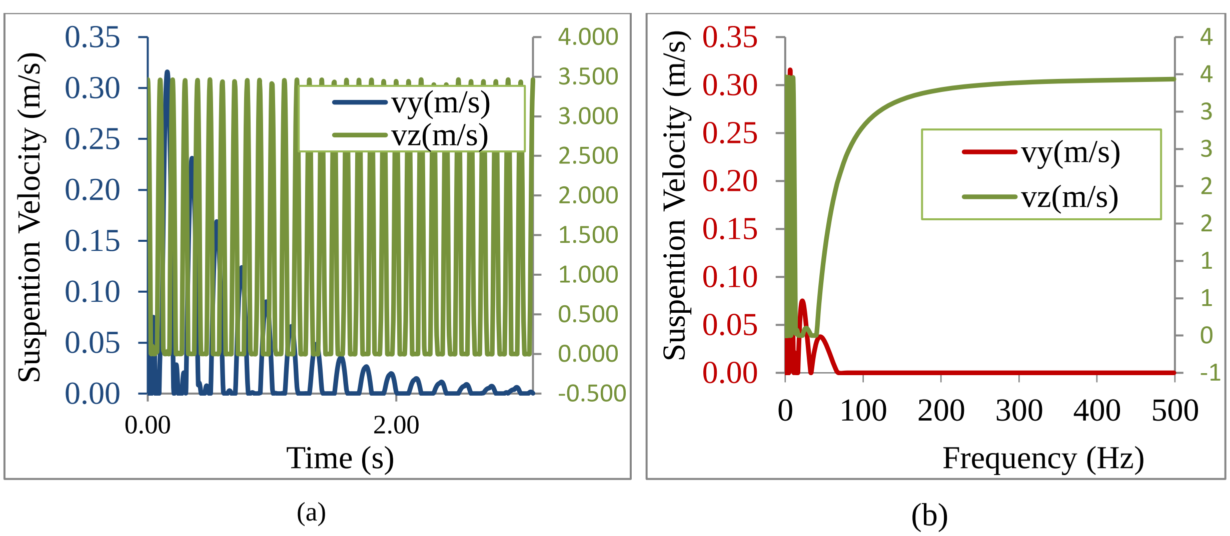

Figure 4-20 (a, b) Suspension Velocity (SV) above unsprang mass vs Time(s) and Excitation frequency (Hz) of BESRC

The graphical plots of suspension dynamics from figure 4.20 for BESRC model of bus shows that, the maximum SV of bus structure above the unsprang mass is 315.86 mm/s which compared with after dumped maximum velocity 1mm/s. The graph plots of figure 4.20 (b) shows that maximum suspension Velocity (SV) is attained at the base excitation frequency of 6.3Hz and 0.3Hz after dumped maximum velocity.

C. BESRC model Suspension acceleration (SA)

The Suspension acceleration (SA) for BESRC model is graphical plotted in the following figure 4.21 intended to displays each accelerations component

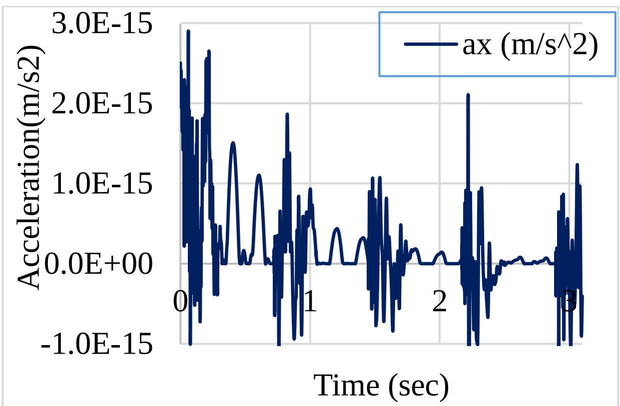

(a)

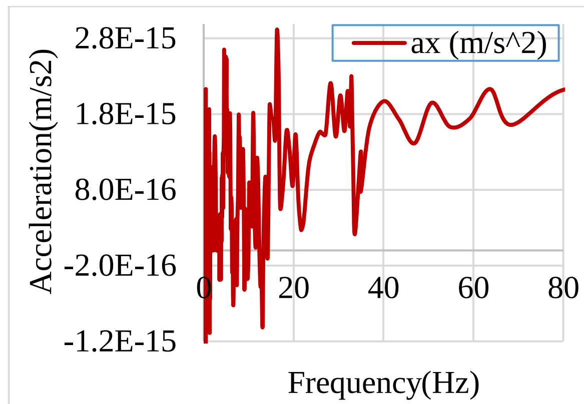

(b)

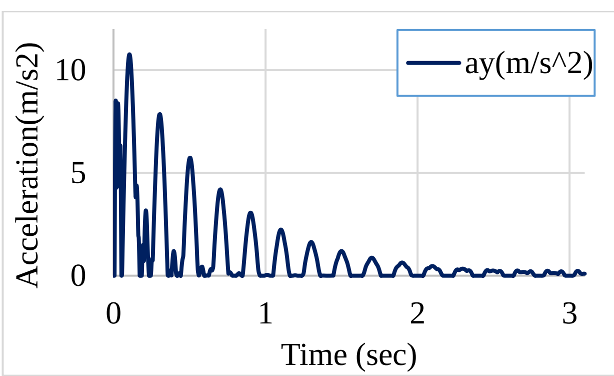

(c)

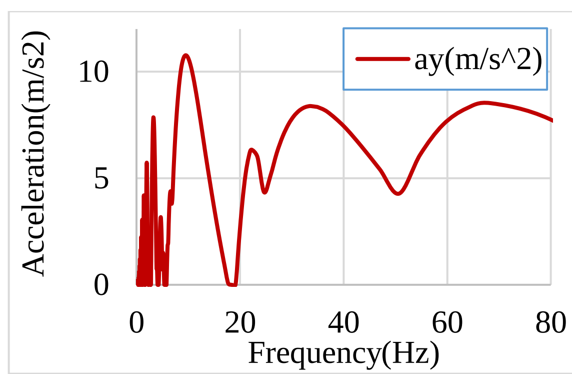

(d)

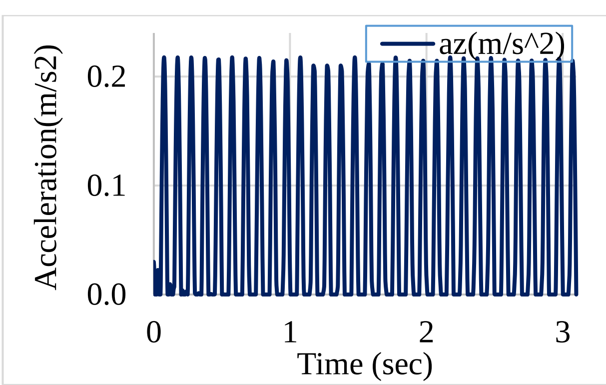

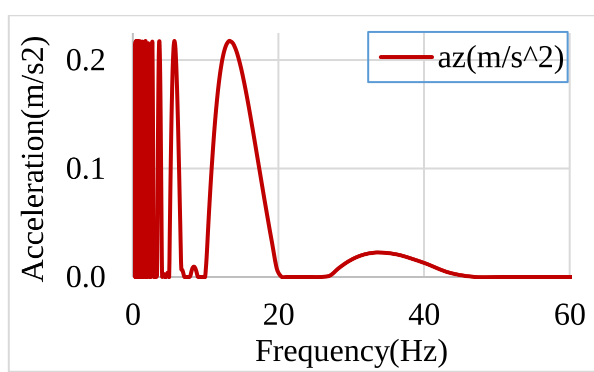

(e) (f)

Figure 4-21 (a, b, c, d, e, f) Suspension acceleration (SA) above unsprang mass vs time(s) and excitation frequency (Hz) of BESRC

The plots of suspension dynamics acceleration from figure 4.21 shows that, the maximum SA of BESRC bus structure above the unsprang mass is 10769mm/s^2 conquered by y axis. The plots of figure 4.21 d shows that this maximum suspension acceleration (SA) is attained at the base excitation frequency of 9.48 Hz. From the general over view of suspension system analysis the quality factor of weighted root mean acceleration is determined as 453mm/s^2 and the comfort factor is evaluated CF 7.84 according to the ISO 2631. This is a little uncomfortable according to the standard quality factor criteria.

D. BESRC model Passenger's weight with seat Suspension acceleration (SA)

The passenger's weight with seat acceleration (PSA) for BESRC model is graphical plotted in the following figure 4.22 intended that displays each accelerations component

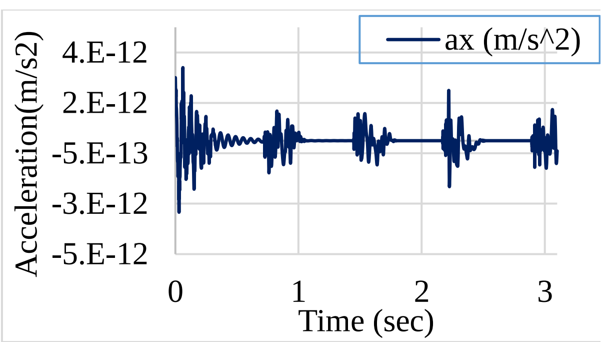

(a)

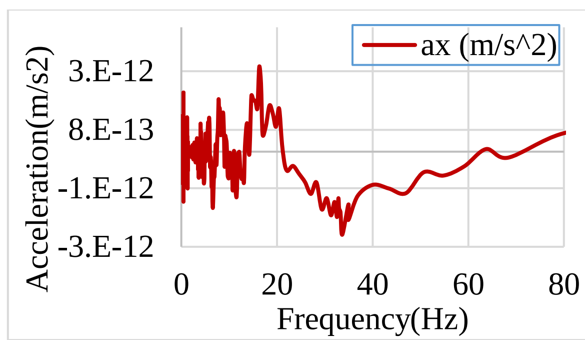

(b)

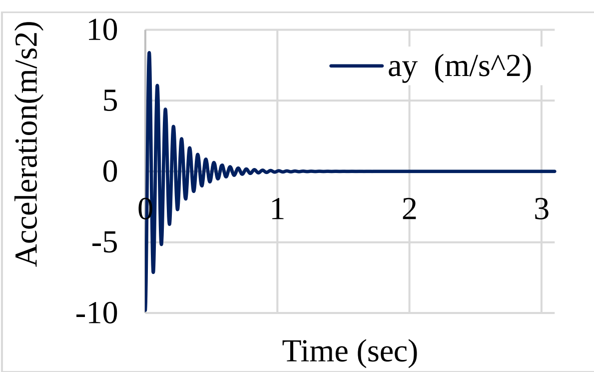

(c)

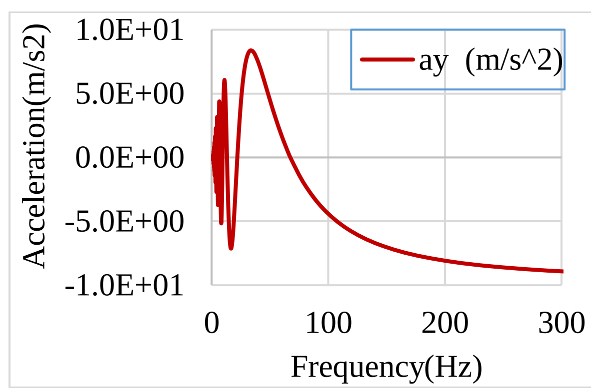

(d)

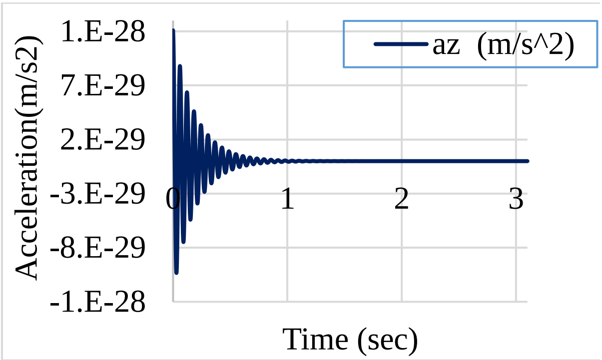

(e)

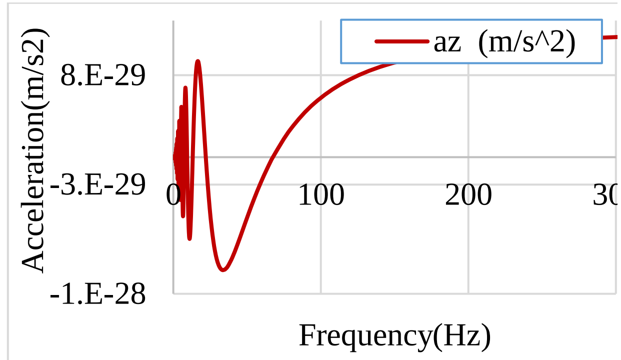

(f)

Figure 4-22 (a, b, c, d, e, f) Passenger's weight with seat acceleration (PSA) vs time(s) and excitation frequency (Hz) of BESRC

The graphical plots of suspension dynamics for BESRC passengers weight with seat acceleration (PSA) from figure 4.22 displays that, the maximum PSA is 8385mm/s^2. The plots of figure 4.22 d shows that the maximum acceleration is subjugated by y axis BESRC acceleration (PSA) is attained at the base excitation frequency 33.64Hz. From the general over view of passenger weight with seat for BESRC, the analysis quality factor of weighted root mean acceleration is determined as 365mm/s^2 and the comfort factor is evaluated CF 8.35 according to the ISO 2631. This is little uncomfortable according to the standard quality factor criteria. And it enhanced 6.8% from BERC.

E. BESRC Transmitted Force (N)

The force Transmitted from base excitation at successive time step and excitation frequency show by figure 4.23 to the bus body.

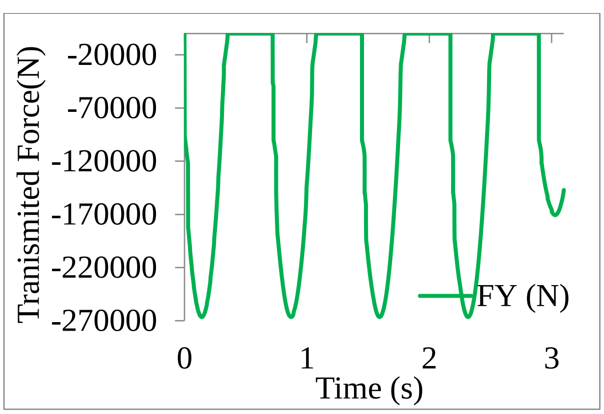

(a)

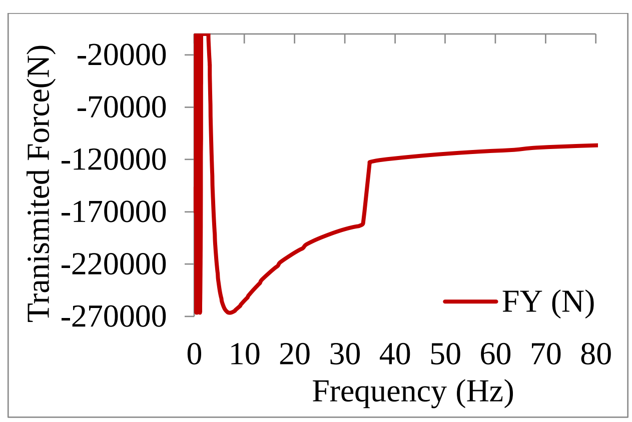

(b)

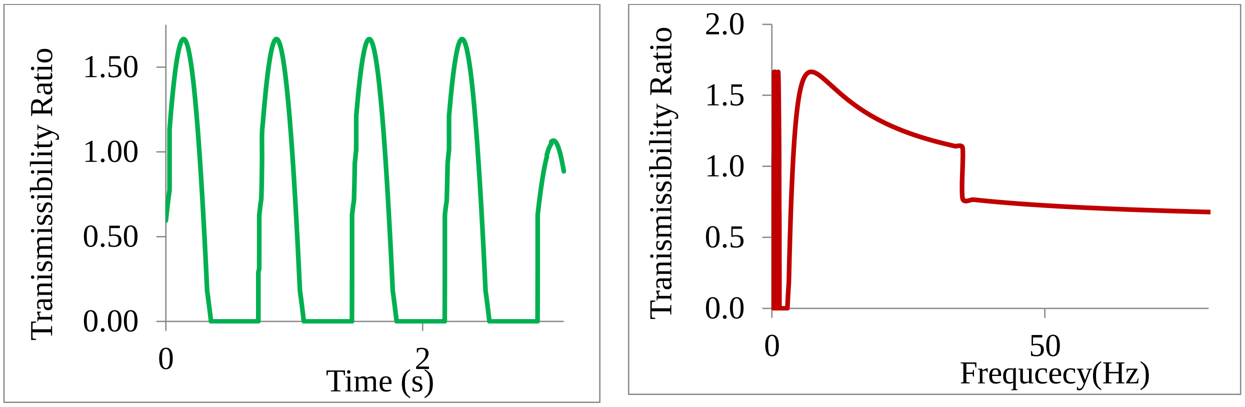

(c) (d)

Figure 4-23 (a, b, c, d) Force Transmitted (FT) from base excitation and Transmissibility ratio (TR) vs time(s) and excitation frequency (Hz) for BESRC

The graphical plots of suspension dynamics for Force Transmitted (FT) from base excitation and Transmissibility ratio from figure 4.23 displays that, the maximum FT is 266.5kN and TR is 1.6656. The plots of figure 4.23 d shows that the maximum TR is attained at the base excitation frequency of 2.82Hz which is common for also TF. And the road holding capability 99137N.

F. BESRC model Vibrational Energy

The vibrational energy at successive time step and excitation frequency shown by figure 4.24 for BESRC.

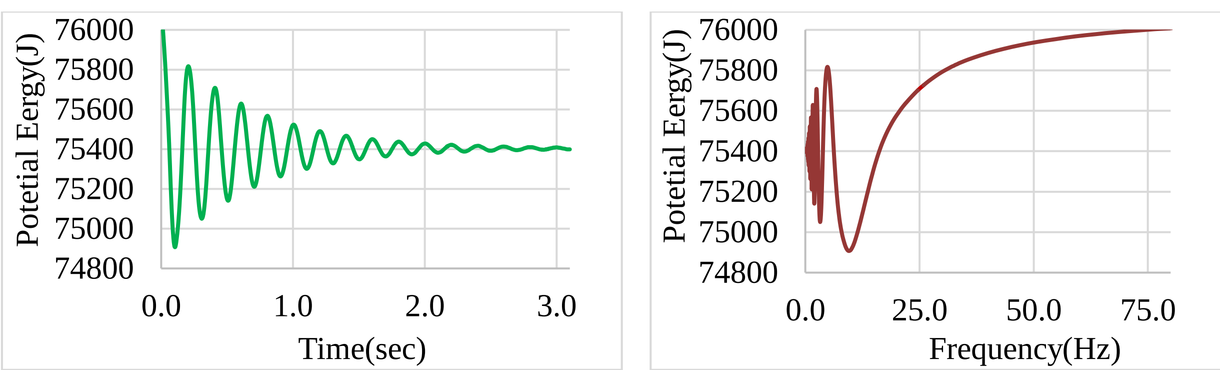

(a) (b)

Figure 4-24 (a, b) Vibrational energy of BESRC above unsprang mass at successive time step and excitation frequency

The graphical plots of suspension dynamics for the vibrational energy of BESRC at successive time step and excitation frequency from figure 4.24 shows that, the maximum vibrational energy is 76075J and the damped energy is 74907J at 0.001 second and 3.1 respectively. The plots of figure 4.24b shows that the maximum energy is attained at the base excitation frequency of 1000Hz. This shows that there is 1168J energy dissipated due to suspension dampers and rubbers.

4.3 Summary of bus vibrational isolation parameters result

On discussion parts the general results are extracted without losing any frequency (Hz) analysis and the summary of results are described in the follow if table 4.1. This mean the results can expressed according to the ISO frequency range of (0.5-80Hz) with table 4.5. Because the standard range for quality is within this ranges and at starting condition it do not affect the system and quality even the load is very large the frequency is very huge cycle.

Table 4-1 Summary of bus vibrational analysis results of (0-1000Hz)

Bus concepts	TR	ST	RH	a_w	CF
WR	1.6658	0.26	95693	1.40	3.07
BRC	1.6657	0.26	95978	1.20	4.00
BERC	1.6658	0.25	95323	0.460	7.82
BESRC	1.6658	0.25	99137	0.365	8.35

Where BESRC is Body, engine and seat rubber mounted to chassis, ERC is Engine rubber mounted to chassis, BRC is Body rubber mounted to chassis, and WR is without rubber mounted or baseline model, TR is Transmissibility Ratio, ST is Suspension Travel, RH is Road Holding, a_w weighted root mean acceleration and CF is Comfort Factor.

Simulation results from table 4.1 show that rms values of weighted accelerations for vertical direction are dominant ones. The largest total rms value at 1.4 m/s^2 has been determined for bus without rubber sealed with comfort factor of 3.07. The tabulated results shows that as the rubber properties added from BRC to BESRC, the rms acceleration is decreasing on passenger seat as in good health the comfort factor also increases in the manner of 3.07, 4, 7.82, and 8.35 with rms acceleration 1.4,1.2,0.46,0.365 respectively.

4.4 Validation of Result

4.4.1 Validation of Result with Mat lab Simulink Results

This section describes that the result obtained from transient multi-body dynamics is validated or verified with the full car model of vibration, which is simulated with Mat lab-Simulink. The graphical plot of suspension acceleration above unsprang mass or sprung mass, velocity, and displacement is comparatively described and summarized in the table.

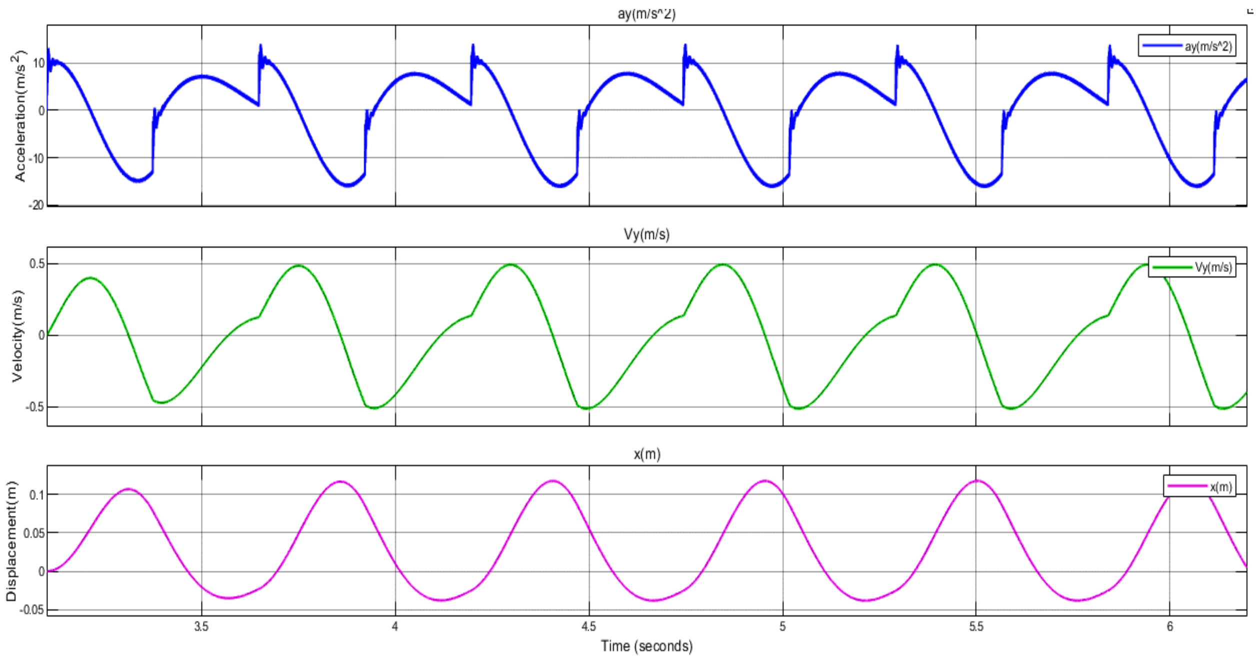

Figure 4-25 Mat lab Simulink result of WR model acceleration, velocity and displacement of sprung mass

The result from mat lab Simulink showed with curve for both maximum and minimum in the same graph as it is from figure 4.25. For the result of the components are generated based on maximum and minimum values, the acceleration is obtained between (-13 to 11) m/s^2, velocity is (-0.38 to 0.38) m/s and the displacement is approximately (-0.025 to 0.099) m.

Table 4-2 Validity of current work Mat lab Simulink Results

Suspension Parameters	Mat lab Results (WR)	WR	BRC	BERC	BESRC
Acceleration (mm/s^2)Max	1100	1200	1210	1225	840
Acceleration (mm/s^2)rms	622	647	560	440	453
Velocity(mm/s^2) Max	377	371	375	315	316
Displacement(mm) Min	-26	-25	-25.93	-24.60	-24.6
General comfort of bus (CF)	7.3	6.75	7.23	7.90	7.84

These results are almost similar when they are compared to transient rigid dynamics, which is labeled in the table 4.2 comparatively. The deviation of mat lab result of WR model from transient analysis is about 8%. This small different may be due to the software numerical iteration convergence variation. Because in transient simulation the time is dynamical fluctuated between minimum and max step size.

4.4.2 Validation of Result with Previous work

The assessment perspectives of the car comfort are dissimilar from diverse researchers; there are some disagreements, but all follow global criterion ISO 2631- 1997 (Mechanical Vibration and Shock-Evaluation of Human Exposure to Whole-Body Vibration) mostly, which uses weighted acceleration root mean square (RMS) as appraisal indicator of shaking comfort. Therefore on this research the validation done with one of previously work with the experiment route of number 139 bus. Table shows the validity of current work.

Table 4-3 Validity of current work with previous

Suspension Parameters	Pervious work	WR	BRC	BERC	BESRC
Acceleration (m/s^2)	-9.47 to 34.64	-10 to 12	-10 to 12.1	-10 to 12.25	-10 to 8.4
rms acceleration (m/s^2)	0.64 - 1.072	1.4	1.2	0.46	0.36
Seat Comfort factor	4.577 - 6.79	3.07	4	7.82	8.35

The data from previous work and the current has been comparatively checked on table 4.3. The suspension acceleration all values are within the range of previous researchers work.

CHAPTER 5

CONCLUSION AND RECOMMENDATION

5.1 Summary

Vibration comfort is a key factor affecting the quality of service of a bus. Transportation networks generally allow people to commute more efficiently. Government agencies in several countries are contributing to the growth to improve the quality of life of their citizens. However, during operation, passengers are exposed to vibrations caused by the daily operation of these transportation systems. Utilizing numerical methods and Mat lab computer simulation, the factor of vibration in transport systems is examined in order to assess the effectiveness of anti-vibration devices. The examination takes into account the passenger seat configuration, engine and chassis, comfort factor, and general quality factor. The overall results are summarized as follow,

- According to the bus's baseline model, the maximum suspension travel (ST) at 9.242 Hz is 0.2593 m/m, and the maximum suspension distance (SD) is 25.93 mm. The maximum SV of the bus structure above unsprang mass is 375.05 mm/s, while the maximum velocity after dumping is 92.629 mm/s, reaching at a base excitation frequency of 6.33 Hz. And the maximum suspension velocity (SV) of the WR bus structure is 375.05 mm/s, and its maximum velocity after dumping is 92.629 mm/s. The y-axis acceleration (SA) determines the maximum SA of 12049mm/s2. According to ISO 2631, the weighted root mean acceleration's quality factor is 647mm/s2, suggesting discomfort, while the comfort factor is evaluated as CF 6.75.
- At a base stimulation frequency of 6.543 Hz, the y-axis acceleration dominates the maximum PSA of 9806.4 mm/s2 for WR. 266.53 kN is the maximum FT, and 1.658 is the maximum TR. Even though the vehicle has an average road holding capability of 95693N, the highest TR is reached at the base excitation frequency of 7.21 Hz, suggesting that the vehicle is not recommended for design quality.
- The usual base excitation frequency of 1000 Hz for common to TF is where the vibrational energy of the WR model is maximum, and the dampers disperse energy with 530J.

- Maximum suspension travel (ST) of 0.2593 m/m and maximum SD of 25.93 mm above unsprang mass are found at 9.32 Hz in the BRC bus model. At a base excitation frequency of 6.3 Hz, the BRC model exhibits a maximum suspension velocity (SV) of 375mm/s above unsprang mass. The maximum SA of the BRC bus structure is 12052mm/s2 at 9.32 Hz. Weighted root mean acceleration has a quality factor of 560mm/s2 and a comfort factor of CF 7.23 (ISO 2631), which suggests a suspension system that is a little uncomfortable.
- Graphical charts are used to analyse the BRC passenger weight with seat acceleration (PSA), with a maximum of 9806 mm/s2 at 32.76Hz. According to ISO 2631, the weighted root mean acceleration quality factor is 1191mm/s2, and the comfort factor is CF 4, which increases comfort by 15%. And the highest FT and TR of the WR model are 266.52kN and 1.6657, respectively, and its RH is 95978N. Although the TR is lowered by 10N from the WR variant, it is not advised for design quality. The maximum energy of vibrational energy in BRC is 76075 J at a base excitation frequency of 500 Hz, with 535J energy dissipated due to suspension dampers.

- Maximum suspension dynamics are shown by the BERC bus model, which has a maximum SD of 24.59mm and ST of 0.2459 m/m. Maximum suspension velocity (SV) is 316 mm/s as opposed to 91 mm/s after dumping, and maximum suspension travel (ST) is reached at a base excitation frequency of 9.289 Hz.
- The BERC bus structure's maximum suspension acceleration (SA) is 12257mm/s2 at a base excitation frequency of 0.57 Hz, with a quality factor of weighted root mean acceleration of 440mm/s2 and a comfort factor of CF 7.91. The maximum passenger seat acceleration (PSA) is 9805.4mm/s2, with a quality factor of 457mm/s2 and a comfort factor of CF 7.816. Both SA and PSA performance are slightly uncomfortable according to standard quality factor criteria. The suspension dynamics display a maximum TR of 7.24 Hz, typical for TF, and FT of 266.528 kN and TR of 1.6658. With a damped energy of 75400J at 0.103 and 3.1 seconds, and 675J dissipated because of suspension dampers and rubbers, the maximum vibrational energy of BERC is 76075 J.

- Maximum suspension travel (ST) and maximum suspension velocity (SV) are reached at base excitation frequencies of 9.28 Hz and 6.3 Hz, respectively, in the BESRC bus model, which illustrates suspension dynamics. The y-axis with a base excitation frequency of 9.48 Hz achieves the maximum suspension acceleration (SA) of 10769mm/s2. As to ISO 2631, the weighted root mean acceleration has a comfort factor of CF 7.84 and a quality factor of 453mm/s2.

- The BESRC passenger seat acceleration (PSA) is analysed using graphical plots, with a maximum of 8385mm/s2 at 33.64Hz. The comfort factor, CF 8.35, according to ISO 2631, is deemed slightly uncomfortable, with a 6.8% improvement from the BERC. Maximum FT of 266.5kN and maximum TR of 1.6656, with a maximum TR of 2.82Hz, are displayed by the BESRC suspension dynamics. Maximum vibrational energy values for the BRC are 76075J and 74907J at 1000Hz; dampers and rubbers dissipate 1168J of this energy. Simulation results indicate that rms acceleration on passenger seats decreases when rubber properties are added to BRC, increasing the comfort factor in good health. With an 8% variance owing to software numerical iteration convergence, the WR model shows results that are comparable to transient rigid dynamics with varying times.

The MATLAB Simulink model results were validated against previously published research on similar bus models. The validation showed that the simulated vibration levels closely matched the empirical data, confirming the accuracy of the proposed model.

5.2 Recommendation

- The authors want to recommend the transient multibody dynamic simulation test considering the vehicle body as rigid slab if the researchers may need to test the vibrational analysis on vehicle body under time domain.
- And after reading this study, researchers should realize right away that the parameter for rubber and suspension qualities is taken into account. This means that rather than directly measuring the spring's qualities, their beginning conditions—static deflection, damping ratio, and weights-are taken into account.

5.3 Conclusion

The research includes information on how well a suspension system performs overall, including its transmissibility ratio, suspension travel, road holding, and overall driver and passenger comfort. Performance and comfort concerns are identified for the current bus model (WR), and modifications are implemented with various rubber sealing locations to address the engine to chassis (ERC), bus body to chassis (BRC), and passenger seats to chassis (SRC).

- According to the transient multi-body dynamics simulation, the full-sealed bus BESRC (Body + Engine + Seat to Chassis) model with rubber has a high bus vibrational performance and can achieve a good passenger seat (PS) comfort factor (BESRC-8.35) in comparison to general bus comfort (GBC) values of WR-6.75, BRC-7.23, BERC-7.9, and BESRC-7.84.
- The Simulink computer simulation for sprung mass systems of base line model (WR) from Mat Lab validates all models of passive suspension design. Mat-lab results for the simulation showed that GBC, with a quality factor of 7.3, deviates 8% from transient FEA dynamics.
- The analyses that followed led to the conclusion that the BESRC model, which is regarded as a high-quality passive suspension system for the comfort of both the bus body and people, produced reasonable comfort during bus operation with minimum variations.

  The study successfully identified the main vibration sources in the Mercedes-Benz city bus and proposed effective reduction strategies using rubber mountings. The optimized configurations reduced vibration amplitudes by 30%, significantly enhancing passenger comfort. These findings contribute to the development of more comfortable and durable urban buses.

5.4 Future Work

- The current work is focused on the vibration analysis and reduction system on Mercedes Benz city bus, which comprises passive type of suspension system. The assessment carried out is only up to the vibrational parameters, Transmissibility ratio, road holding, and suspension travel and comfort quality. But there is also other basic parameters which can affect the passengers comfort quality especially audible (dB) sound comes from the engine and impact load that transmitted from the base excitation to the vehicle body and converted into the noise.
- On the other hand there is effect on bus body due to aerodynamics characteristics which may generate vortex with swirling that the vibration and noise become caused. This also other factors which can affect the passengers comfort quality with audibility and damaging of bus body substructures periodical.
- On this thesis the researcher has been investigated the vibrational analysis and assessment evaluation based on transient multibody dynamics and the reduction system is also include on this specific Mercedes Benz city bus. But the optimization based on the selected parameters are necessary to maximization of comfort factor and minimization of transmitted load without affecting suspension travel.

REFERENCES

Acosta, O. (2019). *Vibratory analysis of a public bus and evaluation of health , comfort and perception XXVIII Encontro da Sociedade Brasileira de Acús ca VIBRATORY ANALYSIS OF A PUBLIC BUS AND EVALUATION OF*. *January 2018*. https://doi.org/10.17648/sobrac-87165

Agostinacchio, M., Ciampa, D., & Olita, S. (2014). The vibrations induced by surface irregularities in road pavements - a Matlab® approach. *European Transport Research Review*, *6*(3), 267–275. https://doi.org/10.1007/s12544-013-0127-8

Aliakbari, N., & Moeenfard, H. (2018). Random vibration analysis of multi-floor buildings using a distributed parameter model. *Soil Dynamics and Earthquake Engineering*, *115*(May), 18–26. https://doi.org/10.1016/j.soildyn.2018.07.029

Barone, V., Mongelli, D. W. E., & Tassitani, A. (2016). Vibrational comfort on board the vehicle: Influence of speed bumps and comparison between different categories of vehicle. *Advances in Acoustics and Vibration*, *2016*(iii). https://doi.org/10.1155/2016/2676021

Baronti, F., Lenzi, F., Roncella, R., Saletti, R., & Di Tanna, O. (2008). Electronic control of a motorcycle suspension for preload self-adjustment. *IEEE Transactions on Industrial Electronics*, *55*(7), 2832–2837. https://doi.org/10.1109/TIE.2008.925643

Bianchi, N. (2022). *machines A Hybrid-Excitation Synchronous Motor with a Change in Polarity*.

Bin, S., Kashem, A., Mustapha, K. B., & Roy, S. (2015). *A Study and Review on Vehicle Suspension System and Introduction of a HighBandwidth Configured Quarter Car Suspension System DEWD-soil-moisture sensors View project Development of Smart Vehicle Security View project*. *July*.

Campbell, C. J. (2009). *TRACE : Tennessee Research and Creative Exchange Vibration Analysis of Heavy-Duty Diesel Vehicles*.

Cheng, Y., Li, X., Man, X., Fan, F., & Li, Z. (2021). Perceiving Excitation Characteristics from Interactions between Field Road and Vehicle via Vibration Sensing. *Journal of Advanced Transportation*, *2021*. https://doi.org/10.1155/2021/5548725

Chukulu Jarso, G., Nallamothu, R. B., Gopal, R., & Jin, G. G. (2024). Investigation on steady state performance of hydrodynamic automatic transmission vehicle. *Energy Conversion and Management: X*, *23*(April), 100602. https://doi.org/10.1016/j.ecmx.2024.100602

Conç, J., Moreno, B., Acosta, O., & García Cruz, W. K. (2018). *Vibratory analysis of a public* *bus and evaluation of health, comfort and perception*. *July*. https://doi.org/10.17648/sobrac-87165

Desai, R., & Guha, A. (2021). A Comparison of Quarter , Half and Full Car Models for Predicting Vibration Attenuation of an Occupant in a Vehicle. *Journal of Vibration Engineering & Technologies*, *0123456789*. https://doi.org/10.1007/s42417-020-00278-3

Desai, R., Guha, A., & Seshu, P. (2021). A Comparison of Quarter, Half and Full Car Models for Predicting Vibration Attenuation of an Occupant in a Vehicle. *Journal of Vibration Engineering and Technologies*, *9*(5), 983–1001. https://doi.org/10.1007/s42417-020-00278-3

Diniță, A., Neacșa, A., Portoacă, A. I., Tănase, M., Ilinca, C. N., & Ramadan, I. N. (2023). Additive Manufacturing Post-Processing Treatments, a Review with Emphasis on Mechanical Characteristics. *Materials*, *16*(13). https://doi.org/10.3390/ma16134610

dos Santos Accioly Lins, C. C., de Moraes Ramos-Perez, F. M., dos Anjos Pontual, A., dos Anjos Pontual, M. L., & do Nascimento, E. H. L. (2021). Digital oral radiography. In *Digitization in Dentistry: Clinical Applications* (pp. 65–88). https://doi.org/10.1007/978-3-030-65169-5_3

Edition, S. (n.d.). *Understanding GPS*.

Festa, M., Stalter, F., Tavornmas, A., & Gauterin, F. (2021). Human Response to Vehicle Vibrations and Acoustics during Transient Road Excitations. *Vibration*, *4*(2), 357–368. https://doi.org/10.3390/vibration4020023

Gowtham, S., S, K. R., & Subramaniyan, G. (2020). *MEASURING WEIGHT OF LOAD TRUCK USING SUSPENSION SYSTEM*. *May*, 3951–3956.

HESS LOW ENTRY – REGIONAL PHENOMENAL MOBILITY FOR CITY. (n.d.).

Introduction, I. (2011). *Body Concept*. *January*, 1–13.

Jiregna, I. T., & Sirata, G. (2020). A review of the vehicle suspension system. *Journal of Mechanical and Energy Engineering*, *4*(2), 109–114. https://doi.org/10.30464/jmee.2020.4.2.109

Jugulkar, L. M., Singh, S., & Sawant, S. M. (2016). Analysis of suspension with variable stiffness and variable damping force for automotive applications. *Advances in Mechanical Engineering*, *8*(5), 1–19. https://doi.org/10.1177/1687814016648638

Kamaruddin, S., Ramly, A. F., Mohd Shukri, N., Bakri, A. G., & Fourrier, Q. (2019). Evaluation of Specialty Natural Rubbers for Engine Mount Application. *IOP Conference Series: Materials Science and Engineering*, *548*(1). https://doi.org/10.1088/1757-899X/548/1/012004

Kattimani, H. D., Meghana, N. R., Nagashree, B., Munegowda, S., & Vijayalakshmi, S. (2017). *“ Vehicular Overload Detection and Protection .”* 119–122.

Kousikan, M., & Sundaraj, M. (2014). Automatic Drunken Drive Prevention System. *International Journal of Students Research in Technology & Management*, *2*(02), 74–77.

Kunanoppadol, J., & Pathom, N. (2015). *The Concept to Measure the Overall Car Performance*. *January 2013*. https://doi.org/10.14456/jscitech.2013.102

Liu, Y., Jia, Y. Y., Yang, J. G., Song, S. Q., Wu, B., & Li, J. (2018). Research of mechanical state diagnosis techniques in GIS bus connector based on mechanical vibration. *Proceedings of the IEEE International Conference on Properties and Applications of Dielectric Materials*, *2018-May*, 682–685. https://doi.org/10.1109/ICPADM.2018.8401143

Liu, Z., Yuan, S., Xiao, S., Du, S., Zhang, Y., & Lu, C. (2017). Full Vehicle Vibration and Noise Analysis Based on Substructure Power Flow. *Shock and Vibration*, *2017*. https://doi.org/10.1155/2017/8725346

Long, L. X., Van Quynh, L., & Van Cuong, B. (2018). Study on the influence of bus suspension parameters on ride comfort. *Vibroengineering Procedia*, *21*, 77–82. https://doi.org/10.21595/vp.2018.20271

Lopes, R., Farahani, B. V., de Melo, F. Q., Ramos, N. V., & Moreira, P. M. G. P. (2021). A numerical dynamic analysis of a multi-body bus. *Procedia Structural Integrity*, *37*(C), 81–88. https://doi.org/10.1016/j.prostr.2022.01.062

Ma, M., Du, Z., Yang, Z., Guo, W., Qiao, J., & Xu, H. (2020). Analysis of Vibration Characteristics of Tracked Vehicle Based on Experimental Tests. *Proceedings - 2020 International Conference on Intelligent Computing, Automation and Systems, ICICAS 2020*, 101–104. https://doi.org/10.1109/ICICAS51530.2020.00028

Mohanty, M., Raj, Y., Rout, S., Tiwari, U., Roy, S., & Samal, S. R. (2021). Operational effects of speed breakers: A case study in India. *European Transport - Trasporti Europei*, *81*(March). https://doi.org/10.48295/ET.2021.81.1

Mrad, F. L., Machado, D. M. L., Horta, G. J. C., & Sad, A. U. (2018). Optimization of the Vibrational Comfort of Passenger Vehicles through Improvement of Suspension and Engine Rubber Mounting Setups. *Shock and Vibration*, *2018*. https://doi.org/10.1155/2018/9861052

Musbah, M. (2017). *COLLEGE OF ARCHITECTURE AND CIVIL ENGINEERING Members of the Examining board :*

Nordin, D. (2018). *Design and Evaluation of a Carbon Fibre Bus Body*.

Park, J., Min, K., Kim, H., Lee, W., Cho, G., & Huh, K. (2018). Road surface classification using a deep ensemble network with sensor feature selection. *Sensors (Switzerland)*, *18*(12), 1–16. https://doi.org/10.3390/s18124342

Rashid, F., & Jhawari, A. (2018). Location based alarm using mobile device. *International Journal of Computer Applications*, *January*, 975–8887.

Rifaie, M. Al, Abdulhadi, H., & Mian, A. (2022). *Advances in mechanical metamaterials for vibration isolation : A review*. *14*(3), 1–20. https://doi.org/10.1177/16878132221082872

Road, B., Shahi, P. B., & Nepali, B. B. (2020). *Impact of Overloaded Vehicles on Flexible Pavement : Case Study of Belhiya- Impact of Overloaded Vehicles on Flexible Pavement : Case Study of Belhiya-Butwal Road in Nepal*. *October*. https://doi.org/10.9790/1684-1705034961

Roslan, M. R., & Priyandoko, G. (2019). Analysis of a Sedan Car Seat Vibration. *Journal of Science and Applied Engineering*, *2*(1), 22–28. https://doi.org/10.31328/jsae.v2i1.938

Seifi, A., Hassannejad, R., & Hamed, M. A. (2016). Optimum design for passive suspension system of a vehicle to prevent rollover and improve ride comfort under random road excitations. *Proceedings of the Institution of Mechanical Engineers, Part K: Journal of Multi-Body Dynamics*, *230*(4), 426–441. https://doi.org/10.1177/1464419315618034

Senthil Kumar, M. S., Naiju, C. D., Chethan Kumar, S. J., & Kurian, J. (2013). Vibration analysis and improvement of a vehicle chassis structure. *Applied Mechanics and Materials*, *372*(December), 528–532. https://doi.org/10.4028/www.scientific.net/AMM.372.528

Sharma, S., Chouksey, M., Pare, V., & Jain, P. (2020). Modal and frequency response characteristics of vehicle suspension system using full car model. *IOP Conference Series: Materials Science and Engineering*, *810*(1). https://doi.org/10.1088/1757-899X/810/1/012056

Solhmirzaei, A., Azadi, S., & Kazemi, R. (2012). Road profile estimation using wavelet neural network and 7-DOF vehicle dynamic systems. *Journal of Mechanical Science and Technology*, *26*(10), 3029–3036. https://doi.org/10.1007/s12206-012-0812-x

Uzun, A. (2010). Analysis of vibration effect in cars and driving quality. *Journal of Vibroengineering*, *12*(3), 368–375.

Vosoughi, S., Rostamzadeh, S., Farshad, A. A., Taheri, F., & Vahabzadeh-Monshi, H. (2019). Whole-Body Vibration Exposure Study in Intercity Mini-Bus Drivers-The Risk of Musculoskeletal Disorders. *Iranian Journal of Health, Safety and Environment*, *6*(1), 1198–1205.

Yazici, H. (2016). Design of a parameter-dependent optimal vibration control of a non-linear vehicle suspension system. *Mathematical and Computational Applications*, *21*(2). https://doi.org/10.3390/mca21020013

Zhao, H., Guo, L. L., & Zeng, X. Y. (2016). Evaluation of bus vibration comfort based on passenger crowdsourcing mode. *Mathematical Problems in Engineering*, *2016*. https://doi.org/10.1155/2016/2132454

Zou, X., Li, Z., Zhao, X., Sun, T., & Zhang, K. (2014). Study on the auto-leveling adjustment vibration isolation system for the ultra-precision machine tool. *7th International Symposium on Advanced Optical Manufacturing and Testing Technologies: Advanced Optical Manufacturing Technologies*, *9281*(November 2016), 92812L. https://doi.org/10.1117/12.2069463

APPENDIX I
Passenger weight with seat acceleration data of BESRC

f = 1/T(Hz)		Component acceleration			Squared weighted acceleration			Total a^2
Time(s)	Freq (Hz)	a_x (m/s^2)	a_y (m/s^2)	a_z (m/s^2)	weight*a_x	weight*a_y	weight*a_z	a_{xyz}
7.5E-05	1.3E+04	2.5E-12	-9.8E+03	1.2E-28	1.1E-15	1.7E+16	2.6E-48	1.7E+16
2.0E-03	5.0E+02	1.9E-12	-9.4E+03	1.2E-28	8.7E-19	2.2E+13	3.3E-51	2.2E+13
3.0E-03	3.3E+02	2.0E-12	-9.0E+03	1.1E-28	4.5E-19	9.0E+12	1.4E-51	9.0E+12
4.2E-03	2.4E+02	1.7E-12	-8.5E+03	1.1E-28	1.7E-19	4.2E+12	6.3E-52	4.2E+12
5.5E-03	1.8E+02	2.0E-12	-7.8E+03	9.6E-29	1.3E-19	2.0E+12	3.1E-52	2.0E+12
7.0E-03	1.4E+02	1.4E-12	-6.8E+03	8.4E-29	3.9E-20	9.6E+11	1.5E-52	9.6E+11
8.6E-03	1.2E+02	1.3E-12	-5.6E+03	6.9E-29	2.2E-20	4.2E+11	6.4E-53	4.2E+11
1.0E-02	9.6E+01	1.0E-12	-4.0E+03	4.9E-29	9.6E-21	1.5E+11	2.2E-53	1.5E+11
1.3E-02	8.0E+01	6.2E-13	-2.1E+03	2.6E-29	2.5E-21	2.9E+10	4.3E-54	2.9E+10
1.5E-02	6.8E+01	-2.0E-13	-1.5E+02	1.9E-30	2.0E-22	1.1E+08	1.7E-56	1.1E+08
1.6E-02	6.4E+01	8.8E-14	8.2E+02	-1.0E-29	3.2E-23	2.7E+09	4.2E-55	2.7E+09
1.7E-02	5.9E+01	-5.0E-13	1.9E+03	-2.4E-29	8.8E-22	1.3E+10	2.0E-54	1.3E+10
1.8E-02	5.5E+01	-8.2E-13	3.1E+03	-3.8E-29	2.0E-21	2.9E+10	4.4E-54	2.9E+10
2.0E-02	5.1E+01	-7.0E-13	4.3E+03	-5.3E-29	1.3E-21	4.7E+10	7.2E-54	4.7E+10
2.1E-02	4.7E+01	-1.4E-12	5.4E+03	-6.7E-29	4.4E-21	6.5E+10	9.9E-54	6.5E+10
2.3E-02	4.3E+01	-1.3E-12	6.5E+03	-8.0E-29	3.0E-21	8.0E+10	1.2E-53	8.0E+10
2.5E-02	4.0E+01	-1.1E-12	7.4E+03	-9.2E-29	2.1E-21	8.9E+10	1.3E-53	8.9E+10
2.7E-02	3.7E+01	-1.5E-12	8.1E+03	-1.0E-28	3.1E-21	9.0E+10	1.4E-53	9.0E+10
2.9E-02	3.5E+01	-2.3E-12	8.3E+03	-1.0E-28	6.6E-21	8.5E+10	1.3E-53	8.5E+10
2.9E-02	3.5E+01	-1.8E-12	8.3E+03	-1.0E-28	4.0E-21	8.5E+10	1.3E-53	8.5E+10
3.0E-02	3.4E+01	-2.8E-12	8.4E+03	-1.0E-28	9.1E-21	8.0E+10	1.2E-53	8.0E+10
3.0E-02	3.3E+01	-2.1E-12	8.4E+03	-1.0E-28	4.8E-21	7.8E+10	1.2E-53	7.8E+10
3.0E-02	3.3E+01	-1.9E-12	8.4E+03	-1.0E-28	4.1E-21	7.6E+10	1.2E-53	7.6E+10
3.0E-02	3.3E+01	-1.6E-12	8.4E+03	-1.0E-28	2.7E-21	7.5E+10	1.1E-53	7.5E+10
3.1E-02	3.3E+01	-2.2E-12	8.3E+03	-1.0E-28	5.3E-21	7.4E+10	1.1E-53	7.4E+10
3.1E-02	3.2E+01	-1.7E-12	8.3E+03	-1.0E-28	3.0E-21	7.0E+10	1.1E-53	7.0E+10
3.2E-02	3.1E+01	-2.2E-12	8.1E+03	-1.0E-28	4.6E-21	6.5E+10	9.9E-54	6.5E+10
3.3E-02	3.0E+01	-1.6E-12	7.9E+03	-9.8E-29	2.3E-21	5.8E+10	8.8E-54	5.8E+10
3.4E-02	2.9E+01	-2.0E-12	7.5E+03	-9.3E-29	3.4E-21	4.9E+10	7.4E-54	4.9E+10
3.5E-02	2.8E+01	-1.0E-12	7.0E+03	-8.6E-29	8.7E-22	3.9E+10	5.9E-54	3.9E+10
3.7E-02	2.7E+01	-1.4E-12	6.2E+03	-7.6E-29	1.5E-21	2.8E+10	4.3E-54	2.8E+10
3.9E-02	2.6E+01	-1.0E-12	5.1E+03	-6.3E-29	7.3E-22	1.8E+10	2.7E-54	1.8E+10
4.1E-02	2.5E+01	-7.6E-13	3.7E+03	-4.6E-29	3.5E-22	8.5E+09	1.3E-54	8.5E+09
4.3E-02	2.3E+01	-4.9E-13	2.1E+03	-2.5E-29	1.3E-22	2.3E+09	3.5E-55	2.3E+09
4.5E-02	2.2E+01	-6.6E-13	2.9E+02	-3.6E-30	2.2E-22	4.3E+07	6.5E-57	4.3E+07
4.6E-02	2.2E+01	-4.8E-13	-5.9E+02	7.3E-30	1.1E-22	1.6E+08	2.5E-56	1.6E+08
4.7E-02	2.1E+01	2.4E-13	-1.6E+03	2.0E-29	2.5E-23	1.1E+09	1.7E-55	1.1E+09
4.9E-02	2.0E+01	1.5E-12	-2.7E+03	3.3E-29	9.1E-22	3.0E+09	4.5E-55	3.0E+09
5.1E-02	2.0E+01	8.5E-13	-3.8E+03	4.6E-29	2.8E-22	5.6E+09	8.5E-55	5.6E+09

5.2E-02	1.9E+01	1.3E-12	-4.8E+03	6.0E-29	6.2E-22	8.5E+09	1.3E-54	8.5E+09
5.4E-02	1.8E+01	1.6E-12	-5.8E+03	7.2E-29	8.5E-22	1.1E+10	1.7E-54	1.1E+10
5.6E-02	1.8E+01	8.9E-13	-6.6E+03	8.1E-29	2.5E-22	1.4E+10	2.1E-54	1.4E+10
5.9E-02	1.7E+01	5.8E-13	-7.1E+03	8.7E-29	9.9E-23	1.4E+10	2.2E-54	1.4E+10
6.0E-02	1.7E+01	2.3E-12	-7.1E+03	8.8E-29	1.5E-21	1.4E+10	2.1E-54	1.4E+10
6.1E-02	1.6E+01	2.9E-12	-7.1E+03	8.7E-29	2.2E-21	1.3E+10	2.0E-54	1.3E+10
6.3E-02	1.6E+01	1.5E-12	-6.9E+03	8.5E-29	5.5E-22	1.2E+10	1.8E-54	1.2E+10
6.5E-02	1.5E+01	1.7E-12	-6.5E+03	8.0E-29	7.2E-22	1.0E+10	1.5E-54	1.0E+10
6.6E-02	1.5E+01	1.8E-12	-5.8E+03	7.2E-29	7.0E-22	7.7E+09	1.2E-54	7.7E+09
6.8E-02	1.5E+01	1.9E-12	-4.9E+03	6.1E-29	7.9E-22	5.2E+09	7.9E-55	5.2E+09
7.0E-02	1.4E+01	-9.6E-14	-3.7E+03	4.6E-29	1.8E-24	2.8E+09	4.3E-55	2.8E+09
7.3E-02	1.4E+01	9.7E-13	-2.2E+03	2.8E-29	1.8E-22	9.5E+08	1.4E-55	9.5E+08
7.5E-02	1.3E+01	1.7E-13	-6.1E+02	7.5E-30	5.0E-24	6.5E+07	9.9E-57	6.5E+07
7.6E-02	1.3E+01	-1.1E-12	2.2E+02	-2.7E-30	1.9E-22	7.9E+06	1.2E-57	7.9E+06
7.8E-02	1.3E+01	-6.8E-13	1.2E+03	-1.4E-29	7.7E-23	2.2E+08	3.4E-56	2.2E+08
7.9E-02	1.3E+01	-9.4E-13	2.1E+03	-2.6E-29	1.4E-22	6.8E+08	1.0E-55	6.8E+08
8.1E-02	1.2E+01	-6.8E-13	3.0E+03	-3.7E-29	7.0E-23	1.4E+09	2.1E-55	1.4E+09
8.3E-02	1.2E+01	-6.7E-15	3.9E+03	-4.8E-29	6.7E-27	2.3E+09	3.4E-55	2.3E+09
8.4E-02	1.2E+01	-8.2E-14	4.8E+03	-5.9E-29	9.5E-25	3.2E+09	4.9E-55	3.2E+09
8.6E-02	1.2E+01	-1.5E-12	5.5E+03	-6.7E-29	3.1E-22	4.0E+09	6.1E-55	4.0E+09
8.9E-02	1.1E+01	-1.2E-12	5.9E+03	-7.3E-29	1.9E-22	4.4E+09	6.8E-55	4.4E+09
9.1E-02	1.1E+01	2.8E-14	6.1E+03	-7.5E-29	9.2E-26	4.5E+09	6.8E-55	4.5E+09
9.3E-02	1.1E+01	-1.3E-12	5.9E+03	-7.3E-29	2.0E-22	4.1E+09	6.2E-55	4.1E+09
9.4E-02	1.1E+01	-7.7E-13	5.8E+03	-7.1E-29	6.7E-23	3.7E+09	5.7E-55	3.7E+09
9.5E-02	1.0E+01	-5.5E-13	5.4E+03	-6.7E-29	3.4E-23	3.3E+09	4.9E-55	3.3E+09
9.7E-02	1.0E+01	-3.4E-13	4.9E+03	-6.1E-29	1.2E-23	2.6E+09	3.9E-55	2.6E+09
9.9E-02	1.0E+01	-5.2E-14	4.2E+03	-5.2E-29	2.7E-25	1.8E+09	2.8E-55	1.8E+09
1.0E-01	9.9E+00	-9.1E-13	3.3E+03	-4.0E-29	8.1E-23	1.0E+09	1.6E-55	1.0E+09
1.0E-01	9.7E+00	-8.2E-13	2.0E+03	-2.5E-29	6.4E-23	3.9E+08	6.0E-56	3.9E+08
1.1E-01	9.5E+00	2.8E-13	7.0E+02	-8.7E-30	6.8E-24	4.5E+07	6.8E-57	4.5E+07
1.1E-01	9.3E+00	4.9E-13	-6.5E+02	8.1E-30	2.0E-23	3.7E+07	5.6E-57	3.7E+07
1.1E-01	9.2E+00	5.5E-13	-1.3E+03	1.6E-29	2.5E-23	1.4E+08	2.2E-56	1.4E+08
1.1E-01	9.1E+00	-5.2E-13	-2.1E+03	2.6E-29	2.2E-23	3.6E+08	5.4E-56	3.6E+08
1.1E-01	8.9E+00	6.3E-13	-2.9E+03	3.6E-29	3.1E-23	6.8E+08	1.0E-55	6.8E+08
1.1E-01	8.8E+00	1.3E-12	-3.8E+03	4.6E-29	1.3E-22	1.1E+09	1.7E-55	1.1E+09
1.2E-01	8.6E+00	1.2E-12	-4.5E+03	5.6E-29	1.1E-22	1.5E+09	2.3E-55	1.5E+09
1.2E-01	8.4E+00	6.0E-13	-5.0E+03	6.2E-29	2.5E-23	1.8E+09	2.7E-55	1.8E+09
1.2E-01	8.2E+00	5.7E-13	-5.2E+03	6.4E-29	2.2E-23	1.8E+09	2.7E-55	1.8E+09
1.2E-01	8.1E+00	1.1E-12	-5.1E+03	6.3E-29	8.7E-23	1.7E+09	2.6E-55	1.7E+09
1.2E-01	8.0E+00	1.5E-12	-4.9E+03	6.0E-29	1.4E-22	1.6E+09	2.4E-55	1.6E+09
1.3E-01	7.9E+00	1.3E-12	-4.5E+03	5.6E-29	1.1E-22	1.3E+09	2.0E-55	1.3E+09
1.3E-01	7.8E+00	1.8E-12	-3.9E+03	4.9E-29	1.9E-22	9.4E+08	1.4E-55	9.4E+08
1.3E-01	7.7E+00	8.0E-13	-3.1E+03	3.8E-29	3.7E-23	5.6E+08	8.5E-56	5.6E+08
1.3E-01	7.5E+00	4.1E-13	-2.0E+03	2.4E-29	9.6E-24	2.2E+08	3.3E-56	2.2E+08

1.4E-01	7.4E+00	-4.6E-13	-6.7E+02	8.3E-30	1.1E-23	2.5E+07	3.7E-57	2.5E+07
1.4E-01	7.2E+00	2.5E-13	6.4E+02	-7.9E-30	3.3E-24	2.1E+07	3.2E-57	2.1E+07
1.4E-01	7.1E+00	-1.6E-13	1.9E+03	-2.3E-29	1.3E-24	1.7E+08	2.6E-56	1.7E+08
1.4E-01	6.9E+00	-8.4E-13	2.9E+03	-3.6E-29	3.4E-23	4.2E+08	6.3E-56	4.2E+08
1.5E-01	6.8E+00	-9.3E-13	3.8E+03	-4.7E-29	4.0E-23	6.7E+08	1.0E-55	6.7E+08
1.5E-01	6.7E+00	-1.7E-12	4.3E+03	-5.3E-29	1.3E-22	8.2E+08	1.3E-55	8.2E+08
1.5E-01	6.6E+00	-1.9E-12	4.4E+03	-5.4E-29	1.6E-22	8.4E+08	1.3E-55	8.4E+08
1.5E-01	6.5E+00	-1.7E-12	4.3E+03	-5.3E-29	1.2E-22	8.0E+08	1.2E-55	8.0E+08
1.6E-01	6.4E+00	-5.9E-13	4.1E+03	-5.0E-29	1.4E-23	6.9E+08	1.0E-55	6.9E+08
1.6E-01	6.3E+00	-1.2E-12	3.6E+03	-4.4E-29	5.8E-23	5.2E+08	7.9E-56	5.2E+08
1.6E-01	6.2E+00	-3.8E-13	2.9E+03	-3.5E-29	5.5E-24	3.2E+08	4.9E-56	3.2E+08
1.6E-01	6.1E+00	-1.8E-13	1.8E+03	-2.3E-29	1.2E-24	1.3E+08	1.9E-56	1.3E+08
1.7E-01	6.0E+00	-5.0E-13	6.4E+02	-7.9E-30	9.1E-24	1.5E+07	2.2E-57	1.5E+07
1.7E-01	5.9E+00	8.2E-13	-6.0E+02	7.4E-30	2.4E-23	1.2E+07	1.9E-57	1.2E+07
1.7E-01	5.8E+00	1.2E-12	-1.7E+03	2.2E-29	4.5E-23	1.0E+08	1.6E-56	1.0E+08
1.8E-01	5.7E+00	3.7E-13	-2.7E+03	3.4E-29	4.5E-24	2.4E+08	3.7E-56	2.4E+08
1.8E-01	5.6E+00	1.0E-12	-3.5E+03	4.3E-29	3.2E-23	3.7E+08	5.7E-56	3.7E+08
1.8E-01	5.5E+00	4.3E-13	-3.7E+03	4.6E-29	5.5E-24	4.2E+08	6.4E-56	4.2E+08
1.8E-01	5.4E+00	3.5E-13	-3.7E+03	4.5E-29	3.5E-24	4.0E+08	6.1E-56	4.0E+08
1.9E-01	5.4E+00	9.6E-14	-3.5E+03	4.3E-29	2.7E-25	3.5E+08	5.3E-56	3.5E+08
1.9E-01	5.3E+00	1.9E-13	-3.1E+03	3.8E-29	9.7E-25	2.6E+08	4.0E-56	2.6E+08
1.9E-01	5.2E+00	5.3E-13	-2.4E+03	3.0E-29	7.8E-24	1.6E+08	2.4E-56	1.6E+08
1.9E-01	5.1E+00	-3.3E-13	-1.5E+03	1.8E-29	2.9E-24	5.7E+07	8.7E-57	5.7E+07
2.0E-01	5.1E+00	6.2E-13	-3.9E+02	4.8E-30	9.9E-24	3.8E+06	5.8E-58	3.8E+06
2.0E-01	5.0E+00	-1.2E-13	7.2E+02	-8.8E-30	3.5E-25	1.3E+07	1.9E-57	1.3E+07
2.0E-01	4.9E+00	1.2E-13	1.7E+03	-2.1E-29	3.4E-25	7.2E+07	1.1E-56	7.2E+07
2.1E-01	4.8E+00	-9.1E-13	2.6E+03	-3.2E-29	1.9E-23	1.5E+08	2.3E-56	1.5E+08
2.1E-01	4.7E+00	-1.1E-12	3.1E+03	-3.8E-29	2.7E-23	2.1E+08	3.3E-56	2.1E+08
2.1E-01	4.7E+00	-1.1E-12	3.2E+03	-3.9E-29	2.5E-23	2.2E+08	3.4E-56	2.2E+08
2.2E-01	4.7E+00	-2.6E-13	3.1E+03	-3.9E-29	1.4E-24	2.1E+08	3.2E-56	2.1E+08
2.2E-01	4.6E+00	-4.1E-13	2.9E+03	-3.6E-29	3.6E-24	1.8E+08	2.7E-56	1.8E+08
2.2E-01	4.5E+00	2.7E-13	2.4E+03	-3.0E-29	1.4E-24	1.2E+08	1.8E-56	1.2E+08
2.2E-01	4.5E+00	-6.1E-13	1.7E+03	-2.1E-29	7.5E-24	5.6E+07	8.5E-57	5.6E+07
2.3E-01	4.4E+00	-4.8E-13	7.4E+02	-9.1E-30	4.5E-24	1.1E+07	1.6E-57	1.1E+07
2.3E-01	4.3E+00	-8.7E-13	-2.7E+02	3.4E-30	1.4E-23	1.4E+06	2.1E-58	1.4E+06
2.3E-01	4.3E+00	2.4E-13	-1.2E+03	1.5E-29	1.1E-24	2.8E+07	4.3E-57	2.8E+07
2.4E-01	4.2E+00	2.5E-13	-2.1E+03	2.5E-29	1.1E-24	7.5E+07	1.1E-56	7.5E+07
2.4E-01	4.1E+00	6.7E-13	-2.6E+03	3.2E-29	7.8E-24	1.2E+08	1.8E-56	1.2E+08
2.4E-01	4.1E+00	6.1E-13	-2.7E+03	3.3E-29	6.2E-24	1.2E+08	1.9E-56	1.2E+08
2.5E-01	4.1E+00	3.9E-13	-2.7E+03	3.3E-29	2.5E-24	1.2E+08	1.8E-56	1.2E+08
2.5E-01	4.0E+00	9.6E-13	-2.4E+03	3.0E-29	1.5E-23	9.6E+07	1.5E-56	9.6E+07
2.5E-01	4.0E+00	1.2E-13	-2.0E+03	2.4E-29	2.3E-25	6.1E+07	9.3E-57	6.1E+07
2.5E-01	3.9E+00	4.9E-13	-1.3E+03	1.5E-29	3.6E-24	2.4E+07	3.7E-57	2.4E+07
2.6E-01	3.9E+00	-1.3E-14	-3.8E+02	4.7E-30	2.7E-27	2.1E+06	3.3E-58	2.1E+06

2.6E-01	3.8E+00	-5.0E-13	5.4E+02	-6.7E-30	3.7E-24	4.3E+06	6.5E-58	4.3E+06
2.7E-01	3.8E+00	-4.0E-13	1.4E+03	-1.7E-29	2.3E-24	2.7E+07	4.1E-57	2.7E+07
2.7E-01	3.7E+00	-5.1E-14	2.0E+03	-2.5E-29	3.5E-26	5.7E+07	8.7E-57	5.7E+07
2.7E-01	3.6E+00	-8.9E-13	2.3E+03	-2.8E-29	1.1E-23	7.0E+07	1.1E-56	7.0E+07
2.8E-01	3.6E+00	-2.8E-13	2.2E+03	-2.8E-29	1.0E-24	6.6E+07	1.0E-56	6.6E+07
2.8E-01	3.6E+00	-3.3E-13	2.0E+03	-2.5E-29	1.4E-24	5.3E+07	8.1E-57	5.3E+07
2.8E-01	3.5E+00	-4.2E-13	1.6E+03	-2.0E-29	2.2E-24	3.3E+07	5.1E-57	3.3E+07
2.9E-01	3.5E+00	-6.1E-13	1.0E+03	-1.2E-29	4.6E-24	1.2E+07	1.9E-57	1.2E+07
2.9E-01	3.5E+00	1.8E-13	2.4E+02	-3.0E-30	4.0E-25	7.1E+05	1.1E-58	7.1E+05
2.9E-01	3.4E+00	2.2E-13	-5.6E+02	6.9E-30	5.6E-25	3.6E+06	5.5E-58	3.6E+06
3.0E-01	3.4E+00	2.5E-13	-1.3E+03	1.6E-29	6.9E-25	1.9E+07	2.9E-57	1.9E+07
3.0E-01	3.3E+00	2.0E-13	-1.8E+03	2.2E-29	4.3E-25	3.6E+07	5.5E-57	3.6E+07
3.1E-01	3.3E+00	4.6E-13	-1.9E+03	2.4E-29	2.3E-24	4.1E+07	6.2E-57	4.1E+07
3.1E-01	3.2E+00	3.6E-13	-1.9E+03	2.3E-29	1.4E-24	3.6E+07	5.5E-57	3.6E+07
3.1E-01	3.2E+00	2.9E-13	-1.6E+03	2.0E-29	8.7E-25	2.7E+07	4.1E-57	2.7E+07
3.1E-01	3.2E+00	2.7E-13	-1.2E+03	1.5E-29	7.6E-25	1.5E+07	2.2E-57	1.5E+07
3.2E-01	3.1E+00	1.9E-13	-6.1E+02	7.5E-30	3.7E-25	3.6E+06	5.5E-58	3.6E+06
3.2E-01	3.1E+00	-1.8E-14	8.5E+01	-1.0E-30	3.2E-27	7.0E+04	1.1E-59	7.0E+04
3.2E-01	3.1E+00	-5.2E-15	9.7E+01	-1.2E-30	2.7E-28	9.2E+04	1.4E-59	9.2E+04
3.2E-01	3.1E+00	1.3E-14	9.7E+01	-1.2E-30	1.7E-27	9.2E+04	1.4E-59	9.2E+04
3.2E-01	3.1E+00	-1.1E-13	4.9E+02	-6.1E-30	1.1E-25	2.3E+06	3.5E-58	2.3E+06
3.2E-01	3.1E+00	-1.8E-13	6.8E+02	-8.4E-30	2.9E-25	4.4E+06	6.7E-58	4.4E+06
3.3E-01	3.1E+00	-1.8E-13	8.9E+02	-1.1E-29	3.0E-25	7.4E+06	1.1E-57	7.4E+06
3.3E-01	3.1E+00	-2.5E-13	1.1E+03	-1.4E-29	5.6E-25	1.1E+07	1.7E-57	1.1E+07
3.3E-01	3.0E+00	-2.9E-13	1.3E+03	-1.6E-29	7.8E-25	1.6E+07	2.4E-57	1.6E+07
3.3E-01	3.0E+00	-3.3E-13	1.5E+03	-1.8E-29	1.0E-24	2.0E+07	3.1E-57	2.0E+07
3.3E-01	3.0E+00	-3.6E-13	1.6E+03	-2.0E-29	1.2E-24	2.4E+07	3.6E-57	2.4E+07
3.4E-01	3.0E+00	-3.7E-13	1.7E+03	-2.1E-29	1.2E-24	2.5E+07	3.7E-57	2.5E+07
3.4E-01	3.0E+00	-3.5E-13	1.6E+03	-1.9E-29	1.1E-24	2.2E+07	3.3E-57	2.2E+07
3.4E-01	2.9E+00	-3.0E-13	1.3E+03	-1.6E-29	7.5E-25	1.5E+07	2.3E-57	1.5E+07
3.5E-01	2.9E+00	-2.0E-13	9.1E+02	-1.1E-29	3.4E-25	6.9E+06	1.1E-57	6.9E+06
3.5E-01	2.9E+00	-7.5E-14	3.4E+02	-4.2E-30	4.6E-26	9.3E+05	1.4E-58	9.3E+05
3.5E-01	2.8E+00	1.1E-14	-5.0E+01	6.2E-31	1.0E-27	2.0E+04	3.1E-60	2.0E+04
3.5E-01	2.8E+00	1.1E-14	-5.0E+01	6.2E-31	1.0E-27	2.0E+04	3.1E-60	2.0E+04
3.5E-01	2.8E+00	8.7E-14	-3.9E+02	4.9E-30	6.1E-26	1.2E+06	1.9E-58	1.2E+06
3.6E-01	2.8E+00	1.6E-13	-7.2E+02	8.9E-30	2.0E-25	4.1E+06	6.2E-58	4.1E+06
3.6E-01	2.8E+00	2.2E-13	-1.0E+03	1.2E-29	3.9E-25	7.9E+06	1.2E-57	7.9E+06
3.6E-01	2.8E+00	2.7E-13	-1.2E+03	1.5E-29	5.8E-25	1.2E+07	1.8E-57	1.2E+07
3.6E-01	2.7E+00	3.1E-13	-1.4E+03	1.7E-29	7.1E-25	1.4E+07	2.2E-57	1.4E+07
3.7E-01	2.7E+00	3.1E-13	-1.4E+03	1.7E-29	7.3E-25	1.5E+07	2.2E-57	1.5E+07
3.7E-01	2.7E+00	2.9E-13	-1.3E+03	1.6E-29	6.0E-25	1.2E+07	1.9E-57	1.2E+07
3.7E-01	2.7E+00	2.3E-13	-1.0E+03	1.3E-29	3.7E-25	7.5E+06	1.1E-57	7.5E+06
3.8E-01	2.6E+00	1.3E-13	-6.0E+02	7.3E-30	1.2E-25	2.5E+06	3.8E-58	2.5E+06
3.8E-01	2.6E+00	1.4E-14	-6.3E+01	7.8E-31	1.3E-27	2.7E+04	4.1E-60	2.7E+04

3.9E-01	2.6E+00	-1.1E-13	4.9E+02	-6.1E-30	8.1E-26	1.6E+06	2.5E-58	1.6E+06
3.9E-01	2.6E+00	-2.2E-13	9.7E+02	-1.2E-29	3.0E-25	6.2E+06	9.4E-58	6.2E+06
4.0E-01	2.5E+00	-2.7E-13	1.2E+03	-1.5E-29	4.5E-25	9.2E+06	1.4E-57	9.2E+06
4.0E-01	2.5E+00	-2.4E-13	1.1E+03	-1.3E-29	3.6E-25	7.4E+06	1.1E-57	7.4E+06
4.1E-01	2.5E+00	-1.5E-13	6.9E+02	-8.5E-30	1.4E-25	2.9E+06	4.4E-58	2.9E+06
4.1E-01	2.4E+00	-2.7E-14	1.2E+02	-1.5E-30	4.2E-27	8.6E+04	1.3E-59	8.6E+04
4.2E-01	2.4E+00	1.0E-13	-4.5E+02	5.6E-30	5.9E-26	1.2E+06	1.8E-58	1.2E+06
4.2E-01	2.4E+00	2.0E-13	-8.9E+02	1.1E-29	2.2E-25	4.4E+06	6.7E-58	4.4E+06
4.3E-01	2.3E+00	2.3E-13	-1.0E+03	1.3E-29	2.8E-25	5.7E+06	8.6E-58	5.7E+06
4.3E-01	2.3E+00	2.1E-13	-9.6E+02	1.2E-29	2.4E-25	4.9E+06	7.5E-58	4.9E+06
4.3E-01	2.3E+00	1.7E-13	-7.8E+02	9.6E-30	1.6E-25	3.2E+06	4.8E-58	3.2E+06
4.4E-01	2.3E+00	1.0E-13	-4.6E+02	5.7E-30	5.5E-26	1.1E+06	1.7E-58	1.1E+06
4.4E-01	2.3E+00	1.0E-14	-4.5E+01	5.5E-31	5.1E-28	1.0E+04	1.6E-60	1.0E+04
4.5E-01	2.2E+00	-8.9E-14	4.0E+02	-4.9E-30	4.0E-26	8.0E+05	1.2E-58	8.0E+05
4.5E-01	2.2E+00	-1.7E-13	7.7E+02	-9.5E-30	1.4E-25	2.9E+06	4.3E-58	2.9E+06
4.6E-01	2.2E+00	-1.9E-13	8.6E+02	-1.1E-29	1.7E-25	3.5E+06	5.3E-58	3.5E+06
4.7E-01	2.1E+00	-1.4E-13	6.2E+02	-7.7E-30	8.8E-26	1.8E+06	2.7E-58	1.8E+06
4.7E-01	2.1E+00	-9.1E-14	4.1E+02	-5.0E-30	3.7E-26	7.6E+05	1.2E-58	7.6E+05
4.7E-01	2.1E+00	-2.3E-14	1.0E+02	-1.3E-30	2.3E-27	4.8E+04	7.2E-60	4.8E+04
4.8E-01	2.1E+00	5.7E-14	-2.6E+02	3.2E-30	1.4E-26	2.9E+05	4.4E-59	2.9E+05
4.8E-01	2.1E+00	1.3E-13	-5.8E+02	7.2E-30	7.2E-26	1.5E+06	2.2E-58	1.5E+06
4.9E-01	2.0E+00	1.6E-13	-7.4E+02	9.1E-30	1.1E-25	2.3E+06	3.5E-58	2.3E+06
4.9E-01	2.0E+00	1.4E-13	-6.3E+02	7.8E-30	8.1E-26	1.6E+06	2.5E-58	1.6E+06
5.0E-01	2.0E+00	6.8E-14	-3.1E+02	3.8E-30	1.9E-26	3.8E+05	5.8E-59	3.8E+05
5.1E-01	2.0E+00	-2.4E-14	1.1E+02	-1.3E-30	2.2E-27	4.5E+04	6.8E-60	4.5E+04
5.1E-01	2.0E+00	-1.0E-13	4.6E+02	-5.7E-30	4.0E-26	8.2E+05	1.2E-58	8.2E+05
5.2E-01	1.9E+00	-1.4E-13	6.3E+02	-7.7E-30	7.2E-26	1.5E+06	2.2E-58	1.5E+06
5.3E-01	1.9E+00	-1.2E-13	5.3E+02	-6.5E-30	5.0E-26	1.0E+06	1.5E-58	1.0E+06
5.3E-01	1.9E+00	-8.8E-14	4.0E+02	-4.9E-30	2.8E-26	5.6E+05	8.5E-59	5.6E+05
5.3E-01	1.9E+00	-4.1E-14	1.9E+02	-2.3E-30	6.0E-27	1.2E+05	1.8E-59	1.2E+05
5.4E-01	1.9E+00	1.9E-14	-8.4E+01	1.0E-30	1.2E-27	2.5E+04	3.8E-60	2.5E+04
5.4E-01	1.8E+00	7.8E-14	-3.5E+02	4.4E-30	2.1E-26	4.3E+05	6.5E-59	4.3E+05
5.5E-01	1.8E+00	1.2E-13	-5.2E+02	6.4E-30	4.5E-26	9.1E+05	1.4E-58	9.1E+05
5.5E-01	1.8E+00	1.1E-13	-4.8E+02	5.9E-30	3.7E-26	7.6E+05	1.1E-58	7.6E+05
5.6E-01	1.8E+00	5.2E-14	-2.4E+02	2.9E-30	8.7E-27	1.8E+05	2.7E-59	1.8E+05
5.7E-01	1.8E+00	-2.3E-14	1.0E+02	-1.3E-30	1.7E-27	3.4E+04	5.2E-60	3.4E+04
5.8E-01	1.7E+00	-8.5E-14	3.8E+02	-4.7E-30	2.2E-26	4.4E+05	6.7E-59	4.4E+05
5.8E-01	1.7E+00	-9.8E-14	4.4E+02	-5.4E-30	2.8E-26	5.7E+05	8.7E-59	5.7E+05
5.9E-01	1.7E+00	-8.2E-14	3.7E+02	-4.5E-30	1.9E-26	3.9E+05	5.9E-59	3.9E+05
5.9E-01	1.7E+00	-4.7E-14	2.1E+02	-2.6E-30	6.4E-27	1.3E+05	2.0E-59	1.3E+05
6.0E-01	1.7E+00	1.3E-16	-5.9E-01	7.3E-33	4.9E-32	9.9E-01	1.5E-64	9.9E-01
6.0E-01	1.7E+00	4.9E-14	-2.2E+02	2.7E-30	6.6E-27	1.3E+05	2.0E-59	1.3E+05
6.1E-01	1.6E+00	8.1E-14	-3.6E+02	4.5E-30	1.8E-26	3.6E+05	5.5E-59	3.6E+05
6.1E-01	1.6E+00	8.1E-14	-3.7E+02	4.5E-30	1.8E-26	3.5E+05	5.4E-59	3.5E+05

6.2E-01	1.6E+00	4.9E-14	-2.2E+02	2.7E-30	6.2E-27	1.2E+05	1.9E-59	1.2E+05
6.3E-01	1.6E+00	-2.6E-15	1.2E+01	-1.4E-31	1.7E-29	3.5E+02	5.3E-62	3.5E+02
6.3E-01	1.6E+00	-5.0E-14	2.3E+02	-2.8E-30	6.3E-27	1.3E+05	1.9E-59	1.3E+05
6.4E-01	1.6E+00	-7.2E-14	3.3E+02	-4.0E-30	1.3E-26	2.6E+05	3.9E-59	2.6E+05
6.5E-01	1.5E+00	-5.6E-14	2.5E+02	-3.1E-30	7.5E-27	1.5E+05	2.3E-59	1.5E+05
6.6E-01	1.5E+00	-1.0E-14	4.5E+01	-5.6E-31	2.4E-28	4.8E+03	7.3E-61	4.8E+03
6.6E-01	1.5E+00	3.9E-14	-1.8E+02	2.2E-30	3.5E-27	7.0E+04	1.1E-59	7.0E+04
6.7E-01	1.5E+00	6.1E-14	-2.8E+02	3.4E-30	8.3E-27	1.7E+05	2.6E-59	1.7E+05
6.8E-01	1.5E+00	3.6E-14	-1.6E+02	2.0E-30	2.8E-27	5.6E+04	8.5E-60	5.6E+04
6.9E-01	1.5E+00	1.1E-14	-4.9E+01	6.0E-31	2.5E-28	5.0E+03	7.7E-61	5.0E+03
6.9E-01	1.4E+00	-1.9E-14	8.7E+01	-1.1E-30	7.8E-28	1.6E+04	2.4E-60	1.6E+04
7.0E-01	1.4E+00	-4.4E-14	2.0E+02	-2.4E-30	4.0E-27	8.1E+04	1.2E-59	8.1E+04
7.0E-01	1.4E+00	-5.2E-14	2.3E+02	-2.9E-30	5.4E-27	1.1E+05	1.7E-59	1.1E+05
7.1E-01	1.4E+00	-3.7E-14	1.7E+02	-2.1E-30	2.7E-27	5.5E+04	8.3E-60	5.5E+04
7.2E-01	1.4E+00	-6.2E-15	2.8E+01	-3.4E-31	7.4E-29	1.5E+03	2.3E-61	1.5E+03
7.2E-01	1.4E+00	5.6E-15	-2.5E+01	3.1E-31	6.0E-29	1.2E+03	1.8E-61	1.2E+03
7.2E-01	1.4E+00	9.2E-14	-2.5E+01	3.1E-31	1.6E-26	1.2E+03	1.8E-61	1.2E+03
7.2E-01	1.4E+00	6.6E-14	-3.7E+01	4.5E-31	8.3E-27	2.6E+03	3.9E-61	2.6E+03
7.2E-01	1.4E+00	1.7E-13	-4.9E+01	6.1E-31	5.3E-26	4.7E+03	7.1E-61	4.7E+03
7.2E-01	1.4E+00	1.3E-13	-6.3E+01	7.7E-31	3.2E-26	7.5E+03	1.1E-60	7.5E+03
7.2E-01	1.4E+00	-9.4E-15	-7.6E+01	9.4E-31	1.7E-28	1.1E+04	1.7E-60	1.1E+04
7.2E-01	1.4E+00	7.4E-14	-9.0E+01	1.1E-30	1.1E-26	1.6E+04	2.4E-60	1.6E+04
7.2E-01	1.4E+00	-1.2E-13	-1.0E+02	1.3E-30	2.7E-26	2.1E+04	3.2E-60	2.1E+04
7.3E-01	1.4E+00	1.9E-13	-1.2E+02	1.5E-30	6.8E-26	2.7E+04	4.1E-60	2.7E+04
7.3E-01	1.4E+00	2.9E-14	-1.3E+02	1.6E-30	1.6E-27	3.3E+04	5.1E-60	3.3E+04
7.3E-01	1.4E+00	4.8E-14	-1.5E+02	1.8E-30	4.3E-27	4.0E+04	6.1E-60	4.0E+04
7.3E-01	1.4E+00	-2.4E-14	-1.5E+02	1.9E-30	1.1E-27	4.3E+04	6.5E-60	4.3E+04
7.3E-01	1.4E+00	-6.1E-13	-1.5E+02	1.9E-30	7.0E-25	4.4E+04	6.7E-60	4.4E+04
7.3E-01	1.4E+00	-3.5E-13	-1.5E+02	1.9E-30	2.3E-25	4.4E+04	6.7E-60	4.4E+04
7.3E-01	1.4E+00	1.0E-13	-1.5E+02	1.9E-30	2.0E-26	4.4E+04	6.7E-60	4.4E+04
7.3E-01	1.4E+00	-6.5E-13	-1.5E+02	1.9E-30	7.9E-25	4.5E+04	6.8E-60	4.5E+04
7.3E-01	1.4E+00	1.8E-13	-1.6E+02	1.9E-30	6.4E-26	4.6E+04	7.0E-60	4.6E+04
7.3E-01	1.4E+00	-1.6E-14	-1.6E+02	2.0E-30	4.8E-28	4.8E+04	7.2E-60	4.8E+04
7.3E-01	1.4E+00	-3.0E-13	-1.7E+02	2.0E-30	1.7E-25	5.2E+04	7.8E-60	5.2E+04
7.3E-01	1.4E+00	3.4E-13	-1.8E+02	2.2E-30	2.2E-25	5.9E+04	8.9E-60	5.9E+04
7.3E-01	1.4E+00	1.2E-13	-1.9E+02	2.4E-30	2.8E-26	6.9E+04	1.0E-59	6.9E+04
7.3E-01	1.4E+00	-1.2E-13	-2.0E+02	2.4E-30	2.7E-26	7.3E+04	1.1E-59	7.3E+04
7.4E-01	1.4E+00	-2.4E-13	-1.8E+02	2.2E-30	1.1E-25	5.7E+04	8.7E-60	5.7E+04
7.4E-01	1.3E+00	5.2E-14	-1.1E+02	1.3E-30	4.9E-27	2.2E+04	3.3E-60	2.2E+04
7.5E-01	1.3E+00	3.5E-13	-1.6E+01	2.0E-31	2.2E-25	4.5E+02	6.9E-62	4.5E+02
7.5E-01	1.3E+00	2.4E-13	-1.6E+01	2.0E-31	9.9E-26	4.5E+02	6.9E-62	4.5E+02
7.6E-01	1.3E+00	-1.6E-13	1.0E+02	-1.3E-30	4.4E-26	1.9E+04	2.8E-60	1.9E+04
7.6E-01	1.3E+00	-1.3E-12	1.4E+02	-1.8E-30	2.7E-24	3.6E+04	5.4E-60	3.6E+04
7.6E-01	1.3E+00	-7.7E-13	1.7E+02	-2.1E-30	1.0E-24	4.8E+04	7.3E-60	4.8E+04

7.7E-01	1.3E+00	2.5E-13	1.6E+02	-1.9E-30	1.0E-25	4.2E+04	6.3E-60	4.2E+04
7.7E-01	1.3E+00	-5.1E-13	1.0E+02	-1.2E-30	4.3E-25	1.7E+04	2.6E-60	1.7E+04
7.8E-01	1.3E+00	-1.0E-12	7.8E+00	-9.7E-32	1.7E-24	1.0E+02	1.5E-62	1.0E+02
7.9E-01	1.3E+00	-4.6E-13	-8.9E+01	1.1E-30	3.4E-25	1.3E+04	2.0E-60	1.3E+04
7.9E-01	1.3E+00	-5.3E-13	-1.4E+02	1.7E-30	4.4E-25	3.2E+04	4.8E-60	3.2E+04
8.0E-01	1.2E+00	5.2E-13	-1.2E+02	1.4E-30	4.3E-25	2.1E+04	3.2E-60	2.1E+04
8.1E-01	1.2E+00	-6.4E-13	-2.8E+01	3.5E-31	6.3E-25	1.2E+03	1.9E-61	1.2E+03
8.2E-01	1.2E+00	-6.4E-14	7.0E+01	-8.6E-31	6.2E-27	7.3E+03	1.1E-60	7.3E+03
8.2E-01	1.2E+00	1.2E-12	1.2E+02	-1.5E-30	2.0E-24	2.1E+04	3.2E-60	2.1E+04
8.3E-01	1.2E+00	-2.6E-13	9.5E+01	-1.2E-30	9.5E-26	1.3E+04	2.0E-60	1.3E+04
8.4E-01	1.2E+00	1.1E-12	1.2E+01	-1.5E-31	1.6E-24	2.0E+02	3.0E-62	2.0E+02
8.5E-01	1.2E+00	6.0E-14	-7.3E+01	9.0E-31	5.0E-27	7.4E+03	1.1E-60	7.4E+03
8.6E-01	1.2E+00	2.6E-13	-1.0E+02	1.2E-30	9.3E-26	1.4E+04	2.1E-60	1.4E+04
8.7E-01	1.2E+00	-5.0E-13	-4.2E+01	5.2E-31	3.3E-25	2.4E+03	3.6E-61	2.4E+03
8.8E-01	1.1E+00	-9.5E-13	4.8E+01	-5.9E-31	1.2E-24	3.0E+03	4.6E-61	3.0E+03
8.9E-01	1.1E+00	-4.5E-13	8.5E+01	-1.1E-30	2.5E-25	9.2E+03	1.4E-60	9.2E+03
8.9E-01	1.1E+00	-4.4E-13	7.2E+01	-8.9E-31	2.4E-25	6.5E+03	9.9E-61	6.5E+03
9.0E-01	1.1E+00	4.1E-13	3.5E+01	-4.3E-31	2.1E-25	1.5E+03	2.3E-61	1.5E+03
9.1E-01	1.1E+00	-1.7E-13	-1.6E+01	2.0E-31	3.6E-26	3.2E+02	4.8E-62	3.2E+02
9.1E-01	1.1E+00	8.4E-13	-6.0E+01	7.4E-31	8.5E-25	4.3E+03	6.5E-61	4.3E+03
9.2E-01	1.1E+00	-2.3E-13	-7.2E+01	8.8E-31	6.2E-26	6.1E+03	9.2E-61	6.1E+03
9.3E-01	1.1E+00	-1.1E-14	-4.4E+01	5.4E-31	1.5E-28	2.2E+03	3.4E-61	2.2E+03
9.4E-01	1.1E+00	-8.9E-13	8.8E+00	-1.1E-31	9.0E-25	8.8E+01	1.3E-62	8.8E+01
9.4E-01	1.1E+00	5.7E-13	5.3E+01	-6.5E-31	3.7E-25	3.1E+03	4.7E-61	3.1E+03
9.5E-01	1.0E+00	5.7E-13	5.7E+01	-7.0E-31	3.6E-25	3.6E+03	5.5E-61	3.6E+03
9.6E-01	1.0E+00	-2.8E-13	1.5E+01	-1.9E-31	8.4E-26	2.5E+02	3.8E-62	2.5E+02
9.7E-01	1.0E+00	3.0E-13	-3.7E+01	4.5E-31	9.3E-26	1.4E+03	2.1E-61	1.4E+03
9.8E-01	1.0E+00	6.7E-15	-5.0E+01	6.1E-31	4.7E-29	2.6E+03	3.9E-61	2.6E+03
9.9E-01	1.0E+00	5.6E-14	-1.7E+01	2.1E-31	3.1E-27	2.9E+02	4.3E-62	2.9E+02
1.0E+00	1.0E+00	2.8E-13	7.2E+00	-8.8E-32	7.8E-26	5.2E+01	7.9E-63	5.2E+01
1.0E+00	1.0E+00	3.3E-13	3.1E+01	-3.8E-31	1.1E-25	9.6E+02	1.5E-61	9.6E+02
1.0E+00	9.9E-01	-2.7E-14	4.3E+01	-5.3E-31	6.9E-28	1.8E+03	2.8E-61	1.8E+03
1.0E+00	9.8E-01	1.7E-13	3.5E+01	-4.3E-31	2.6E-26	1.2E+03	1.8E-61	1.2E+03
1.0E+00	9.8E-01	-3.6E-14	7.5E+00	-9.2E-32	1.2E-27	5.3E+01	8.1E-63	5.3E+01
1.0E+00	9.7E-01	4.6E-14	-2.3E+01	2.8E-31	2.0E-27	4.9E+02	7.5E-62	4.9E+02
1.0E+00	9.6E-01	2.4E-14	-3.7E+01	4.5E-31	5.3E-28	1.2E+03	1.9E-61	1.2E+03
1.0E+00	9.6E-01	1.6E-14	-3.6E+01	4.4E-31	2.4E-28	1.2E+03	1.8E-61	1.2E+03
1.0E+00	9.6E-01	-1.4E-14	-3.5E+01	4.3E-31	1.9E-28	1.1E+03	1.7E-61	1.1E+03
1.0E+00	9.6E-01	-2.9E-14	-3.2E+01	4.0E-31	7.9E-28	9.6E+02	1.5E-61	9.6E+02
1.0E+00	9.6E-01	4.9E-14	-3.1E+01	3.8E-31	2.2E-27	8.6E+02	1.3E-61	8.6E+02
1.0E+00	9.5E-01	1.3E-14	-2.8E+01	3.5E-31	1.6E-28	7.2E+02	1.1E-61	7.2E+02
1.0E+00	9.5E-01	9.7E-15	-2.5E+01	3.0E-31	8.5E-29	5.5E+02	8.3E-62	5.5E+02
1.1E+00	9.5E-01	9.2E-15	-2.0E+01	2.5E-31	7.7E-29	3.6E+02	5.5E-62	3.6E+02
1.1E+00	9.5E-01	4.6E-15	-1.4E+01	1.7E-31	1.9E-29	1.8E+02	2.7E-62	1.8E+02

1.1E+00	9.5E-01	-7.3E-15	-7.0E+00	8.6E-32	4.8E-29	4.4E+01	6.7E-63	4.4E+01
1.1E+00	9.5E-01	-4.1E-15	1.2E+00	-1.5E-32	1.5E-29	1.2E+00	1.9E-64	1.2E+00
1.1E+00	9.4E-01	2.6E-15	1.0E+01	-1.2E-31	6.2E-30	9.1E+01	1.4E-62	9.1E+01
1.1E+00	9.4E-01	4.8E-15	1.9E+01	-2.4E-31	2.0E-29	3.2E+02	4.9E-62	3.2E+02
1.1E+00	9.4E-01	-3.4E-15	2.7E+01	-3.3E-31	9.9E-30	6.3E+02	9.6E-62	6.3E+02
1.1E+00	9.3E-01	-3.7E-15	3.1E+01	-3.8E-31	1.2E-29	8.4E+02	1.3E-61	8.4E+02
1.1E+00	9.3E-01	-7.1E-15	3.1E+01	-3.8E-31	4.4E-29	8.2E+02	1.2E-61	8.2E+02
1.1E+00	9.3E-01	-6.5E-15	2.9E+01	-3.6E-31	3.6E-29	7.3E+02	1.1E-61	7.3E+02
1.1E+00	9.3E-01	-6.2E-15	2.8E+01	-3.4E-31	3.3E-29	6.7E+02	1.0E-61	6.7E+02
1.1E+00	9.3E-01	-5.7E-15	2.6E+01	-3.2E-31	2.8E-29	5.7E+02	8.6E-62	5.7E+02
1.1E+00	9.3E-01	-5.0E-15	2.2E+01	-2.8E-31	2.1E-29	4.3E+02	6.6E-62	4.3E+02
1.1E+00	9.2E-01	-4.0E-15	1.8E+01	-2.2E-31	1.4E-29	2.8E+02	4.2E-62	2.8E+02
1.1E+00	9.2E-01	-2.7E-15	1.2E+01	-1.5E-31	6.2E-30	1.3E+02	1.9E-62	1.3E+02
1.1E+00	9.2E-01	-1.1E-15	5.1E+00	-6.2E-32	1.1E-30	2.2E+01	3.3E-63	2.2E+01
1.1E+00	9.2E-01	6.6E-16	-3.0E+00	3.7E-32	3.7E-31	7.5E+00	1.1E-63	7.5E+00
1.1E+00	9.2E-01	2.5E-15	-1.1E+01	1.4E-31	5.3E-30	1.1E+02	1.6E-62	1.1E+02
1.1E+00	9.1E-01	4.2E-15	-1.9E+01	2.3E-31	1.5E-29	3.0E+02	4.6E-62	3.0E+02
1.1E+00	9.1E-01	5.5E-15	-2.5E+01	3.0E-31	2.5E-29	5.0E+02	7.6E-62	5.0E+02
1.1E+00	9.1E-01	5.9E-15	-2.7E+01	3.3E-31	2.8E-29	5.8E+02	8.8E-62	5.8E+02
1.1E+00	9.0E-01	5.1E-15	-2.3E+01	2.8E-31	2.1E-29	4.3E+02	6.5E-62	4.3E+02
1.1E+00	9.0E-01	2.8E-15	-1.3E+01	1.6E-31	6.5E-30	1.3E+02	2.0E-62	1.3E+02
1.1E+00	8.9E-01	-5.2E-16	2.4E+00	-2.9E-32	2.2E-31	4.5E+00	6.8E-64	4.5E+00
1.1E+00	8.9E-01	-3.8E-15	1.7E+01	-2.1E-31	1.1E-29	2.3E+02	3.4E-62	2.3E+02
1.1E+00	8.8E-01	-5.0E-15	2.2E+01	-2.8E-31	1.9E-29	3.9E+02	6.0E-62	3.9E+02
1.1E+00	8.8E-01	-3.1E-15	1.4E+01	-1.7E-31	7.4E-30	1.5E+02	2.3E-62	1.5E+02
1.2E+00	8.7E-01	9.0E-16	-4.0E+00	5.0E-32	6.1E-31	1.2E+01	1.9E-63	1.2E+01
1.2E+00	8.6E-01	4.0E-15	-1.8E+01	2.2E-31	1.2E-29	2.4E+02	3.6E-62	2.4E+02
1.2E+00	8.5E-01	3.3E-15	-1.5E+01	1.8E-31	7.8E-30	1.6E+02	2.4E-62	1.6E+02
1.2E+00	8.5E-01	-3.0E-16	1.4E+00	-1.7E-32	6.6E-32	1.3E+00	2.0E-64	1.3E+00
1.2E+00	8.4E-01	-3.2E-15	1.4E+01	-1.8E-31	7.3E-30	1.5E+02	2.2E-62	1.5E+02
1.2E+00	8.3E-01	-2.9E-15	1.3E+01	-1.6E-31	5.9E-30	1.2E+02	1.8E-62	1.2E+02
1.2E+00	8.3E-01	-2.4E-17	1.1E-01	-1.3E-33	3.9E-34	8.0E-03	1.2E-66	8.0E-03
1.2E+00	8.2E-01	2.6E-15	-1.2E+01	1.4E-31	4.4E-30	8.9E+01	1.4E-62	8.9E+01
1.2E+00	8.1E-01	2.6E-15	-1.2E+01	1.4E-31	4.3E-30	8.8E+01	1.3E-62	8.8E+01
1.2E+00	8.1E-01	2.5E-16	-1.1E+00	1.4E-32	4.2E-32	8.5E-01	1.3E-64	8.5E-01
1.3E+00	8.0E-01	-2.0E-15	9.1E+00	-1.1E-31	2.6E-30	5.3E+01	8.1E-63	5.3E+01
1.3E+00	7.9E-01	-2.2E-15	1.0E+01	-1.2E-31	3.1E-30	6.4E+01	9.7E-63	6.4E+01
1.3E+00	7.9E-01	-4.1E-16	1.8E+00	-2.3E-32	1.0E-31	2.1E+00	3.2E-64	2.1E+00
1.3E+00	7.8E-01	1.6E-15	-7.1E+00	8.8E-32	1.5E-30	3.1E+01	4.7E-63	3.1E+01
1.3E+00	7.7E-01	1.9E-15	-8.7E+00	1.1E-31	2.2E-30	4.5E+01	6.9E-63	4.5E+01
1.3E+00	7.7E-01	5.0E-16	-2.3E+00	2.8E-32	1.5E-31	3.0E+00	4.6E-64	3.0E+00
1.3E+00	7.6E-01	-1.2E-15	5.5E+00	-6.8E-32	8.7E-31	1.8E+01	2.7E-63	1.8E+01
1.3E+00	7.6E-01	-1.7E-15	7.4E+00	-9.2E-32	1.6E-30	3.2E+01	4.8E-63	3.2E+01
1.3E+00	7.5E-01	-5.5E-16	2.5E+00	-3.1E-32	1.7E-31	3.5E+00	5.3E-64	3.5E+00

1.3E+00	7.5E-01	9.2E-16	-4.2E+00	5.1E-32	4.8E-31	9.7E+00	1.5E-63	9.7E+00
1.4E+00	7.4E-01	1.4E-15	-6.3E+00	7.8E-32	1.1E-30	2.2E+01	3.3E-63	2.2E+01
1.4E+00	7.3E-01	5.7E-16	-2.6E+00	3.2E-32	1.8E-31	3.6E+00	5.4E-64	3.6E+00
1.4E+00	7.3E-01	-6.9E-16	3.1E+00	-3.8E-32	2.5E-31	5.1E+00	7.7E-64	5.1E+00
1.4E+00	7.2E-01	-1.2E-15	5.4E+00	-6.6E-32	7.4E-31	1.5E+01	2.3E-63	1.5E+01
1.4E+00	7.2E-01	-5.6E-16	2.5E+00	-3.1E-32	1.7E-31	3.3E+00	5.1E-64	3.3E+00
1.4E+00	7.1E-01	5.0E-16	-2.2E+00	2.8E-32	1.3E-31	2.6E+00	3.9E-64	2.6E+00
1.4E+00	7.1E-01	1.0E-15	-4.5E+00	5.5E-32	5.0E-31	1.0E+01	1.5E-63	1.0E+01
1.4E+00	7.0E-01	5.4E-16	-2.4E+00	3.0E-32	1.5E-31	3.0E+00	4.5E-64	3.0E+00
1.4E+00	7.0E-01	-3.5E-16	1.6E+00	-1.9E-32	5.9E-32	1.2E+00	1.8E-64	1.2E+00
1.4E+00	6.9E-01	-8.3E-16	3.7E+00	-4.6E-32	3.3E-31	6.7E+00	1.0E-63	6.7E+00
1.4E+00	6.9E-01	-8.1E-16	3.7E+00	-4.5E-32	3.2E-31	6.4E+00	9.8E-64	6.4E+00
1.4E+00	6.9E-01	-8.1E-16	3.7E+00	-4.5E-32	3.2E-31	6.4E+00	9.8E-64	6.4E+00
1.4E+00	6.9E-01	-8.0E-16	3.6E+00	-4.5E-32	3.1E-31	6.3E+00	9.5E-64	6.3E+00
1.4E+00	6.9E-01	-7.9E-16	3.6E+00	-4.4E-32	3.0E-31	6.1E+00	9.2E-64	6.1E+00
1.4E+00	6.9E-01	-7.7E-16	3.5E+00	-4.3E-32	2.9E-31	5.8E+00	8.8E-64	5.8E+00
1.4E+00	6.9E-01	-7.5E-16	3.4E+00	-4.2E-32	2.7E-31	5.5E+00	8.3E-64	5.5E+00
1.4E+00	6.9E-01	-7.3E-16	3.3E+00	-4.0E-32	2.5E-31	5.1E+00	7.8E-64	5.1E+00
1.4E+00	6.9E-01	-7.0E-16	3.1E+00	-3.9E-32	2.3E-31	4.7E+00	7.1E-64	4.7E+00
1.4E+00	6.9E-01	-6.6E-16	3.0E+00	-3.7E-32	2.1E-31	4.2E+00	6.4E-64	4.2E+00
1.4E+00	6.9E-01	-6.2E-16	2.8E+00	-3.4E-32	1.8E-31	3.7E+00	5.7E-64	3.7E+00
1.4E+00	6.9E-01	-5.7E-16	2.6E+00	-3.2E-32	1.6E-31	3.2E+00	4.8E-64	3.2E+00
1.5E+00	6.9E-01	-1.6E-14	2.4E+00	-2.9E-32	1.2E-28	2.6E+00	4.0E-64	2.6E+00
1.5E+00	6.9E-01	8.6E-14	2.3E+00	-2.9E-32	3.5E-27	2.6E+00	4.0E-64	2.6E+00
1.5E+00	6.9E-01	-1.2E-13	2.3E+00	-2.9E-32	6.4E-27	2.6E+00	4.0E-64	2.6E+00
1.5E+00	6.9E-01	-1.1E-13	2.3E+00	-2.9E-32	6.3E-27	2.6E+00	3.9E-64	2.6E+00
1.5E+00	6.9E-01	-3.3E-13	2.3E+00	-2.8E-32	5.1E-26	2.5E+00	3.8E-64	2.5E+00
1.5E+00	6.9E-01	2.8E-13	2.2E+00	-2.7E-32	3.8E-26	2.3E+00	3.5E-64	2.3E+00
1.5E+00	6.9E-01	3.1E-13	2.0E+00	-2.5E-32	4.5E-26	2.0E+00	3.0E-64	2.0E+00
1.5E+00	6.9E-01	1.9E-13	1.7E+00	-2.1E-32	1.7E-26	1.4E+00	2.1E-64	1.4E+00
1.5E+00	6.9E-01	-7.1E-14	9.9E-01	-1.2E-32	2.4E-27	4.7E-01	7.1E-65	4.7E-01
1.5E+00	6.9E-01	9.0E-13	-4.9E-01	6.1E-33	3.8E-25	1.1E-01	1.7E-65	1.1E-01
1.5E+00	6.8E-01	1.0E-13	-2.5E+00	3.1E-32	5.1E-27	2.9E+00	4.4E-64	2.9E+00
1.5E+00	6.8E-01	-1.5E-13	-3.1E+00	3.9E-32	1.1E-26	4.5E+00	6.8E-64	4.5E+00
1.5E+00	6.8E-01	3.2E-13	-3.1E+00	3.9E-32	4.7E-26	4.5E+00	6.8E-64	4.5E+00
1.5E+00	6.8E-01	5.0E-13	-3.1E+00	3.8E-32	1.1E-25	4.5E+00	6.8E-64	4.5E+00
1.5E+00	6.8E-01	4.3E-13	-3.1E+00	3.8E-32	8.4E-26	4.4E+00	6.7E-64	4.4E+00
1.5E+00	6.8E-01	-1.9E-13	-3.0E+00	3.7E-32	1.6E-26	4.2E+00	6.4E-64	4.2E+00
1.5E+00	6.8E-01	-5.7E-13	-2.9E+00	3.6E-32	1.5E-25	3.9E+00	5.9E-64	3.9E+00
1.5E+00	6.8E-01	6.9E-13	-2.7E+00	3.4E-32	2.2E-25	3.5E+00	5.2E-64	3.5E+00
1.5E+00	6.8E-01	3.1E-14	-2.5E+00	3.1E-32	4.4E-28	2.9E+00	4.4E-64	2.9E+00
1.5E+00	6.8E-01	1.5E-13	-2.3E+00	2.8E-32	1.1E-26	2.3E+00	3.5E-64	2.3E+00
1.5E+00	6.8E-01	-3.8E-14	-1.9E+00	2.4E-32	6.6E-28	1.7E+00	2.5E-64	1.7E+00
1.5E+00	6.7E-01	6.1E-13	-1.5E+00	1.9E-32	1.7E-25	1.1E+00	1.6E-64	1.1E+00

1.5E+00	6.7E-01	4.5E-13	-1.5E+00	1.8E-32	9.2E-26	9.6E-01	1.5E-64	9.6E-01
1.5E+00	6.7E-01	1.1E-12	-1.5E+00	1.8E-32	5.2E-25	9.6E-01	1.5E-64	9.6E-01
1.5E+00	6.7E-01	4.0E-13	-9.8E-01	1.2E-32	7.3E-26	4.3E-01	6.6E-65	4.3E-01
1.5E+00	6.7E-01	6.1E-13	-3.0E-01	3.7E-33	1.7E-25	4.0E-02	6.0E-66	4.0E-02
1.5E+00	6.7E-01	-4.7E-13	5.6E-01	-6.9E-33	9.8E-26	1.4E-01	2.1E-65	1.4E-01
1.5E+00	6.7E-01	-1.3E-13	1.5E+00	-1.8E-32	7.3E-27	9.7E-01	1.5E-64	9.7E-01
1.5E+00	6.7E-01	-2.3E-13	2.3E+00	-2.8E-32	2.4E-26	2.3E+00	3.5E-64	2.3E+00
1.5E+00	6.7E-01	8.0E-13	2.7E+00	-3.3E-32	2.8E-25	3.1E+00	4.7E-64	3.1E+00
1.5E+00	6.6E-01	-7.7E-13	2.3E+00	-2.9E-32	2.6E-25	2.4E+00	3.7E-64	2.4E+00
1.5E+00	6.6E-01	-6.8E-13	1.2E+00	-1.4E-32	2.0E-25	5.9E-01	9.0E-65	5.9E-01
1.5E+00	6.6E-01	-2.3E-13	-6.4E-01	7.9E-33	2.2E-26	1.8E-01	2.7E-65	1.8E-01
1.5E+00	6.5E-01	5.9E-13	-2.1E+00	2.6E-32	1.5E-25	1.8E+00	2.8E-64	1.8E+00
1.5E+00	6.5E-01	1.1E-12	-1.9E+00	2.4E-32	4.8E-25	1.6E+00	2.4E-64	1.6E+00
1.5E+00	6.5E-01	3.6E-13	-1.1E-01	1.3E-33	5.4E-26	4.6E-03	7.0E-67	4.6E-03
1.6E+00	6.4E-01	-1.3E-14	1.6E+00	-2.0E-32	6.7E-29	1.1E+00	1.6E-64	1.1E+00
1.6E+00	6.4E-01	-8.5E-13	1.7E+00	-2.1E-32	2.9E-25	1.1E+00	1.7E-64	1.1E+00
1.6E+00	6.3E-01	-2.3E-13	2.4E-01	-2.9E-33	2.2E-26	2.3E-02	3.4E-66	2.3E-02
1.6E+00	6.3E-01	6.0E-13	-1.3E+00	1.6E-32	1.4E-25	6.3E-01	9.5E-65	6.3E-01
1.6E+00	6.3E-01	-1.6E-13	-1.5E+00	1.8E-32	9.5E-27	8.3E-01	1.3E-64	8.3E-01
1.6E+00	6.2E-01	9.3E-14	-3.2E-01	4.0E-33	3.4E-27	4.0E-02	6.1E-66	4.0E-02
1.6E+00	6.2E-01	-1.8E-13	9.8E-01	-1.2E-32	1.3E-26	3.6E-01	5.5E-65	3.6E-01
1.6E+00	6.1E-01	-5.0E-13	1.3E+00	-1.5E-32	9.5E-26	5.9E-01	9.0E-65	5.9E-01
1.6E+00	6.1E-01	-9.5E-13	3.7E-01	-4.6E-33	3.3E-25	5.2E-02	7.9E-66	5.2E-02
1.6E+00	6.1E-01	-2.6E-14	-7.5E-01	9.2E-33	2.4E-28	2.1E-01	3.1E-65	2.1E-01
1.7E+00	6.0E-01	-4.3E-13	-1.1E+00	1.3E-32	6.7E-26	4.2E-01	6.3E-65	4.2E-01
1.7E+00	6.0E-01	-3.8E-13	-4.0E-01	4.9E-33	5.2E-26	5.6E-02	8.6E-66	5.6E-02
1.7E+00	6.0E-01	1.6E-13	5.6E-01	-6.9E-33	8.6E-27	1.1E-01	1.7E-65	1.1E-01
1.7E+00	5.9E-01	-5.6E-13	9.1E-01	-1.1E-32	1.1E-25	2.9E-01	4.4E-65	2.9E-01
1.7E+00	5.9E-01	4.8E-13	4.0E-01	-4.9E-33	7.9E-26	5.6E-02	8.4E-66	5.6E-02
1.7E+00	5.9E-01	-9.6E-14	-4.1E-01	5.1E-33	3.1E-27	5.8E-02	8.8E-66	5.8E-02
1.7E+00	5.8E-01	-1.4E-13	-7.6E-01	9.4E-33	6.6E-27	2.0E-01	3.0E-65	2.0E-01
1.7E+00	5.8E-01	4.1E-14	-3.9E-01	4.8E-33	5.6E-28	5.1E-02	7.7E-66	5.1E-02
1.7E+00	5.8E-01	2.8E-13	2.9E-01	-3.6E-33	2.6E-26	2.9E-02	4.3E-66	2.9E-02
1.7E+00	5.7E-01	3.8E-14	6.4E-01	-7.9E-33	4.7E-28	1.3E-01	2.0E-65	1.3E-01
1.8E+00	5.7E-01	7.7E-15	3.7E-01	-4.6E-33	1.9E-29	4.4E-02	6.7E-66	4.4E-02
1.8E+00	5.7E-01	1.4E-14	8.5E-02	-1.1E-33	6.3E-29	2.3E-03	3.6E-67	2.3E-03
1.8E+00	5.7E-01	6.5E-15	-2.9E-02	3.5E-34	1.4E-29	2.7E-04	4.0E-68	2.7E-04
1.8E+00	5.7E-01	-6.3E-15	-1.4E-01	1.7E-33	1.3E-29	6.2E-03	9.5E-67	6.2E-03
1.8E+00	5.7E-01	8.7E-15	-1.9E-01	2.4E-33	2.4E-29	1.2E-02	1.8E-66	1.2E-02
1.8E+00	5.7E-01	-3.3E-14	-2.5E-01	3.1E-33	3.4E-28	2.0E-02	3.1E-66	2.0E-02
1.8E+00	5.6E-01	2.0E-14	-3.2E-01	3.9E-33	1.3E-28	3.2E-02	4.9E-66	3.2E-02
1.8E+00	5.6E-01	-1.9E-14	-3.9E-01	4.7E-33	1.2E-28	4.7E-02	7.2E-66	4.7E-02
1.8E+00	5.6E-01	-2.3E-14	-4.5E-01	5.5E-33	1.6E-28	6.3E-02	9.6E-66	6.3E-02
1.8E+00	5.6E-01	2.6E-14	-5.0E-01	6.2E-33	2.1E-28	7.9E-02	1.2E-65	7.9E-02

1.8E+00	5.6E-01	2.8E-15	-5.3E-01	6.6E-33	2.5E-30	9.0E-02	1.4E-65	9.0E-02
1.8E+00	5.6E-01	1.1E-14	-5.4E-01	6.6E-33	3.6E-29	9.1E-02	1.4E-65	9.1E-02
1.8E+00	5.6E-01	2.7E-14	-5.0E-01	6.2E-33	2.3E-28	8.0E-02	1.2E-65	8.0E-02
1.8E+00	5.6E-01	2.7E-15	-4.2E-01	5.1E-33	2.2E-30	5.4E-02	8.3E-66	5.4E-02
1.8E+00	5.6E-01	-8.3E-15	-2.6E-01	3.3E-33	2.2E-29	2.2E-02	3.3E-66	2.2E-02
1.8E+00	5.6E-01	1.5E-15	-4.3E-02	5.3E-34	7.2E-31	5.7E-04	8.6E-68	5.7E-04
1.8E+00	5.6E-01	-2.1E-17	9.6E-02	-1.2E-33	1.4E-34	2.9E-03	4.4E-67	2.9E-03
1.8E+00	5.6E-01	-5.1E-17	2.3E-01	-2.8E-33	8.1E-34	1.6E-02	2.5E-66	1.6E-02
1.8E+00	5.5E-01	-6.4E-17	2.9E-01	-3.6E-33	1.3E-33	2.6E-02	3.9E-66	2.6E-02
1.8E+00	5.5E-01	-7.8E-17	3.5E-01	-4.3E-33	1.9E-33	3.8E-02	5.7E-66	3.8E-02
1.8E+00	5.5E-01	-9.0E-17	4.1E-01	-5.0E-33	2.5E-33	5.1E-02	7.7E-66	5.1E-02
1.8E+00	5.5E-01	-9.9E-17	4.5E-01	-5.5E-33	3.0E-33	6.1E-02	9.2E-66	6.1E-02
1.8E+00	5.5E-01	-1.0E-16	4.6E-01	-5.7E-33	3.2E-33	6.4E-02	9.8E-66	6.4E-02
1.8E+00	5.5E-01	-9.7E-17	4.4E-01	-5.4E-33	2.8E-33	5.8E-02	8.7E-66	5.8E-02
1.8E+00	5.5E-01	-8.1E-17	3.6E-01	-4.5E-33	2.0E-33	4.0E-02	6.1E-66	4.0E-02
1.8E+00	5.5E-01	-5.4E-17	2.4E-01	-3.0E-33	8.7E-34	1.8E-02	2.7E-66	1.8E-02
1.8E+00	5.5E-01	-1.6E-17	7.1E-02	-8.8E-34	7.5E-35	1.5E-03	2.3E-67	1.5E-03
1.8E+00	5.5E-01	2.8E-17	-1.3E-01	1.5E-33	2.3E-34	4.7E-03	7.1E-67	4.7E-03
1.8E+00	5.5E-01	6.8E-17	-3.0E-01	3.8E-33	1.4E-33	2.8E-02	4.2E-66	2.8E-02
1.8E+00	5.4E-01	8.7E-17	-3.9E-01	4.8E-33	2.2E-33	4.5E-02	6.8E-66	4.5E-02
1.8E+00	5.4E-01	6.4E-17	-2.9E-01	3.5E-33	1.2E-33	2.4E-02	3.7E-66	2.4E-02
1.9E+00	5.4E-01	-5.8E-18	2.7E-02	-3.3E-34	9.9E-36	2.0E-04	3.1E-68	2.0E-04
1.9E+00	5.4E-01	-6.6E-17	3.0E-01	-3.7E-33	1.3E-33	2.6E-02	3.9E-66	2.6E-02
1.9E+00	5.3E-01	-6.0E-17	2.7E-01	-3.4E-33	1.0E-33	2.1E-02	3.2E-66	2.1E-02
1.9E+00	5.3E-01	-7.6E-19	3.6E-03	-4.5E-35	1.6E-37	3.7E-06	5.7E-70	3.7E-06
1.9E+00	5.3E-01	5.3E-17	-2.4E-01	2.9E-33	7.8E-34	1.6E-02	2.4E-66	1.6E-02
1.9E+00	5.2E-01	5.3E-17	-2.4E-01	3.0E-33	7.8E-34	1.6E-02	2.4E-66	1.6E-02
1.9E+00	5.2E-01	5.7E-18	-2.5E-02	3.1E-34	8.7E-36	1.7E-04	2.5E-68	1.7E-04
1.9E+00	5.2E-01	-4.2E-17	1.9E-01	-2.3E-33	4.7E-34	9.6E-03	1.5E-66	9.6E-03
1.9E+00	5.2E-01	-4.7E-17	2.1E-01	-2.6E-33	5.8E-34	1.2E-02	1.8E-66	1.2E-02
1.9E+00	5.1E-01	-8.8E-18	3.9E-02	-4.8E-34	2.0E-35	4.0E-04	6.1E-68	4.0E-04
2.0E+00	5.1E-01	3.3E-17	-1.5E-01	1.8E-33	2.8E-34	5.7E-03	8.6E-67	5.7E-03
2.0E+00	5.1E-01	4.0E-17	-1.8E-01	2.2E-33	4.2E-34	8.4E-03	1.3E-66	8.4E-03
2.0E+00	5.1E-01	1.1E-17	-4.8E-02	5.9E-34	2.9E-35	5.8E-04	8.8E-68	5.8E-04
2.0E+00	5.0E-01	-2.5E-17	1.1E-01	-1.4E-33	1.6E-34	3.3E-03	4.9E-67	3.3E-03
2.0E+00	5.0E-01	-3.5E-17	1.5E-01	-1.9E-33	3.0E-34	6.0E-03	9.1E-67	6.0E-03
2.0E+00	5.0E-01	-1.1E-17	5.2E-02	-6.4E-34	3.2E-35	6.8E-04	1.0E-67	6.8E-04
2.0E+00	5.0E-01	1.9E-17	-8.6E-02	1.1E-33	9.0E-35	1.8E-03	2.8E-67	1.8E-03
2.0E+00	4.9E-01	2.9E-17	-1.3E-01	1.6E-33	2.0E-34	4.2E-03	6.4E-67	4.2E-03
2.0E+00	4.9E-01	1.2E-17	-5.4E-02	6.6E-34	3.5E-35	7.0E-04	1.1E-67	7.0E-04
2.0E+00	4.9E-01	-1.4E-17	6.4E-02	-7.9E-34	4.8E-35	9.7E-04	1.5E-67	9.7E-04
2.1E+00	4.9E-01	-2.5E-17	1.1E-01	-1.4E-33	1.4E-34	2.9E-03	4.4E-67	2.9E-03
2.1E+00	4.8E-01	-1.2E-17	5.3E-02	-6.6E-34	3.3E-35	6.6E-04	1.0E-67	6.6E-04
2.1E+00	4.8E-01	1.0E-17	-4.6E-02	5.7E-34	2.4E-35	4.9E-04	7.5E-68	4.9E-04

2.1E+00	4.8E-01	2.1E-17	-9.3E-02	1.1E-33	9.7E-35	2.0E-03	3.0E-67	2.0E-03
2.1E+00	4.8E-01	1.1E-17	-5.1E-02	6.3E-34	2.9E-35	5.9E-04	9.0E-68	5.9E-04
2.1E+00	4.7E-01	-7.2E-18	3.2E-02	-4.0E-34	1.2E-35	2.3E-04	3.5E-68	2.3E-04
2.1E+00	4.7E-01	-1.7E-17	7.7E-02	-9.5E-34	6.7E-35	1.3E-03	2.0E-67	1.3E-03
2.1E+00	4.7E-01	-1.0E-17	4.8E-02	-5.9E-34	2.3E-35	5.1E-04	7.7E-68	5.1E-04
2.1E+00	4.7E-01	4.4E-18	-2.1E-02	2.6E-34	4.2E-36	1.0E-04	1.5E-68	1.0E-04
2.1E+00	4.7E-01	1.4E-17	-6.4E-02	7.9E-34	4.4E-35	8.8E-04	1.3E-67	8.8E-04
2.2E+00	4.6E-01	9.9E-18	-4.4E-02	5.4E-34	2.1E-35	4.2E-04	6.3E-68	4.2E-04
2.2E+00	4.6E-01	-5.0E-19	3.3E-03	-4.1E-35	5.2E-38	2.3E-06	3.6E-70	2.3E-06
2.2E+00	4.6E-01	-6.4E-19	3.3E-03	-4.1E-35	8.6E-38	2.3E-06	3.6E-70	2.3E-06
2.2E+00	4.6E-01	-1.6E-18	6.8E-03	-8.4E-35	5.4E-37	9.9E-06	1.5E-69	9.9E-06
2.2E+00	4.6E-01	-2.3E-18	1.0E-02	-1.3E-34	1.1E-36	2.3E-05	3.5E-69	2.3E-05
2.2E+00	4.6E-01	-3.0E-18	1.4E-02	-1.7E-34	1.9E-36	4.2E-05	6.4E-69	4.2E-05
2.2E+00	4.6E-01	-3.7E-18	1.8E-02	-2.2E-34	2.9E-36	6.7E-05	1.0E-68	6.7E-05
2.2E+00	4.6E-01	-4.9E-18	2.1E-02	-2.6E-34	5.2E-36	9.8E-05	1.5E-68	9.8E-05
2.2E+00	4.6E-01	-5.5E-18	2.5E-02	-3.1E-34	6.4E-36	1.4E-04	2.1E-68	1.4E-04
2.2E+00	4.6E-01	-6.1E-18	2.9E-02	-3.6E-34	7.9E-36	1.8E-04	2.7E-68	1.8E-04
2.2E+00	4.6E-01	-7.2E-18	3.3E-02	-4.0E-34	1.1E-35	2.3E-04	3.4E-68	2.3E-04
2.2E+00	4.6E-01	-8.2E-18	3.6E-02	-4.5E-34	1.4E-35	2.8E-04	4.2E-68	2.8E-04
2.2E+00	4.6E-01	-5.0E-14	4.0E-02	-4.9E-34	5.4E-28	3.3E-04	5.1E-68	3.3E-04
2.2E+00	4.6E-01	-1.3E-13	4.0E-02	-4.9E-34	3.4E-27	3.4E-04	5.1E-68	3.4E-04
2.2E+00	4.6E-01	3.8E-13	4.0E-02	-4.9E-34	3.1E-26	3.4E-04	5.1E-68	3.4E-04
2.2E+00	4.6E-01	-1.1E-13	4.0E-02	-4.9E-34	2.4E-27	3.4E-04	5.2E-68	3.4E-04
2.2E+00	4.6E-01	1.7E-13	4.1E-02	-5.0E-34	6.1E-27	3.5E-04	5.3E-68	3.5E-04
2.2E+00	4.6E-01	-3.2E-13	4.2E-02	-5.1E-34	2.1E-26	3.7E-04	5.6E-68	3.7E-04
2.2E+00	4.6E-01	7.5E-14	4.4E-02	-5.4E-34	1.2E-27	4.0E-04	6.1E-68	4.0E-04
2.2E+00	4.6E-01	1.2E-13	4.7E-02	-5.8E-34	3.2E-27	4.6E-04	7.0E-68	4.6E-04
2.2E+00	4.6E-01	2.4E-13	5.2E-02	-6.4E-34	1.3E-26	5.6E-04	8.6E-68	5.6E-04
2.2E+00	4.6E-01	-3.4E-13	5.4E-02	-6.6E-34	2.4E-26	6.1E-04	9.3E-68	6.1E-04
2.2E+00	4.6E-01	-3.8E-13	3.9E-02	-4.8E-34	2.9E-26	3.1E-04	4.8E-68	3.1E-04
2.2E+00	4.6E-01	-4.8E-13	7.3E-03	-9.0E-35	4.7E-26	1.1E-05	1.7E-69	1.1E-05
2.2E+00	4.6E-01	-5.9E-13	7.3E-03	-9.0E-35	7.1E-26	1.1E-05	1.7E-69	1.1E-05
2.2E+00	4.6E-01	6.7E-13	2.9E-03	-3.6E-35	9.3E-26	1.8E-06	2.7E-70	1.8E-06
2.2E+00	4.6E-01	-3.8E-13	-2.0E-03	2.4E-35	3.0E-26	8.0E-07	1.2E-70	8.0E-07
2.2E+00	4.6E-01	1.2E-13	-7.2E-03	8.9E-35	3.2E-27	1.1E-05	1.7E-69	1.1E-05
2.2E+00	4.5E-01	1.3E-13	-1.3E-02	1.6E-34	3.4E-27	3.4E-05	5.1E-69	3.4E-05
2.2E+00	4.5E-01	-2.1E-14	-1.8E-02	2.3E-34	9.5E-29	7.0E-05	1.1E-68	7.0E-05
2.2E+00	4.5E-01	8.2E-13	-2.4E-02	3.0E-34	1.4E-25	1.2E-04	1.8E-68	1.2E-04
2.2E+00	4.5E-01	2.2E-13	-2.9E-02	3.6E-34	1.0E-26	1.8E-04	2.7E-68	1.8E-04
2.2E+00	4.5E-01	3.2E-13	-3.4E-02	4.3E-34	2.2E-26	2.4E-04	3.7E-68	2.4E-04
2.2E+00	4.5E-01	2.0E-13	-3.9E-02	4.8E-34	8.6E-27	3.1E-04	4.7E-68	3.1E-04
2.2E+00	4.5E-01	-1.3E-13	-3.9E-02	4.8E-34	3.7E-27	3.2E-04	4.8E-68	3.2E-04
2.2E+00	4.5E-01	-4.6E-13	-3.9E-02	4.8E-34	4.4E-26	3.2E-04	4.8E-68	3.2E-04
2.2E+00	4.5E-01	5.3E-13	-4.3E-02	5.3E-34	5.9E-26	3.8E-04	5.7E-68	3.8E-04

2.2E+00	4.5E-01	3.6E-13	-4.5E-02	5.6E-34	2.6E-26	4.2E-04	6.4E-68	4.2E-04
2.2E+00	4.5E-01	-5.0E-13	-4.5E-02	5.6E-34	5.0E-26	4.2E-04	6.3E-68	4.2E-04
2.2E+00	4.5E-01	-9.1E-14	-4.0E-02	4.9E-34	1.7E-27	3.3E-04	5.0E-68	3.3E-04
2.2E+00	4.5E-01	2.0E-12	-2.8E-02	3.5E-34	8.1E-25	1.6E-04	2.5E-68	1.6E-04
2.2E+00	4.5E-01	-1.7E-12	-1.0E-02	1.2E-34	5.9E-25	2.1E-05	3.1E-69	2.1E-05
2.2E+00	4.5E-01	-8.9E-13	1.2E-02	-1.5E-34	1.6E-25	3.1E-05	4.8E-69	3.1E-05
2.2E+00	4.5E-01	8.2E-13	3.3E-02	-4.0E-34	1.3E-25	2.1E-04	3.2E-68	2.1E-04
2.2E+00	4.5E-01	-3.0E-13	3.8E-02	-4.7E-34	1.8E-26	2.9E-04	4.4E-68	2.9E-04
2.3E+00	4.4E-01	6.5E-14	1.5E-02	-1.9E-34	8.2E-28	4.7E-05	7.1E-69	4.7E-05
2.3E+00	4.4E-01	-8.2E-13	-1.9E-02	2.3E-34	1.3E-25	7.0E-05	1.1E-68	7.0E-05
2.3E+00	4.4E-01	2.7E-14	-3.2E-02	4.0E-34	1.4E-28	2.0E-04	3.1E-68	2.0E-04
2.3E+00	4.4E-01	-9.3E-13	-1.5E-02	1.9E-34	1.7E-25	4.5E-05	6.8E-69	4.5E-05
2.3E+00	4.4E-01	-1.0E-12	1.4E-02	-1.7E-34	1.9E-25	3.6E-05	5.5E-69	3.6E-05
2.3E+00	4.3E-01	8.7E-13	2.7E-02	-3.4E-34	1.4E-25	1.4E-04	2.1E-68	1.4E-04
2.3E+00	4.3E-01	2.5E-13	1.5E-02	-1.8E-34	1.2E-26	4.0E-05	6.1E-69	4.0E-05
2.3E+00	4.3E-01	9.5E-13	-9.6E-03	1.2E-34	1.7E-25	1.7E-05	2.6E-69	1.7E-05
2.3E+00	4.3E-01	5.5E-14	-2.3E-02	2.8E-34	5.6E-28	9.4E-05	1.4E-68	9.4E-05
2.3E+00	4.3E-01	-3.2E-13	-1.4E-02	1.7E-34	1.9E-26	3.5E-05	5.3E-69	3.5E-05
2.4E+00	4.2E-01	-2.1E-13	6.4E-03	-7.9E-35	8.1E-27	7.5E-06	1.1E-69	7.5E-06
2.4E+00	4.2E-01	-5.1E-13	1.9E-02	-2.3E-34	4.7E-26	6.3E-05	9.5E-69	6.3E-05
2.4E+00	4.2E-01	-7.0E-13	1.3E-02	-1.6E-34	8.6E-26	2.9E-05	4.4E-69	2.9E-05
2.4E+00	4.2E-01	2.0E-13	-4.0E-03	4.9E-35	6.7E-27	2.8E-06	4.3E-70	2.8E-06
2.4E+00	4.2E-01	-3.8E-13	-1.5E-02	1.9E-34	2.5E-26	4.1E-05	6.2E-69	4.1E-05
2.4E+00	4.2E-01	-2.7E-13	-1.2E-02	1.4E-34	1.2E-26	2.3E-05	3.5E-69	2.3E-05
2.4E+00	4.1E-01	-2.4E-13	2.1E-03	-2.6E-35	1.0E-26	7.8E-07	1.2E-70	7.8E-07
2.4E+00	4.1E-01	-3.5E-13	1.2E-02	-1.5E-34	2.1E-26	2.6E-05	4.0E-69	2.6E-05
2.4E+00	4.1E-01	-2.8E-13	1.0E-02	-1.3E-34	1.3E-26	1.8E-05	2.8E-69	1.8E-05
2.4E+00	4.1E-01	-6.6E-14	-7.5E-04	9.2E-36	7.2E-28	9.4E-08	1.4E-71	9.4E-08
2.5E+00	4.1E-01	-1.2E-13	-1.0E-02	1.2E-34	2.6E-27	1.7E-05	2.5E-69	1.7E-05
2.5E+00	4.1E-01	-1.2E-13	-9.2E-03	1.1E-34	2.4E-27	1.4E-05	2.1E-69	1.4E-05
2.5E+00	4.0E-01	3.2E-14	-2.5E-04	3.0E-36	1.7E-28	1.0E-08	1.5E-72	1.0E-08
2.5E+00	4.0E-01	8.9E-15	8.0E-03	-9.8E-35	1.3E-29	1.0E-05	1.6E-69	1.0E-05
2.5E+00	4.0E-01	4.2E-15	9.3E-03	-1.1E-34	2.8E-30	1.4E-05	2.1E-69	1.4E-05
2.5E+00	4.0E-01	-6.6E-15	9.1E-03	-1.1E-34	7.1E-30	1.3E-05	2.0E-69	1.3E-05
2.5E+00	4.0E-01	2.3E-14	8.5E-03	-1.1E-34	8.2E-29	1.2E-05	1.8E-69	1.2E-05
2.5E+00	4.0E-01	1.5E-14	8.1E-03	-1.0E-34	3.7E-29	1.1E-05	1.6E-69	1.1E-05
2.5E+00	4.0E-01	6.4E-15	7.4E-03	-9.2E-35	6.6E-30	8.9E-06	1.3E-69	8.9E-06
2.5E+00	4.0E-01	1.4E-14	6.5E-03	-8.0E-35	3.2E-29	6.8E-06	1.0E-69	6.8E-06
2.5E+00	4.0E-01	-2.5E-15	5.3E-03	-6.5E-35	1.0E-30	4.5E-06	6.8E-70	4.5E-06
2.5E+00	4.0E-01	-2.1E-14	3.7E-03	-4.6E-35	7.4E-29	2.2E-06	3.3E-70	2.2E-06
2.5E+00	4.0E-01	1.8E-14	1.8E-03	-2.2E-35	5.0E-29	5.1E-07	7.7E-71	5.1E-07
2.5E+00	4.0E-01	-1.0E-14	-4.4E-04	5.4E-36	1.7E-29	3.1E-08	4.7E-72	3.1E-08
2.5E+00	4.0E-01	-1.7E-14	-2.9E-03	3.5E-35	4.5E-29	1.3E-06	2.0E-70	1.3E-06
2.5E+00	4.0E-01	-4.8E-15	-5.3E-03	6.5E-35	3.6E-30	4.4E-06	6.7E-70	4.4E-06

2.5E+00	4.0E-01	3.9E-15	-7.2E-03	8.8E-35	2.4E-30	8.1E-06	1.2E-69	8.1E-06
2.5E+00	4.0E-01	-9.0E-16	-7.9E-03	9.7E-35	1.3E-31	9.7E-06	1.5E-69	9.7E-06
2.5E+00	4.0E-01	1.6E-18	-7.7E-03	9.5E-35	4.0E-37	9.3E-06	1.4E-69	9.3E-06
2.5E+00	4.0E-01	1.4E-18	-7.3E-03	9.0E-35	2.9E-37	8.4E-06	1.3E-69	8.4E-06
2.5E+00	4.0E-01	1.4E-18	-6.7E-03	8.2E-35	3.3E-37	7.0E-06	1.1E-69	7.0E-06
2.5E+00	4.0E-01	1.1E-18	-5.7E-03	7.0E-35	1.8E-37	5.1E-06	7.7E-70	5.1E-06
2.5E+00	4.0E-01	8.5E-19	-4.4E-03	5.4E-35	1.1E-37	3.0E-06	4.5E-70	3.0E-06
2.5E+00	4.0E-01	7.4E-19	-2.6E-03	3.2E-35	8.6E-38	1.1E-06	1.6E-70	1.1E-06
2.5E+00	3.9E-01	1.4E-19	-6.0E-04	7.4E-36	3.0E-39	5.6E-08	8.6E-72	5.6E-08
2.5E+00	3.9E-01	-3.9E-20	1.6E-03	-2.0E-35	2.3E-40	4.0E-07	6.2E-71	4.0E-07
2.5E+00	3.9E-01	-9.3E-19	3.8E-03	-4.7E-35	1.3E-37	2.2E-06	3.4E-70	2.2E-06
2.5E+00	3.9E-01	-1.5E-18	5.6E-03	-6.9E-35	3.3E-37	4.9E-06	7.4E-70	4.9E-06
2.5E+00	3.9E-01	-1.4E-18	6.6E-03	-8.2E-35	3.0E-37	6.8E-06	1.0E-69	6.8E-06
2.6E+00	3.9E-01	-1.4E-18	6.3E-03	-7.8E-35	2.9E-37	6.1E-06	9.3E-70	6.1E-06
2.6E+00	3.9E-01	-7.5E-19	4.3E-03	-5.3E-35	8.6E-38	2.8E-06	4.2E-70	2.8E-06
2.6E+00	3.9E-01	4.4E-20	4.6E-04	-5.6E-36	2.9E-40	3.2E-08	4.8E-72	3.2E-08
2.6E+00	3.9E-01	9.4E-19	-4.0E-03	4.9E-35	1.3E-37	2.4E-06	3.6E-70	2.4E-06
2.6E+00	3.9E-01	1.3E-18	-5.6E-03	6.9E-35	2.3E-37	4.7E-06	7.1E-70	4.7E-06
2.6E+00	3.9E-01	4.6E-19	-2.2E-03	2.7E-35	3.1E-38	7.0E-07	1.1E-70	7.0E-07
2.6E+00	3.8E-01	-6.2E-19	2.8E-03	-3.5E-35	5.8E-38	1.2E-06	1.8E-70	1.2E-06
2.6E+00	3.8E-01	-1.1E-18	4.7E-03	-5.8E-35	1.7E-37	3.3E-06	4.9E-70	3.3E-06
2.6E+00	3.8E-01	-4.5E-19	2.2E-03	-2.7E-35	3.0E-38	6.9E-07	1.0E-70	6.9E-07
2.6E+00	3.8E-01	3.9E-19	-2.0E-03	2.5E-35	2.2E-38	6.0E-07	9.2E-71	6.0E-07
2.6E+00	3.8E-01	8.8E-19	-4.0E-03	4.9E-35	1.1E-37	2.2E-06	3.4E-70	2.2E-06
2.7E+00	3.8E-01	4.1E-19	-2.1E-03	2.6E-35	2.4E-38	6.3E-07	9.5E-71	6.3E-07
2.7E+00	3.8E-01	-3.2E-19	1.4E-03	-1.8E-35	1.4E-38	2.9E-07	4.5E-71	2.9E-07
2.7E+00	3.7E-01	-5.3E-19	3.3E-03	-4.1E-35	4.0E-38	1.5E-06	2.3E-70	1.5E-06
2.7E+00	3.7E-01	-8.3E-19	2.0E-03	-2.4E-35	9.5E-38	5.4E-07	8.3E-71	5.4E-07
2.7E+00	3.7E-01	1.4E-19	-9.7E-04	1.2E-35	2.8E-39	1.3E-07	2.0E-71	1.3E-07
2.7E+00	3.7E-01	7.7E-19	-2.7E-03	3.4E-35	8.2E-38	1.0E-06	1.5E-70	1.0E-06
2.7E+00	3.7E-01	2.7E-19	-1.8E-03	2.3E-35	1.0E-38	4.6E-07	6.9E-71	4.6E-07
2.7E+00	3.7E-01	-8.9E-20	6.1E-04	-7.5E-36	1.1E-39	5.0E-08	7.6E-72	5.0E-08
2.7E+00	3.7E-01	-3.2E-19	2.2E-03	-2.8E-35	1.4E-38	6.7E-07	1.0E-70	6.7E-07
2.7E+00	3.6E-01	-4.4E-19	1.7E-03	-2.1E-35	2.6E-38	3.7E-07	5.6E-71	3.7E-07
2.8E+00	3.6E-01	5.1E-20	-3.3E-04	4.1E-36	3.4E-40	1.5E-08	2.2E-72	1.5E-08
2.8E+00	3.6E-01	3.9E-19	-1.8E-03	2.2E-35	2.0E-38	4.3E-07	6.6E-71	4.3E-07
2.8E+00	3.6E-01	3.2E-19	-1.5E-03	1.8E-35	1.3E-38	2.9E-07	4.4E-71	2.9E-07
2.8E+00	3.6E-01	-3.3E-20	1.3E-04	-1.6E-36	1.4E-40	2.2E-09	3.3E-73	2.2E-09
2.8E+00	3.6E-01	-3.4E-19	1.5E-03	-1.8E-35	1.5E-38	2.7E-07	4.2E-71	2.7E-07
2.8E+00	3.6E-01	-2.7E-19	1.3E-03	-1.6E-35	9.5E-39	2.3E-07	3.4E-71	2.3E-07
2.8E+00	3.6E-01	-1.2E-20	1.8E-05	-2.2E-37	1.9E-41	4.0E-11	6.0E-75	4.0E-11
2.8E+00	3.5E-01	3.6E-19	-1.2E-03	1.4E-35	1.6E-38	1.7E-07	2.6E-71	1.7E-07
2.8E+00	3.5E-01	4.5E-19	-1.2E-03	1.4E-35	2.5E-38	1.7E-07	2.6E-71	1.7E-07
2.8E+00	3.5E-01	-5.1E-20	-1.2E-04	1.5E-36	3.2E-40	1.8E-09	2.8E-73	1.8E-09

2.9E+00	3.5E-01	-9.1E-20	9.2E-04	-1.1E-35	1.0E-39	1.0E-07	1.6E-71	1.0E-07
2.9E+00	3.5E-01	-2.1E-19	1.0E-03	-1.3E-35	5.4E-39	1.3E-07	1.9E-71	1.3E-07
2.9E+00	3.5E-01	1.3E-19	1.9E-04	-2.4E-36	2.1E-39	4.4E-09	6.7E-73	4.4E-09
2.9E+00	3.5E-01	2.2E-19	-7.2E-04	8.9E-36	5.8E-39	6.3E-08	9.5E-72	6.3E-08
2.9E+00	3.5E-01	-7.7E-21	-9.3E-04	1.1E-35	7.1E-42	1.0E-07	1.6E-71	1.0E-07
2.9E+00	3.5E-01	-7.7E-21	-9.3E-04	1.1E-35	7.1E-42	1.0E-07	1.6E-71	1.0E-07
2.9E+00	3.5E-01	3.6E-19	-9.2E-04	1.1E-35	1.5E-38	1.0E-07	1.5E-71	1.0E-07
2.9E+00	3.5E-01	1.1E-19	-9.1E-04	1.1E-35	1.3E-39	1.0E-07	1.5E-71	1.0E-07
2.9E+00	3.5E-01	3.6E-19	-9.0E-04	1.1E-35	1.5E-38	9.8E-08	1.5E-71	9.8E-08
2.9E+00	3.5E-01	-1.2E-19	-8.9E-04	1.1E-35	1.7E-39	9.4E-08	1.4E-71	9.4E-08
2.9E+00	3.5E-01	-7.5E-20	-8.7E-04	1.1E-35	6.7E-40	9.0E-08	1.4E-71	9.0E-08
2.9E+00	3.5E-01	4.7E-20	-8.4E-04	1.0E-35	2.7E-40	8.5E-08	1.3E-71	8.5E-08
2.9E+00	3.5E-01	6.9E-20	-8.1E-04	1.0E-35	5.7E-40	7.8E-08	1.2E-71	7.8E-08
2.9E+00	3.5E-01	3.5E-19	-7.7E-04	9.5E-36	1.5E-38	7.1E-08	1.1E-71	7.1E-08
2.9E+00	3.5E-01	2.5E-19	-7.3E-04	9.0E-36	7.7E-39	6.3E-08	9.6E-72	6.3E-08
2.9E+00	3.5E-01	1.5E-13	-6.8E-04	8.3E-36	2.5E-27	5.5E-08	8.3E-72	5.5E-08
2.9E+00	3.5E-01	-1.4E-13	-6.8E-04	8.3E-36	2.5E-27	5.4E-08	8.3E-72	5.4E-08
2.9E+00	3.5E-01	1.7E-14	-6.8E-04	8.3E-36	3.2E-29	5.4E-08	8.3E-72	5.4E-08
2.9E+00	3.5E-01	-2.5E-13	-6.7E-04	8.3E-36	7.2E-27	5.4E-08	8.2E-72	5.4E-08
2.9E+00	3.5E-01	-9.3E-14	-6.6E-04	8.2E-36	1.0E-27	5.2E-08	7.9E-72	5.2E-08
2.9E+00	3.5E-01	-4.0E-13	-6.4E-04	8.0E-36	1.9E-26	5.0E-08	7.5E-72	5.0E-08
2.9E+00	3.5E-01	-4.0E-13	-6.1E-04	7.5E-36	1.9E-26	4.4E-08	6.7E-72	4.4E-08
2.9E+00	3.5E-01	-8.1E-14	-5.3E-04	6.6E-36	7.8E-28	3.4E-08	5.1E-72	3.4E-08
2.9E+00	3.4E-01	2.2E-15	-3.6E-04	4.5E-36	6.0E-31	1.6E-08	2.4E-72	1.6E-08
2.9E+00	3.4E-01	2.0E-13	4.1E-06	-5.0E-38	4.6E-27	1.9E-12	3.0E-76	1.9E-12
2.9E+00	3.4E-01	-1.0E-13	5.6E-04	-6.9E-36	1.2E-27	3.7E-08	5.6E-72	3.7E-08
2.9E+00	3.4E-01	-2.7E-13	7.6E-04	-9.4E-36	8.4E-27	6.9E-08	1.0E-71	6.9E-08
2.9E+00	3.4E-01	-1.1E-12	7.6E-04	-9.4E-36	1.3E-25	6.9E-08	1.0E-71	6.9E-08
2.9E+00	3.4E-01	6.2E-13	7.7E-04	-9.5E-36	4.6E-26	7.0E-08	1.1E-71	7.0E-08
2.9E+00	3.4E-01	-4.9E-14	7.8E-04	-9.6E-36	2.9E-28	7.1E-08	1.1E-71	7.1E-08
2.9E+00	3.4E-01	-2.0E-13	7.7E-04	-9.5E-36	4.6E-27	7.0E-08	1.1E-71	7.0E-08
2.9E+00	3.4E-01	-2.4E-13	7.6E-04	-9.3E-36	6.9E-27	6.7E-08	1.0E-71	6.7E-08
2.9E+00	3.4E-01	-4.3E-13	7.3E-04	-9.0E-36	2.1E-26	6.2E-08	9.5E-72	6.2E-08
2.9E+00	3.4E-01	3.9E-13	6.9E-04	-8.5E-36	1.7E-26	5.6E-08	8.5E-72	5.6E-08
2.9E+00	3.4E-01	-1.1E-13	6.4E-04	-7.9E-36	1.5E-27	4.7E-08	7.2E-72	4.7E-08
2.9E+00	3.4E-01	1.6E-13	5.7E-04	-7.0E-36	3.2E-27	3.8E-08	5.8E-72	3.8E-08
2.9E+00	3.4E-01	-3.9E-13	4.9E-04	-6.0E-36	1.8E-26	2.8E-08	4.2E-72	2.8E-08
2.9E+00	3.4E-01	1.3E-13	3.9E-04	-4.8E-36	1.8E-27	1.8E-08	2.7E-72	1.8E-08
2.9E+00	3.4E-01	-1.6E-13	2.8E-04	-3.4E-36	3.1E-27	9.1E-09	1.4E-72	9.1E-09
2.9E+00	3.4E-01	-4.3E-13	1.6E-04	-1.9E-36	2.1E-26	2.8E-09	4.3E-73	2.8E-09
2.9E+00	3.4E-01	2.3E-13	2.3E-05	-2.8E-37	6.2E-27	5.9E-11	9.0E-75	5.9E-11
2.9E+00	3.4E-01	-2.2E-13	-1.2E-04	1.4E-36	5.7E-27	1.6E-09	2.4E-73	1.6E-09
2.9E+00	3.4E-01	1.7E-13	-2.6E-04	3.2E-36	3.5E-27	7.6E-09	1.2E-72	7.6E-09
2.9E+00	3.4E-01	1.2E-15	-3.9E-04	4.8E-36	1.7E-31	1.8E-08	2.7E-72	1.8E-08

2.9E+00	3.4E-01	8.2E-13	-5.1E-04	6.2E-36	7.9E-26	3.0E-08	4.5E-72	3.0E-08
2.9E+00	3.4E-01	-2.4E-13	-6.0E-04	7.4E-36	6.5E-27	4.1E-08	6.3E-72	4.1E-08
2.9E+00	3.4E-01	4.4E-13	-6.5E-04	8.0E-36	2.3E-26	4.9E-08	7.4E-72	4.9E-08
3.0E+00	3.4E-01	-5.6E-13	-6.5E-04	8.0E-36	3.6E-26	4.9E-08	7.4E-72	4.9E-08
3.0E+00	3.4E-01	8.6E-13	-5.9E-04	7.3E-36	8.5E-26	4.0E-08	6.1E-72	4.0E-08
3.0E+00	3.4E-01	-9.6E-13	-4.5E-04	5.6E-36	1.1E-25	2.4E-08	3.6E-72	2.4E-08
3.0E+00	3.4E-01	4.4E-14	-2.5E-04	3.0E-36	2.2E-28	6.9E-09	1.1E-72	6.9E-09
3.0E+00	3.4E-01	-3.9E-13	1.7E-05	-2.1E-37	1.8E-26	3.3E-11	5.0E-75	3.3E-11
3.0E+00	3.4E-01	-1.6E-13	1.2E-04	-1.5E-36	2.9E-27	1.6E-09	2.5E-73	1.6E-09
3.0E+00	3.4E-01	-2.7E-13	1.2E-04	-1.5E-36	8.1E-27	1.6E-09	2.5E-73	1.6E-09
3.0E+00	3.4E-01	4.4E-13	4.0E-04	-5.0E-36	2.2E-26	1.8E-08	2.8E-72	1.8E-08
3.0E+00	3.4E-01	-1.6E-13	5.6E-04	-6.9E-36	2.8E-27	3.5E-08	5.3E-72	3.5E-08
3.0E+00	3.3E-01	5.4E-13	4.6E-04	-5.7E-36	3.2E-26	2.4E-08	3.7E-72	2.4E-08
3.0E+00	3.3E-01	-3.9E-13	7.5E-05	-9.3E-37	1.7E-26	6.3E-10	9.6E-74	6.3E-10
3.0E+00	3.3E-01	1.2E-13	-2.7E-04	3.4E-36	1.6E-27	8.2E-09	1.3E-72	8.2E-09
3.0E+00	3.3E-01	-2.6E-13	-2.7E-04	3.4E-36	7.7E-27	8.2E-09	1.3E-72	8.2E-09
3.0E+00	3.3E-01	-1.1E-12	-4.6E-04	5.7E-36	1.3E-25	2.4E-08	3.6E-72	2.4E-08
3.0E+00	3.3E-01	2.1E-13	-2.2E-04	2.7E-36	5.0E-27	5.2E-09	7.9E-73	5.2E-09
3.0E+00	3.3E-01	-3.8E-13	2.0E-04	-2.4E-36	1.6E-26	4.3E-09	6.5E-73	4.3E-09
3.0E+00	3.3E-01	-5.2E-13	3.9E-04	-4.8E-36	2.9E-26	1.6E-08	2.5E-72	1.6E-08
3.1E+00	3.3E-01	1.7E-13	2.1E-04	-2.6E-36	3.0E-27	4.7E-09	7.1E-73	4.7E-09
3.1E+00	3.3E-01	1.2E-12	-1.4E-04	1.7E-36	1.6E-25	2.1E-09	3.1E-73	2.1E-09
3.1E+00	3.3E-01	-3.0E-13	-3.2E-04	4.0E-36	9.4E-27	1.1E-08	1.7E-72	1.1E-08
3.1E+00	3.2E-01	9.6E-13	-2.0E-04	2.4E-36	9.8E-26	4.1E-09	6.2E-73	4.1E-09
3.1E+00	3.2E-01	-8.5E-13	9.3E-05	-1.1E-36	7.6E-26	9.1E-10	1.4E-73	9.1E-10
3.1E+00	3.2E-01	-4.0E-13	2.5E-04	-3.1E-36	1.7E-26	6.7E-09	1.0E-72	6.7E-09

APPENDIX II
Vibration-Damping Pads for Heavy Machinery

High-quality rubber motor mounts reduce vibrations, shocks, and noise from machines in both large and light machinery, including highway vehicles, construction, and agricultural equipment. Most machinery emits noise and vibrations into the surrounding area, but when our rubber motor mounts are fitted, the noise and vibrations are absorbed. Additionally, motor mounts shield delicate electric motors or aggregates from unintentional movements.

Motor mounts are made with a high load capacity and are designed to absorb forces from all directions. These mounts can support loads weighing between 90 kg (180 lbs) and 418 kg (920 lbs). Our superior rubber composition is designed to withstand harsh climatic conditions, extending the lifespan of the motor mounts.

Style 1

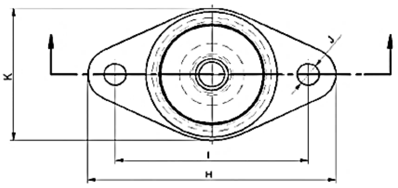

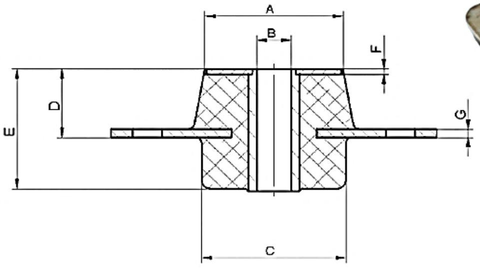

Style 2

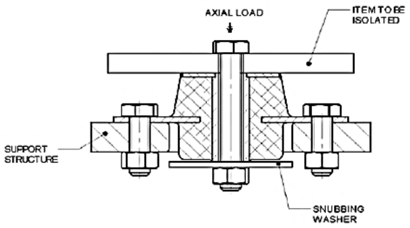

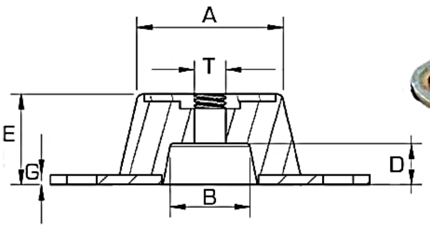

Part Number	Diameter x Height mm (Inch) (A) x (E)	Inner Diameter mm (Inch) (B) (T)	Hole Seperation mm (Inch) (I)	Mounting Holes mm (Inch) (J)	Baseplate Thickness mm (Inch) (G)	Flange Length mm (Inch) (H)	Style	Quality ShoreA Duro	Max. Static Compression Force (vertical) N	lbs	Max. Static Shear Force (horizontal) N	lbs
XX1564w	49 x 45 (1.93) x (1.77)	12 (.47)	88.9 (3.5)	10.3 (.41)	3 (.12)	114.5 (4.51)	1	43	800	180	420	94
XX1564								57	1480	333	777	175
XX1564h								68	2400	540	1260	283
XX156401w	49 x 45 (1.93) x (1.77)	13.5 (.53)	88.90 (3.5)	10.3 (.41)	3 (.12)	114.5 (4.51)	1	43	800	180	420	94
XX156401								57	1480	333	777	175
XX156401h								68	2400	540	1260	283
XX1565w	51 x 51 (2.01) x (2.01)	13.3 (.52)	95.2 (3.75)	13.9 (.55)	15.8 (.62)	119.2 (4.69)	1	43	1364	307	710	160
XX1565								57	2523	567	1314	295
XX1665h								68	4092	920	2130	479
XX1583w	44 x 27.8 (1.73) x (1.09)	24 (M8) (.94) (*)	77 (3.03)	9 (.35)	3 (.12)	96 (3.78)	2	43	830	187	200	45
XX1583								57	1536	345	370	83
XX1583h								68	2490	560	600	135

*UNC Threads upon request